NON-HERMITIAN QUANTUM AND CLASSICAL INTEGRATED NONLINEAR PHOTONICS

A thesis submitted for the degree
of Doctor of Philosophy of
the Australian National University

Diana A. Antonosyan

29 November 2016

This thesis contains no material which has been accepted for the award of any other degree or diploma in any university. To the best of the author's knowledge and belief, it contains no material previously published or written by another person, except where due reference is made in the text.

Diana Antonosyan
29 November 2016

Acknowledgements

I would like to thank my supervisory panel A/Prof. Andrey A. Sukhorukov, Dr. Alexander S. Solntsev, A/Prof. Ilya V. Shadrivov and Prof. Yuri S. Kivshar for their support and guidance, interesting research and everything new I have learnt. I am grateful in particular to Prof. Ilya Shadrivov who helped me a lot both at work and in everyday life. Many thanks to Alexander S. Solntsev who was not only a mentor but also a friend all this years. I want to thank all my colleagues and friends at the Nonlinear Physics Centre for an opportunity to work in a unique research environment, for all their support and and making my PhD journey pleasant and enjoyable. Next, I want to thank Prof. Alexander Szameit and Markus Gräfe from the University of Jena for productive collaboration. My theoretical studies benefitted from the beautiful experiments and femtosecond laser direct-writing waveguide fabrication. I also want to thank Kathy Hicks for the excellent administrative support.

I acknowledge financial support provided by the Centre for Ultrahigh bandwidth Devices for Optical Systems (CUDOS). I also acknowledge the Australian National University and Optical Society of America (OSA) for the support of my overseas conferences.

Finally and most importantly I want to thank my family, mainly my parents dear daddy Alexander Antonosyan and loving mummy Yermone Boyajyan for their unconditional love, constant support and belief in me, without which I wouldn't be able to complete the research presented in this thesis.

Abstract

Integrated optical quantum circuits based on photonic waveguiding structures are increasingly gaining attention as a possible solution for scalable quantum technologies with important applications to quantum simulations. Quantum communication provides secure information transmission, but the distance over which quantum states of light can be distributed without significant disturbance is limited due to inescapable losses and noise in optical elements. Loss is the greatest challenge facing the implementation of integrated photonic technologies, and it is inescapable in experimental reality. In recent years there is a rise of interest in structures with spatially inhomogeneous losses. Light propagation in waveguiding structures with spatially distributed sections of loss can be used for implementation of quantum plasmonic circuits, which are able to strongly confine light to sub-wavelength dimensions, as well as for parity-time (PT) symmetric structures, with phase transition associated with PT-symmetry breaking, which opens new possibilities for light manipulation. The PhD thesis contains research on the controllable classical and quantum dynamics of optical frequency conversion processes in quadratically nonlinear photonic integrated circuites in the presence of losses. Namely, I discuss spontaneous parametric down-conversion (SPDC), sum-frequency generation (SFG) and optical parametric amplification (OPA) in nonlinear structures governed by non-Hermition Hamiltonians. I explore the fundamental features of multi-photon generation in integrated nonlinear waveguides. I have been shown that arrays of coupled nonlinear waveguides can serve as a robust integrated platform for the generation of entangled photon states with nonclassical spatial correlations through spontaneous parametric down-conversion (SPDC), and that the operation of such quantum circuit is tolerant even to relatively high losses. Furthermore, I have studied the bi-photon multimode quantum emission tomography in waveguide structures with spatially inhomegeneous losses. The PhD thesis also covers the research on the effect of these losses in waveguide couplers possessing parity-time (PT) symmetry. I have identified an anti-PT spectral symmetry of a parametric amplifier based on those

couplers. Finally, I describe the single-photon conversion to a photon pair, and identify opportunities for the efficient enhancement of this process.

Contents

Chapter 1

Introduction

Optics and photonics technologies are ubiquitous; they are responsible for the displays on smart-phones and computing devices, optical fiber that carries the information in the internet, advanced precision manufacturing, enhanced defense capabilities, and a variety of medical diagnostics tools. All of these were developed and improved through research. Science and technology are separate, but forever interweaved, subjects.

Several areas of research, such as spectroscopy, semiconductor analysis, photochemistry, and remote sensing, need a tunable coherent source of high-power or high-energy radiation. This thesis is devoted to the research of the controllable optical frequency conversion processes in quadratically nonlinear photonic integrated circuites in presence of losses.

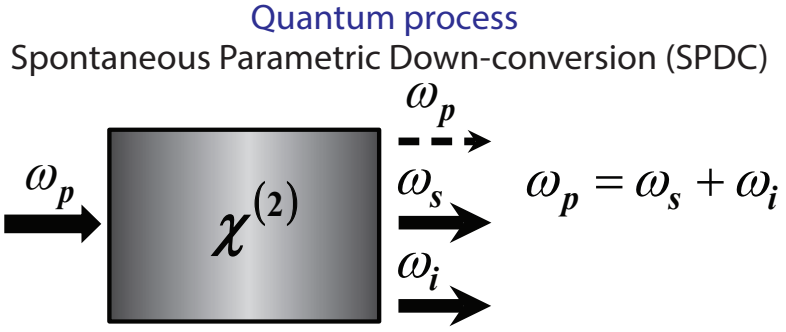

Figure 1.1: Schematic analysis of spontaneous parametric down-conversion (SPDC) in $\chi^{(2)}$ nonlinear media. Explicitly involved fields in the $\chi^{(2)}$ process are shown in black, residual fields are dashed.

The theoretical and experimental advances of 1960s helped to show that any frequency manipulation that could be performed at radio frequencies, could, in principle, be performed at optical frequencies. In the last few years both strong

up and down conversion sources have been developed. The advent of novel higher-damage-threshold nonlinear-optical materials and improved pump lasers has renewed interest in parametric devices and has permitted these devices to make the transition from being a research curiosity to being an actual tool used in a wide variety of applications. In this thesis we examine the classical and quantum dynamics of optical frequency conversion in nonlinear media.

Nonlinear optics is feasible only when powerful laser beams, containing a large number of photons, interact in nonlinear materials. Under the interaction of an applied optical electric field, the atoms or molecules of the dielectric material may respond as follows. Optical field-induced electric dipole moment acts as a new source to emit a secondary electromagnetic wave. This is the fundamental process describing the optical field-induced dipole moment of a molecular system and the re-emission of a secondary wave radiation. It was realized that the electric polarization induced in the medium is the key for studying the physics of nonlinear optics and so in general the polarization of the medium should be expressed as a power series of applied electric field [1, 2]:

$$\mathbf{P} = \chi^{(1)}\mathbf{E} + \chi^{(2)}\mathbf{EE} + \chi^{(3)}\mathbf{EEE} + ..., \tag{1.1}$$

where $\mathbf{P}$ is the polarization, $\chi^{(i)}$ is the ith order susceptibility tensor (material coefficient) of a given medium and $\mathbf{E}$ is applied electric field. Electric polarization of a medium is determined by two factors: one is the field induced dipole moment of each individual molecule of the medium, and the other is the statistically averaged property of a great number of molecules. That is the molecular dipole moment is determined by the microscopic structure and depends on the microscopic symmetry.

In this thesis we consider optical $\chi^{(2)}$ processes. Second order processes are useful non destructive techniques for the study of surfaces and deep interfaces, with a resolution better than the inherent penetration depth of the probe.

Optical processes in $\chi^{(2)}$ media are always three photon processes. Figs. 1.1, 1.2 (optical fields are shown for lossless $\chi^{(2)}$ material) illustrates a schematic analysis of the $\chi^{(2)}$ processes discussed throughout the thesis. Three wave interaction Hamiltonian is written in the following form,

$$H(t) = S\sum_{\alpha,\beta,\gamma}\int_0^L dz\chi^{(2)}_{\alpha,\beta,\gamma}(z)E_\alpha(z,t)E_\beta(z,t)E_\gamma(z,t) = H^{(-)}(t) + H^{(+)}(t), \tag{1.2}$$

where $\chi^{(2)}_{\alpha,\beta,\gamma}(z)$ is the second order nonlinear susceptibility tensor of the one dimensional media with the length L, and interaction area S. $E_\alpha(z,t)$ is the elec-

trical field operator, which is a superposition of three components, corresponding to the pump field $E_{L,\alpha}(z,t)$ and two sub-harmonics marked by $(j=1,2)$ indexes. These sub-harmonic fields consist of electrical field operators with positive $E^{(+)}_{j,\alpha}(z,t)$ and negative $E^{(-)}_{j,\alpha}(z,t)$ frequencies, α,β,γ are the polarization states of the electromagnetic fields. Further we will consider that each field is linearly polarized and has its own polarization, thus we'll skip the polarization indexes of the electric fields and the nonlinear susceptibility tensor. The negative part of the Hamiltonian has the following form,

$$H^{-}(t)=\int_0^L dz\chi^{(2)}(z)E_p^{+}(z,t)E_1^{(-)}(z,t)E_2^{(-)}(z,t), \tag{1.3}$$

where E_p, $E_1^{(-)}$ and $E_2^{(-)}$ are interacting fields, and the positive frequency part of each of them has the following form [3]

$$E_j^{(+)}(z,t)=i\int\frac{d\omega}{2\pi}N_j(\omega)a_j(\omega)e^{i(k_j(\omega,z)z-\omega t)}, \tag{1.4}$$

where $a_j(\omega)$ $(j=1,2)$ is the sub-harmonic mode operator, $a_j^{\dagger}$ and a_j are the creation and annihilation operators for sub-harmonic modes with the commutators $[a_j(\omega),a_j^{\dagger}(\omega')]=\delta(\omega-\omega')$ and $[a_1(\omega),a_2(\omega)]=[a_1^{\dagger}(\omega),a_2^{\dagger}(\omega)]=0$, while the pump field has classical form,

$$E_p^{(+)}(z,t)=i\int\frac{d\omega}{2\pi}E_L(\omega)e^{i(k_L(\omega,z)z-\omega t)}. \tag{1.5}$$

Here $N_j(\omega)=\sqrt{\frac{\pi\hbar\omega}{c\epsilon_0 n_j^2(\omega)S}}$ is the normalization term, $n_j(\omega)$ - refractive index of the media for certain frequency, S - cross-section area of two beams, $\beta_j(z,\omega)=\frac{\omega_j}{c}n_j(z,\omega)$. The quantum state in the low order perturbation theory is presented as follows:

$$|\psi(t)\rangle=\frac{-i}{\hbar}\int_{-\infty}^{t}dt'H(t')|0\rangle, \tag{1.6}$$

Down-conversion is a nonlinear processes where a photon with high energy at ω_p frequency splits into two photons with lower energies at frequencies ω_s,ω_i. The daughter photons are called signal (ω_s) and idler (ω_i) [see Fig. 1.1]. Spontaneous parametric down-conversion can be presented as a process stimulated by random vacuum fluctuations. The conversion efficiency is very low, on the order of 1 pair per every $10^{-8}-10^{-6}$ incoming photons [4]. The signal and idler fields are perfectly correlated to each other, as each pair of low frequency photons is produced by the one high frequency photon. This type of correlation is called entanglement. Entanglement was observed for the first time by Schrödinger, is a phenomena where the wave function of a quantum system consisting of two sub-

systems cannot be factorized into a product of wavefunctions of the subsystem. This phenomena is widely used in quantum technologies for quantum communication and computation. Quantum optics started its intensive development at the end of the twentieth century, when so called non-classical states of light, such as superposition states, squeezed states of light, entangled states and the Einstein-Padolski-Rosen states, were observed theoretically and further investigated experimentally. Nowadays the non-classical states of light have interesting applications in very precise measurements, metrology and spectroscopy, as well as in quantum communication [5–8]. Starting with the pioneering work of Mandel and co-authors [9] many different schemes and the structures were used for generation of photon pairs in nonlinear media. Quantum entanglement plays a key role in all schemes of quantum computation, quantum cryptography and quantum teleportation [10–21]. Spontaneous parametric down-conversion has already become a working horse for generation of high quality entangled states [20, 21].

Sum Frequency Generation (SFG) is a nonlinear process, where two fields at ω_s, ω_i frequencies generate a beam with sum frequency ω_{SFG} [see, Fig. 1.2(a)]. SFG is implemented in frequency chains, and in detection of weak signals at low optical frequencies. One application of sum-frequency generation is to produce tunable radiation in the ultraviolet region by choosing one of the input waves to be a fixed-frequency visible laser and the other to be a frequency-tunable visible laser [2]. In many ways the process of sum-frequency generation is analogous to that of second-harmonic generation, except that in sum-frequency generation the two input waves are at different frequencies. Sum-frequency generation in the range of infrared − visible light is very functional tool for studies of surfaces and interfaces. They can be used to study surface dynamics and reactions with sub-picosecond time resolution, thus SFG is able to provide rich surface-specific vibrational information on bonding and orientation of molecules and ions at interfaces [22, 23]. SFG is used for improvement of upconversion spectrometers for the measurement of time-resolved luminescence spectra with subpicosecond time resolution [24].

Difference frequency generation (DFG) can occur, where two pump beams at frequencies ω_p and ω_s generate another beam, called the idler, with frequency ω_i such that $\omega_p - \omega_s = \omega_i$ [see, Fig. 1.2(b)]. Such a process requires phase matching to be efficient, and usually there is no simultaneous phase matching for sum and difference frequency generation. DFG is often referred to as Optical Parametric Amplification (OPA). Parametric amplification is a phenomenon where a signal can be amplified using a parametric nonlinearity and a pump wave. More precisely, the signal beam propagates through the crystal together with a pump beam of higher energy. Photons of the pump wave are then converted into signal photons and the same number of idler photons; the photon energy of the idler wave is the difference between the photon energies of pump and signal wave.

DFG most often finds application in frequency chains. A tunable mid-IR source has been implemented based on difference frequency generation, which is perfect for spectroscopic applications as it is mechanically robust and stable during temperature fluctuations [25]. The high-sensitivity detection that can be achieved using a DFG spectrometer, which can be used for sensing gases [26], high sensitivity molecular detection as well as sub-Doppler saturated spectroscopy [27]. It is possible to obtain tunable, room-temperature, electrically pumped c.w. semiconductor tunable terahertz (THz) source based on DFG [28]. THz light can be used to simultaneously image the structure of samples while identifying their chemical composition. THz imaging can measure multiple layers.

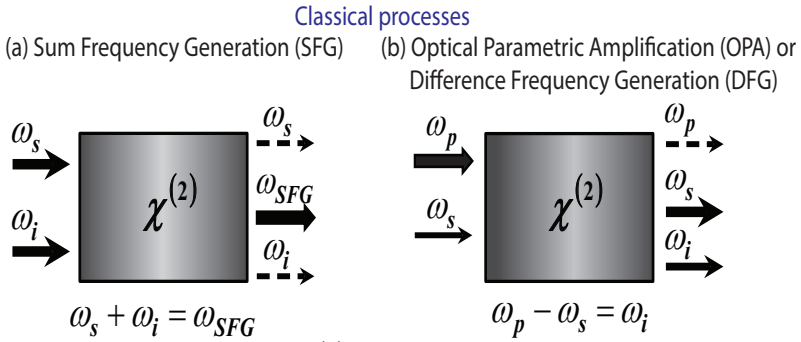

Figure 1.2: Schematic of the $\chi^{(2)}$ processes discussed throughout the thesis. Explicitly involved fields in the $\chi^{(2)}$ process are shown in black, residual fields are dashed. (a) sum frequency generation (SFG) and (b) difference frequency generation DFG, which is often referred to as optical parametric amplification (OPA).

Various kinds of optical components, in addition to light sources, optical fibres and detectors, are required in constructing optical fibre communication systems with higher transmission efficiency and network flexibility [29–31]. These components include optical beam splitters, optical switches, wavelength multiplexers for introducing multiple optical channels into a single optical fibre. Most of these optical components have been realized in bulk-optic configurations using microlenses and prisms. These bulk-optic approaches appear to have some limitations in terms of production, device stability and suitability for integration. A possible way to overcoming this problem is to introduce channel waveguide technologies to form integrated-optic components. One of the most practical and promising approaches in the integrated-optic area seems to be the designing of optical circuits based on low-loss glass waveguides.

Electronic integrated circuits are the most significant technology of the 20th century. They have changed the way we work enabling the computer industry. The photonic equivalents of these devices have been equally challenging to develop and are widely used to manipulate and control the signals in optical fibres.

A Photonic Integrated Circuit (PIC) is conceptually very similar to an electronic integrated circuit (IC). While IC integrates many transistors, capacitors and resistors, a PIC integrates multiple optical components such as lasers, modulators, detectors, attenuators, multiplexers/demultiplexers and optical amplifiers. By integrating many optical devices into a single device, PICs enable improvements in system size, power consumption, reliability and cost. On-chip integrated photonic circuits are crucial to further progress towards quantum technologies and in the science of quantum optics [20, 32, 33].

Overall, integrated optical quantum circuits utilizing coupled waveguides are increasingly gaining attention as a possible solution for scalable quantum technologies with important applications to quantum simulations. Integrated optical circuits enable a stable and scalable realization of quantum logic devices, which can form a basis for the mass production of photonic chips for quantum communication and computation [34–39]. Quantum gates were implemented using pairs of waveguides acting as integrated beam splitters [35], and lattices of coupled waveguides were used for the study of Bloch oscillations [40] and propagation of squeezed light [41]. Recently, there has been growing interest in the study of the propagation of nonclassical light in coupled waveguides. An important challenge is the integration of single-photon sources, which should enable on-chip generation and preparation of quantum states [42–44]. Spontaneous parametric down-conversion (SPDC) in nonlinear waveguides provides an attractive solution for the on-chip generation of correlated and entangled photon pairs [45–49]. A key mechanism for quantum simulations can be provided by the process of quantum walks in an optical waveguide array (WGA) [50, 51], with applications to boson sampling [52–55]. It was recently suggested [56–59] that a nonlinear waveguide array can be used for both photon-pair generation through spontaneous parametric down-conversion and quantum walks of the generated biphotons with strong spatial entanglement between the waveguides. Importantly, such an integrated scheme avoids input losses since in an integrated nonlinear waveguide array photon pairs can be generated inside the quantum-walk circuit.

Conventional photonic chips are based on dielectric platforms, but there is an increasing interest in the development of quantum plasmonic circuits. Such metal-dielectric structures are able to strongly confine light to sub-wavelength dimensions, which can enhance the light-matter interactions. Although metals introduce loss at optical wavelengths, the robust operation of plasmonic circuits with quantum states was recently demonstrated through the observation of quantum interference between single plasmons [60, 61]. The realization of spontaneous frequency conversion in plasmonic structures would provide a route for integrated entangled state generation. However, the nontrivial effect of losses needs to be carefully considered since they can nontrivially affect the emerging photon state [62–66].

Quantum communication provides secure information transmission [67], but the distance over which quantum states of light can be distributed without significant disturbance is limited due to inescapable losses and noise in optical elements. In contrast to classical communication, losses in quantum communication cannot be compensated by amplifying the signal because the laws of quantum mechanics imply that any deterministic phase-insensitive signal amplification is unavoidably accompanied by the addition of noise [68, 69].

Loss is the greatest challenge facing the implementation of integrated photonic technologies, and it is inescapable in experimental reality. Transport phenomena are at the heart of many fundamental problems in physics, chemistry, and biology [70–72]. Of special interest is the realization of novel classes of integrated photonic devices such as isolators [73], optical diodes based on asymmetric nonlinear absorption [74], second harmonic generation in asymmetric waveguides [75] and nonlinear photonic crystals [76].

The motivation for derivation of non-Hermitian quantum mechanics is twofold. Firstly, there are problems which can be answered only in this formalism, for instance, in optics in case of use of complex refractive indexes. Secondly, there are problems that can be, in principle, solved within the conventional Hermitian framework, but only with extreme difficulty, while non-Hermitan formalism enables a much simpler and straightforward solution [77]. Namely, one of the most useful problems is exploration of the resonance phenomena, where particles are trapped by the potential. The systems described in classical statistic mechanics, diffusion in biological systems, or propagation of light in waveguides can be described by quantum language. In such cases the Hamiltonians are not Hermitian since the system is open to interaction with its environment, which interpreted as losses.

In recent years the interest has arisen in structures with spatially inhomogeneous losses. One of the fundamental axioms of quantum mechanics is associated with the Hermiticity of physical observables. In the case of the Hamiltonian operator, this requirement guaranties real spectrum [5–7]. There is a wide class of non-Hermitian Hamiltonians can still show entirely real spectra. Among these are Hamiltonians respecting paritytime (PT) symmetry [78, 79]. The parity operator $\hat{\mathcal{P}}$, responsible for spatial reflections, is defined through the operations $\hat{p} \to -\hat{p}$, $\hat{x} \to -\hat{x}$, while the time reversal operator $\hat{\mathcal{T}}$ leads to $\hat{p} \to -\hat{p}$, $\hat{x} \to \hat{x}$ and to complex conjugation $i \to -i$. PT symmetry requires that the real part of the potential V is an even function of position x, whereas the imaginary part is odd; $V(\hat{x}) = V^*(-\hat{x})$ [80–82]. Quite recently, the prospect of realizing complex PT-symmetric potentials within the framework of optics has been suggested theoretically [80, 83–85] and realized experimentally [80–82]. This is possible because of the formal equivalence between the quantum mechanical Schrödinger equation and the coupled mode equations. We are interested in study of optical beam

propagation in PT-symmetric complex potentials, which can be realized through a composition of gain/loss regions. Given that the complex refractive-index distribution $n(x) = n_R(x) + in_I(x)$ plays the role of an optical potential, we can then design a PT-symmetric system by satisfying the conditions $n_R(x) = n_R(-x)$ and $n_I(x) = -n_I(-x)$ [77, 82].

Light propagation in waveguiding structures with spatially distributed sections of loss and gain can be analogous to quantum wavepacket dynamics governed by a parity-time (PT) symmetric Hamiltonian [81]. Below a certain gain/loss level, such systems support PT-symmetric optical modes, which then exhibit the same average loss or gain [80, 86]. However when gain or loss is increased, the PT-symmetry of modes breaks, and a mode with the strongest gain (or smallest loss) dominates, as demonstrated experimentally [80–82]. The phase transition associated with such PT-symmetry breaking opens new possibilities for light manipulation, such as PT-symmetric lasers [87, 88]. Such lasers can achieve single-mode operation, where small difference in medium gain leads to a dramatic difference in mode amplification below and above the PT breaking threshold. We

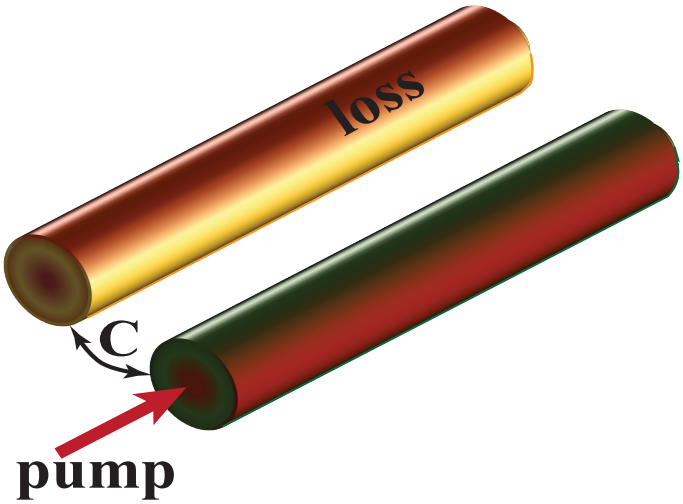

Figure 1.3: Scheme of PT-symmetric coupler with linear absorption in one waveguide.

consider a directional coupler composed of two waveguides, where modes exhibit different loss in each waveguide. The loss can be introduced, for example, by depositing a thin layer of metal [81]. An illustration of such a structure with loss in one waveguide is presented in Fig. 1.3. To analyze the behavior of this structure we employ a coupled-mode formalism where the exact profiles of the isolated modes are obtained [82, 89]

$$
\begin{aligned}
i\frac{\mathrm{d}a_1(z)}{\mathrm{d}z} &= \beta a_1 - C a_2, \\
i\frac{\mathrm{d}a_2(z)}{\mathrm{d}z} &= \left(\beta^* - i\gamma\right) a_2 - C^* a_1.
\end{aligned} \tag{1.7}
$$

where β and β^* represent the two propagation constants, C are the complex coupling coefficients, and γ is a scaled loss coefficient. The Hamiltonian corresponding to the linear problem of Eq. (1.7), is written as:

$$
\mathcal{H} = \begin{pmatrix} \beta & -C \\ -C^* & \beta^* - i\gamma \end{pmatrix}. \tag{1.8}
$$

The Hamiltonian possesses PT symmetry when applied together with Gauge transformation [81, 90],

$$
\mathcal{PT}\left(\mathcal{H} - \bar{\rho}\mathcal{I}\right) = \left(\mathcal{H} - \bar{\rho}\mathcal{I}\right)\mathcal{PT}, \tag{1.9}
$$

where I is an identity matrix, and $\bar{\rho} = \gamma/2$ defines the average gain or loss between the two waveguides. PT-symmetry breaking occurs whenever $|\gamma| \geq 2|C|$.

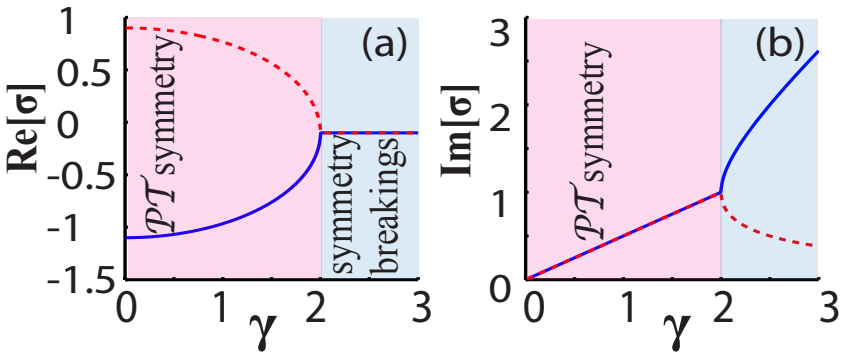

Figure 1.4: Complex bifurcation of the supermode propagation constants. (a) Real part defining propagation constant. (b) Imaginary part propagation constant

This marks the onset of a phase transition beyond which the oscillatory coupling between the two modes disappears and is replaced by a hyperbolic behavior [82]. We present characteristic dependencies of the eigenvalues on the loss in Fig. 1.4. The complex bifurcation of the supermode propagation constants around the transition point is shown in Fig. 1.4(a) and (b). After this point, the spectrum ceases being entirely real and becomes complex, which marks the onset of a phase transition.

There can be input [33, 49] and propagation losses [60, 61] in integrated photonic circuits. The losses can be Markovian and non-Markovian. A Markov

process can be thought of as a memoryless stochastic process, where the conditional probability distribution of future states depends only upon the present state, not on the sequence of events that forerun it. The developed waveguide platform can be further applied to optically simulate the effects of non-Markovian decay and quantum decoherence phenomena [91].

Non-Markovian process has dynamics, which is governed by memory effects. Many quantum systems exhibit non-Markovian behaviour with a flow of information from the environment back to the system [92–94]. Recently important steps towards the development of a general consistent theory of non-Markovian quantum dynamics have been made which try to rigorously define the border between Markovian and non-Markovian quantum evolution and to quantify memory effects in the open system dynamics [95, 96].

The research presented in the thesis is twofold: firstly, I have investigated the effect of losses on the generation and the propagation of the quantum parametric processes in the nonlinear waveguides. Secondly, I have researched the correspondences and the links between quantum and classical dynamics of optical frequency conversion in the glass nonlinear lossy waveguides. The establishment of quantum-classical analogies is an active research topic due to the cross-fertilization of ideas [97], with recent examples including simulated quantum walks of entangled photons [58] and development of classical characterization methods to predict quantum device performance [98, 99].

We anticipate that the proposed concept and achieved results will spark a broad interest. Our results may open a door to not only next-generation optical devices, offering unique advantages in ultrafast selective signal amplification and switching, but also they suggest possibilities for light control in plasmonic waveguides.

Chapter 2 is devoted to theoretical research on the process of spontaneous parametric down-conversion in quadratic nonlinear waveguide arrays in the presence of linear loss. We derive a set of discrete Schrödinger-type equations for the biphoton wavefunction and the wavefunction of one photon when the other photon in a pair is lost. We demonstrate effects arising from loss-affected interference between the generated photon pairs and show that nonlinear waveguide arrays can serve as a robust loss-tolerant integrated platform for the generation of entangled photon states with nonclassical spatial correlations.

Chapter 3 is devoted to the theoretical and experimental analysis of classical emulation of spontaneous parametric down conversion (SPDC) in a single nonlinear lossy waveguide. It is shown theoretically and proved experimentally the possibility to realize photon pair generation in semi-infinite array of weakly coupled single-mode optical waveguides similar to the photon pairs generated through SPDC in the single nonlinear waveguide.

Chapter 4 discuss the spatially inhomogeneous losses in waveguide arrays.

We show useful connection between spontaneous parametric down-conversion and sum frequency generation in the multimode system with arbitrary scattering loss. This result enables the characterization of the quantum performance of a nonlinear optical device based on classical measurements only. We analyse the behaviour of the SPDC and SFG on the base of the passive PT-symmetric coupler and compare the results. The chapter contain results which show the identical behavior of the SPDC and SFG in the low conversion regime.

Chapter 5 focuses on research of the process of parametric amplification in a directional coupler of quadratically nonlinear and lossy waveguides, which belongs to a class of optical systems with spatial parity-time (PT) symmetry. We identify a distinct spectral PT anti-symmetry associated with optical parametric interaction and establish a connection between the breaking of spectral and spatial mode symmetries, revealing the potential to implement unconventional regimes of spatial light switching through ultrafast control of PT breaking by pump pulses.

Chapter 6 is the last chapter where the conservative system is discussed in contrast to all cases researched before. We describe spontaneous parametric down-conversion of a single-photon pump in quadratic nonlinear waveguides and waveguide arrays, taking into account spectral broadening of the signal and idler photons. We perform a detailed analysis of the photon-pair intensities, spectral and spatial correlations for different types of phase-matching conditions and identify suppression of Rabi-like oscillations due to spectral dispersion. We also discuss distinct features of signal and idler photon correlations related to the single-photon nature of the pump.

Chapter 2

Photon pair generation in quadratic waveguide arrays with loss

Optical quantum communications and computation schemes rely on controlled preparation of well-defined photonic states [100, 101]. Spontaneous parametric down-conversion (SPDC) in nonlinear crystals [7, 63, 102] has become a source for experimental generation of correlated and entangled photon pairs with demonstrations of such effects as quantum teleportation [10, 13, 103, 104], quantum cryptography [105], Bell-inequality violations [106] and quantum imaging [107].

The mode confinement in a waveguide enables a significant increase of the SPDC source brightness in comparison to bulk crystal setups [108]. Even more importantly, waveguide integration provides interferometric stability, which is essential for quantum simulations and cryptography. SPDC in nonlinear waveguides can be implemented to produce photon pairs in distinct spatial modes [45, 109–112]. Overall, nonlinear waveguides can serve as photon-pair sources ideally suited for applications in quantum communications [113].

Overall integrated optical quantum circuits utilising coupled waveguides are increasingly gaining attention as a possible solution for scalable quantum technologies with important applications to quantum simulations. A key mechanism for quantum simulations can be provided by the process of quantum walks in an optical waveguide array (WGA) [51], with applications to boson sampling [52–55]. Furthermore, it was recently suggested [56–59] that a nonlinear waveguide array can be used for both photon-pair generation through spontaneous parametric down-conversion and quantum walks of the generated biphotons with strong spatial entanglement between the waveguides. Importantly, such an integrated scheme avoids input losses, since in an integrated nonlinear waveguide array photon pairs are generated inside the quantum walk circuit. Internal losses in the waveguides however may still be present. In this chapter, we research an important question of the tolerance of the biphoton generation to possible losses in the

waveguides.

This Chapter is devoted to the theoretical analysis of the process of spontaneous parametric down-conversion in quadratic nonlinear waveguide arrays in the presence of linear loss. We derive a set of discrete Schrodinger-type equations for the biphoton wave function and the wave function of one photon when the other photon in a pair is lost. It is demonstrated the effects arising from loss-affected interference between the generated photon pairs and show that nonlinear waveguide arrays can serve as a robust loss-tolerant integrated platform for the generation of entangled photon states with nonclassical spatial correlations.

2.1 Spontaneous parametric down conversion in a single waveguide

The process of SPDC can occur in a $\chi^{(2)}$ nonlinear waveguide pumped by a pump laser, where a pump photon at frequency ω_p can be spontaneously split into signal and idler photons with corresponding frequencies ω_s and ω_i, such that $\omega_p = \omega_s + \omega_i$. The effect of linear losses on SPDC was previously considered in various contexts [62–64]. Here, we perform a detailed analysis of the emerging photon intensities and correlations, in the regime of photon-pair generation. We analyze the photon-pair generation while neglecting multi-photon-pair processes for the appropriately attenuated pump power. Due to losses, one or both photons from a pair can be lost. Nevertheless, the two-photon state can be distinguished from the single-photon or vacuum state by performing correlation measurements with two single-photon detectors, as schematically illustrated in Fig. 2.1.

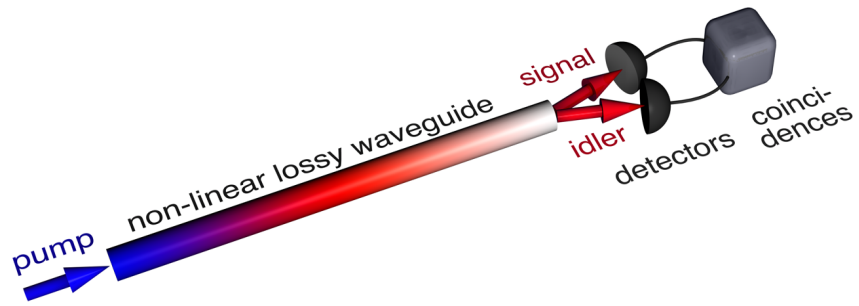

Figure 2.1: Scheme of photon-pair generation through SPDC in a nonlinear waveguide with loss; the photon states are defined by frequency-dependent phase mismatch and losses.

To describe waveguide losses, it is possible to introduce them through series of virtual asymmetric beam-splitters in an otherwise conservative medium [62, 114], see Fig. 2.2. At each step during propagation from z to $z + \Delta z$ the photon pairs can be generated through SPDC. On the other hand there is a probability for signal and idler photons to be reflected by beam-splitters, corresponding to the loss

of photons from the waveguide. Then, according to the general principles [115], the photon dynamics is governed by a sum of Hamiltonians which individually describe SPDC in lossless nonlinear medium ($\hat{H}_{nl}$) and linear losses due to virtual beam-splitters ($\hat{H}_{bs}$),

$$\hat{H} = \hat{H}_{nl} + \hat{H}_{bs}. \tag{2.1}$$

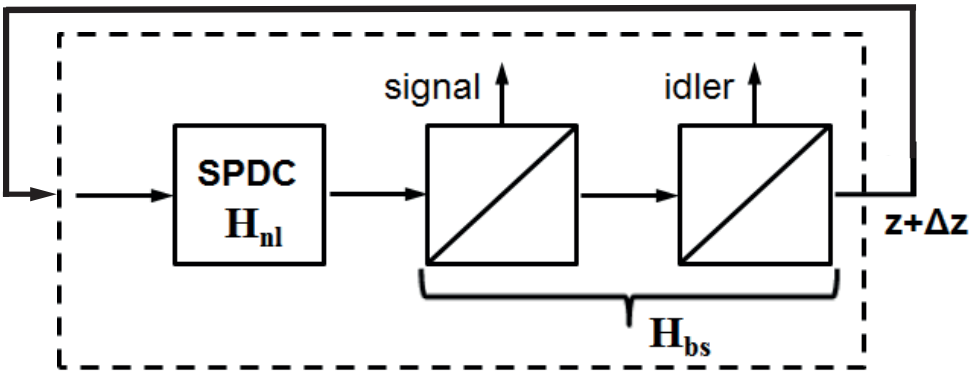

Figure 2.2: Scheme of the Hamiltonian describing the photon-pair propagation involving SPDC and losses in a single waveguide. Losses are represented by beam splitters [62, 114].

The SPDC process in the absence of losses, in the undepleted classical pump approximation, is governed by a Hamiltonian [7]:

$$\begin{aligned}\hat{H}_{nl}(z) &= \int d\omega_s \beta_s^{(0)}(\omega_s) a_s^\dagger(\omega_s) a_s(\omega_s) \\ &+ \int d\omega_i \beta_i^{(0)}(\omega_i) a_i^\dagger(\omega_i) a_i(\omega_i) \\ &+ \int d\omega_s \int d\omega_i \Big[E_p(z, \omega_s + \omega_i) a_s^\dagger(\omega_s) a_i^\dagger(\omega_i) \\ &\qquad + E_p^*(z, \omega_s + \omega_i) a_s(\omega_s) a_i(\omega_i) \Big] ,\end{aligned} \tag{2.2}$$

where $a_{s,i}^\dagger$ and $a_{s,i}$ are the creation and annihilation operators for the signal and idler photons with the commutators $[a_s(\omega_1), a_s^\dagger(\omega_2)] = \delta(\omega_1 - \omega_2)$ and $[a_i(\omega_1), a_i^\dagger(\omega_2)] = \delta(\omega_1 - \omega_2)$, $\delta(z)$ is a Dirac delta-function, $\beta_{s,i}^{(0)}$ are the signal and idler propagation constants relative to the pump. $E_p(z, \omega_p)$ is proportional to the pump amplitude A at frequency ω_p and to the quadratic nonlinearity χ; we also account for a possible pump absorption with the loss coefficient γ_p:

$$E_p(z, \omega_p) = \chi(z) A \exp(-\gamma_p z). \tag{2.3}$$

Throughout the paper we assume weak pump regime, which means that we focus

on the generation of a single photon pair and consider multi-photon-pair processes to be negligible for the appropriately attenuated pump power. For simplicity and to avoid working with very small numbers we renormalize $A \ll 1$ to $A = 1$, and also consider constant nonlinear coefficient renormalized to unity, $\chi(z) = 1$. Such renormalization rescales all results accordingly and does not affect photon-pair dynamics or any considered relations.

We now analyze the effect of Markovian losses under the conditions of negligible thermal fluctuations. Then, the losses can be described by introducing a series of beam-splitters [62, 114, 116], and the corresponding Hamiltonian can be written as follows:

$$\begin{aligned} \hat{H}_{bs}(z) &= \int d\omega_s \sqrt{2\gamma_s(\omega_s)} \left[a_s(\omega_s) b_s^\dagger(z,\omega_s) + a_s^\dagger(\omega_s) b_s(z,\omega_s) \right] \\ &+ \int d\omega_i \sqrt{2\gamma_i(\omega_i)} \left[a_i(\omega_i) b_i^\dagger(z,\omega_i) + a_i^\dagger(\omega_i) b_i(z,\omega_i) \right], \end{aligned} \tag{2.4}$$

where the operators $b_{s,i}^\dagger(z,\omega)$ describe creation of photons which are lost from a waveguide after a beam-splitter at coordinate z, with the commutators $[b_s(z_1,\omega_1), b_s^\dagger(z_2,\omega_2)] = \delta(z_1 - z_2)\delta(\omega_1 - \omega_2)$ and $[b_i(z_1,\omega_1), b_i^\dagger(z_2,\omega_2)] = \delta(z_1 - z_2)\delta(\omega_1 - \omega_2)$, and $\gamma_{s,i}$ are the linear loss coefficients.

Such interpretation of losses as an interaction with a reservoir is a standard approach and has been used for example to describe losses in plasmonic waveguides [117]. This rigorous formalism provides a clear interpretation of results for our analysis, with separation of two-photon and one-photon states. As we discuss below, the results obtained using this method are consistent with the asymptotic analysis of the case of strong idler absorption in Ref. [63], and can also be used to calculate the corresponding density matrices.

Since we consider a weak pump regime, the generation of photon pairs with different frequencies occurs independently, due to the absence of cascading processes. We will therefore omit $\omega_{s,i,p}$ in the following to simplify the notations. We will also analyze the properties of the generated photons in a narrow frequency band, assuming corresponding filtering around particular signal and idler frequencies, such that the model coefficients can be considered constant in the vicinity of the chosen frequencies.

We seek the solution for a two-photon state at distance z as:

$$\begin{aligned} |\Psi(z)\rangle &= \Phi(z) a_s^\dagger a_i^\dagger |0\rangle + \int_0^z dz_l \tilde{\Phi}^{(s)}(z,z_l) a_s^\dagger b_i^\dagger(z_l)|0\rangle \\ &+ \int_0^z dz_l \tilde{\Phi}^{(i)}(z,z_l) b_s^\dagger(z_l) a_i^\dagger |0\rangle \\ &+ \int_0^z dz_{l_s} \int_0^z dz_{l_i} \tilde{\Phi}^{(si)}(z_{l_s}, z_{l_i}) b_s^\dagger(z_{l_s}) b_i^\dagger(z_{l_i})|0\rangle, \end{aligned} \tag{2.5}$$

where $|0\rangle$ denotes a vacuum state with zero number of signal and idler photons. First term corresponds to biphoton state without losses, while the next two terms correspond to the states with the lost signal or idler photons, respectively. The loss happens at an arbitrary position z_l. The last term is the term with both signal and idler photons being lost. We trace the terms with losses over the propagation distance to take into account the probabilistic nature of the process.

The equation for the evolution of the state vector is $d\Psi(z)/dz \simeq -i\hat{H}(z)[|0\rangle + |\Psi(z)\rangle]$, where we neglect vacuum state perturbation due to the generation of a single photon pair, in which we substitute Eq. (2.5) for the Hamiltonian provided by the Eqs. (2.2),(2.4). After performing the calculations (see Appendix A for details), we obtain the following equations for the non-unitary evolution of biphoton wave functions:

$$\Phi(0) = 0,$$

$$\frac{\partial\Phi(z)}{\partial z} = -(i\Delta\beta^{(0)} + \gamma_s + \gamma_i)\Phi(z) + Ae^{-\gamma_p z}, \tag{2.6}$$

$$\frac{\partial\tilde{\Phi}^{(s)}(z,z_l)}{\partial z} = -(i\beta_s^{(0)} + \gamma_s)\tilde{\Phi}^{(s)}(z,z_l),\ z \geq z_l, \tag{2.7}$$

$$\frac{\partial\tilde{\Phi}^{(i)}(z,z_l)}{\partial z} = -(i\beta_i^{(0)} + \gamma_i)\tilde{\Phi}^{(i)}(z,z_l),\ z \geq z_l, \tag{2.8}$$

$$\tilde{\Phi}^{(s)}(z_l,z_l) = -i\sqrt{2\gamma_i}\Phi(z_l),\ \tilde{\Phi}^{(i)}(z_l,z_l) = -i\sqrt{2\gamma_s}\Phi(z_l), \tag{2.9}$$

where $\Delta\beta^{(0)} = \beta_s^{(0)} + \beta_i^{(0)}$, and we consider the pump in the form of Eq. (2.3). We disregard the evolution of $\tilde{\Phi}^{(si)}$ wavefunction, since it corresponds to the case when both photons are lost. We also neglect the generation of more than two photons, as discussed above.

Equation (2.6) can be solved analytically:

$$\Phi(z) = zA\mathrm{sinc}\left\{\frac{z}{2}\left[\Delta\beta^{(0)} - i(\gamma_s + \gamma_i - \gamma_p)\right]\right\} \times$$
$$\exp\left\{-\frac{iz}{2}\left[\Delta\beta^{(0)} - i(\gamma_s + \gamma_i + \gamma_p)\right]\right\}. \tag{2.10}$$

We now calculate the normalized intensity of photons generated through SPDC, which is proportional to an average number of photons per unit time. The expressions for the signal and idler photons are analogous, and to be specific we consider the signal mode. We now calculate the total signal intensity $I_s(z)$ by

tracing over all possible idler photon states, and find that:

$$I_s(z) = I_s^{(0)}(z) + \tilde{I}_s(z),\ I_s^{(0)}(z) = |\Phi(z)|^2,\ \tilde{I}_s(z) = \int_0^z dz_l \left|\tilde{\Phi}^{(s)}(z, z_l)\right|^2, \quad (2.11)$$

where $I_s^{(0)}(z)$ is the contribution when both photons are not absorbed and $\tilde{I}_s(z)$ is a contribution from the states with lost idler photons. Note that the sum of modules appears in the in the expression for $\tilde{I}_s(z)$, since one signal photon remains in a mixed state when idler is lost [64, 118]. By performing differentiation d/dz and using Eq. (2.7), we derive a balance equation for the intensity of the states with lost idler photons:

$$\frac{d\tilde{I}_s(z)}{dz} = 2\gamma_i I_s^{(0)}(z) - 2\gamma_s \tilde{I}_s(z). \quad (2.12)$$

Here the first term corresponds to the creation of the state with the lost idler photon while the second one shows the loss probability of the remaining unpaired signal photon. The intensity contributions can be calculated analytically:

$$I_s^{(0)} = \frac{2A^2 e^{-(\gamma_s+\gamma_i+\gamma_p)z}\ \left\{\cosh\left[(\gamma_s+\gamma_i-\gamma_p)z\right] - \cos\left(\Delta\beta^{(0)}z\right)\right\}}{\left(\Delta\beta^{(0)}\right)^2 + (\gamma_s+\gamma_i-\gamma_p)^2}, \quad (2.13)$$

$$\tilde{I}_s = \frac{4A^2\gamma_i e^{-2\gamma_s z}}{(\Delta\beta^{(0)})^2 + (\gamma_s+\gamma_i-\gamma_p)^2}\Big\{G\left[z, i(\gamma_s+\gamma_i-\gamma_p)\right] - G(z, \Delta\beta^{(0)})\Big\}, \quad (2.14)$$

where

$$\begin{aligned} G(z,p) &= \int_0^L \cos(\xi p) e^{-\xi(\gamma_i+\gamma_p-\gamma_s)} d\xi \\ &= \frac{\gamma_i+\gamma_p-\gamma_s+e^{-z(\gamma_i+\gamma_p-\gamma_s)}\Big[p\sin(zp) - \cos(zp)(\gamma_i+\gamma_p-\gamma_s)\Big]}{p^2+(\gamma_i+\gamma_p-\gamma_s)^2}. \end{aligned} \quad (2.15)$$

The total intensity can be measured by a sensitive camera, which will provide an overall number of detected photons per unit time. The intensity contributions can be separated using a scheme with single-photon detectors: $I_s^{(0)}$ will be proportional to the number of coincidence counts of signal and idler photons, and $\tilde{I}_s$ will be proportional to the signal counts without the corresponding idler photon.

It is instructive to consider a number of limiting cases. In particular, zero pump loss ($\gamma_p = 0$) can be achieved in various conventional waveguides, where losses at pump frequency can be significantly smaller than losses at signal and idler frequencies due to the difference in the fundamental mode cross-section sizes for different wavelengths. In this case both components of signal intensity $I_s^{(0)}(z)$

and $\tilde{I}_s(z)$ approach stationary values for large distances:

$$\begin{aligned} \lim_{z\to\infty}[I_s^{(0)}(z)] &= \lim_{z\to\infty}[\tilde{I}_s(z)]\gamma_s\gamma_i^{-1} \\ &= \frac{A^2}{(\Delta\beta^{(0)})^2+(\gamma_s+\gamma_i)^2}, \end{aligned} \tag{2.16}$$

We see that if there is no idler loss ($\gamma_i = 0$), then $\tilde{I}_s(z) \to 0$, which means that all signal photons are paired with an idler photon, as expected. If the signal and idler exhibit the same loss ($\gamma_s = \gamma_i$), then half of signal photons remains paired. This result is in the agreement with the Eq. (2.12).

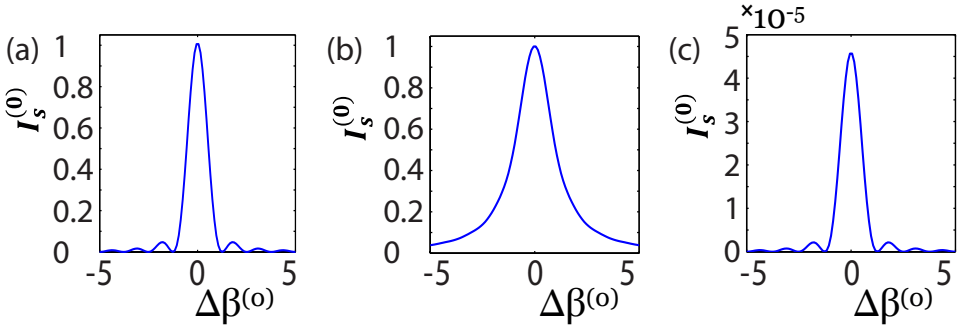

Figure 2.3: Normalized number of photon pairs, $I_s^{(0)}$, generated through SPDC in a single waveguide vs. the phase mismatch $\Delta\beta^{(0)}$ for $z = 5$, $A = 1$ and different losses: (a) $\gamma_p = \gamma_s = \gamma_i = 0$, (b) $\gamma_p = 0$, $\gamma_s = \gamma_i = 0.5$, (c) $\gamma_s = \gamma_i = 0.5$, $\gamma_p = \gamma_s + \gamma_i = 1$.

For degenerate SPDC regime with indistinguishable signal and idler photons ($\gamma_s = \gamma_i = \gamma$) and no pump losses ($\gamma_p = 0$), we have:

$$I_s^{(0)}(z) = \frac{2A^2e^{-2z\gamma}\left[\cosh(2z\gamma)-\cos(z\Delta\beta^{(0)})\right]}{(\Delta\beta^{(0)})^2+4\gamma^2}, \tag{2.17}$$

$$\tilde{I}_s(z) = \frac{2A^2e^{-2z\gamma}\left[\sinh(2z\gamma)-2z\gamma\,\mathrm{sinc}(z\Delta\beta^{(0)})\right]}{(\Delta\beta^{(0)})^2+4\gamma^2}. \tag{2.18}$$

In the case of strongly non-degenerate SPDC, when signal and idler photons are generated with significantly different frequencies, pump and signal losses may become negligible $\gamma_p = \gamma_s = 0$, while idler absorption may be substantial [63]. In this case the biphoton-related component of the signal intensity for long propagation distances is:

$$\lim_{z\to\infty}[I_s^{(0)}(z)] = \frac{2A_{s,i}\gamma_i}{(\Delta\beta^{(0)})^2+\gamma_i^2}. \tag{2.19}$$

We check that Eq. (2.19) agrees with the result derived in Ref. [63] through the application of fluctuation-dissipation theorem.

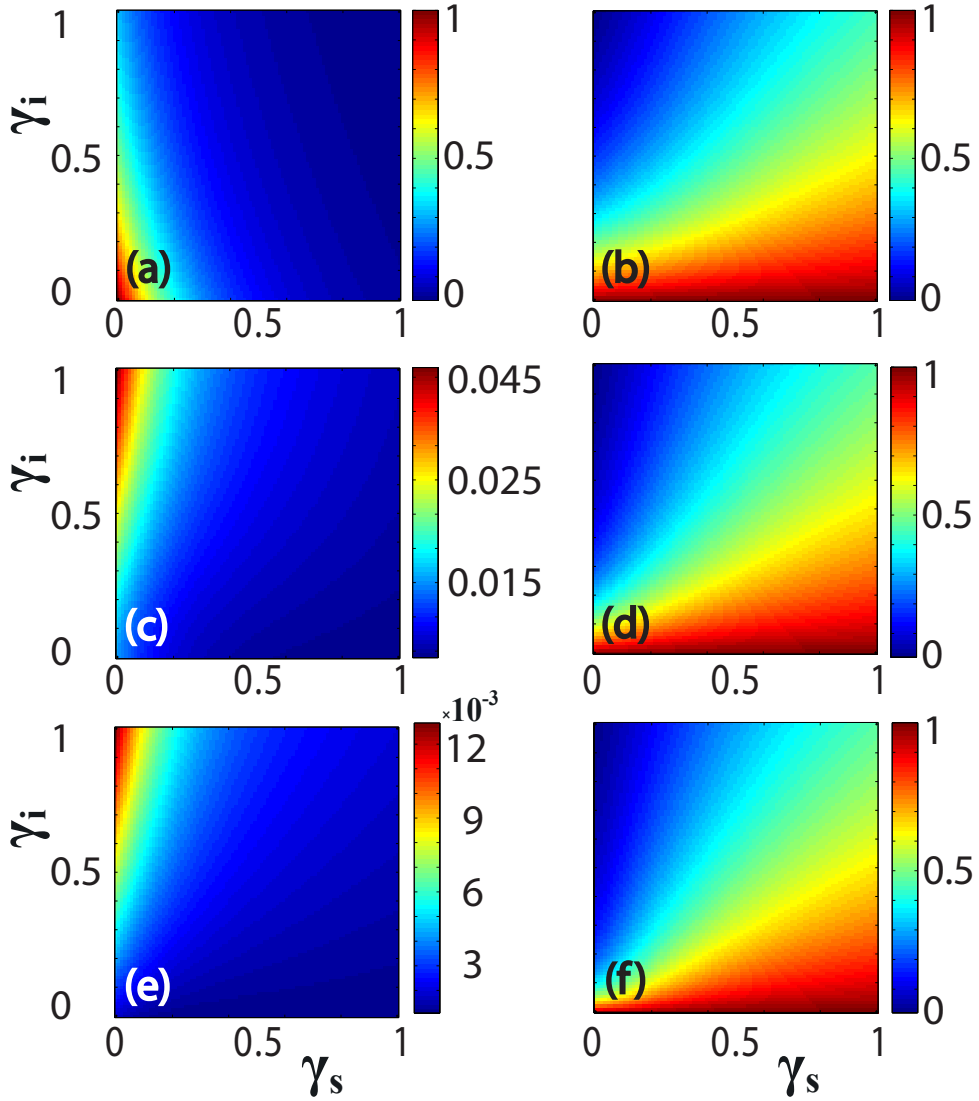

Figure 2.4: (a,c,e) Total signal intensity $I_s(z)$ and (b,d,f) ratio of intensity contribution when both photons are not absorbed and the full intensity $I_s^{(0)}(z)/I_s(z)$ vs. the signal and idler losses in a single waveguide for different values of phase mismatch (a,b) $\Delta\beta^{(0)} = 0$, (c,d) $\Delta\beta^{(0)} = 3$, (e,f) $\Delta\beta^{(0)} = 6$. Parameters are $\gamma_p = 0$, $z = 5$, $A = 1$.

It is interesting to analyze the dependence of the biphoton-related component of the signal intensity $I_s^{(0)}$ on the phase mismatch $\Delta\beta^{(0)}$. The losses are distributed inside the nonlinear region, that is why they affect SPDC [119, 120]. When losses are absent ($\gamma_p = \gamma_s = \gamma_i = 0$), it has a well-known [63] shape of

sinc-function [Fig. 2.3(a)]:

$$I_s^{(0)}(z) = A^2 L^2 \mathrm{sinc}^2\left(\frac{\Delta\beta^{(0)} z}{2}\right). \tag{2.20}$$

For negligible pump losses ($\gamma_p = 0$) and large signal or idler losses $\{\exp[-(\gamma_s+\gamma_i)z] \ll 1\}$ the dependence is transformed into a Lorenzian shape [Fig. 2.3(b)] according to Eq. (2.16).

Interestingly, when pump losses are increased to match the combined idler and signal losses ($\gamma_p = \gamma_s + \gamma_i$) the spectrum returns to a sinc shape [Fig. 2.3(c)]:

$$I_s^{(0)}(z) = A^2 z^2 e^{-2(\gamma_s+\gamma_i)z} \mathrm{sinc}^2\left(\frac{\Delta\beta^{(0)} z}{2}\right). \tag{2.21}$$

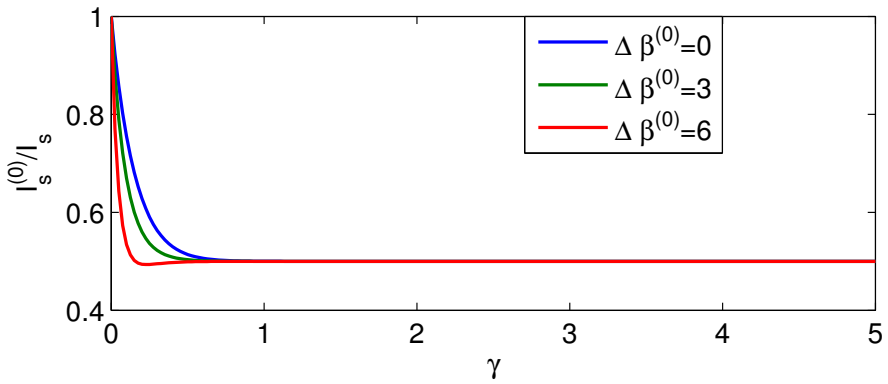

Figure 2.5: Ratio of intensity contribution when both photons are not absorbed and the full intensity $I_s^{(0)}(z)/I_s(z)$ vs. the signal and idler loss γ ($\gamma_s = \gamma_i = \gamma$, $\gamma_p = 0$) in a single waveguide. Parameters are $A = 1$, $z = 5$, and $\Delta\beta^{(0)} = \{0, 3, 6\}$ as indicated by labels.

Next we present a detailed investigation of the signal mode intensity depending on the loss (Figs. 2.4 and 2.5) and propagation distance (Fig. 2.6) in the absence of pump loss $\gamma_p = 0$. We normalized all our graphs to the maximum value of the displayed variable to make sure that everything is normalized to 1. Figures 2.4 (a,c,e) show that the signal intensity I_s is decreasing with the increase of signal loss, however the dependence on the idler loss in relation to the phase mismatch $\Delta\beta^{(0)}$ is nontrivial due to additional signal intensity component $\tilde{I}_s$ related to the disruption of interference when the idler photon is lost. The ratio between the pure biphoton and the full signal intensity, $I_s^{(0)}/I_s$, depends weakly on the phase mismatch, see Figs. 2.4 (b,d,f). Indeed, Fig. 2.5 demonstrates that regardless of the phase mismatch $\Delta\beta^{(0)}$ the proportion of signal photons paired with idler to all signal photons, $I_s^{(0)}/I_s$, becomes independent on the loss above

certain loss threshold. Moreover, for the long distances $I_s^{(0)}/I_s$ ratio became constant as the independent of the losses the number of the lost photons became equal to the number of the paired photons according to the Eq. (2.16) and (2.12).

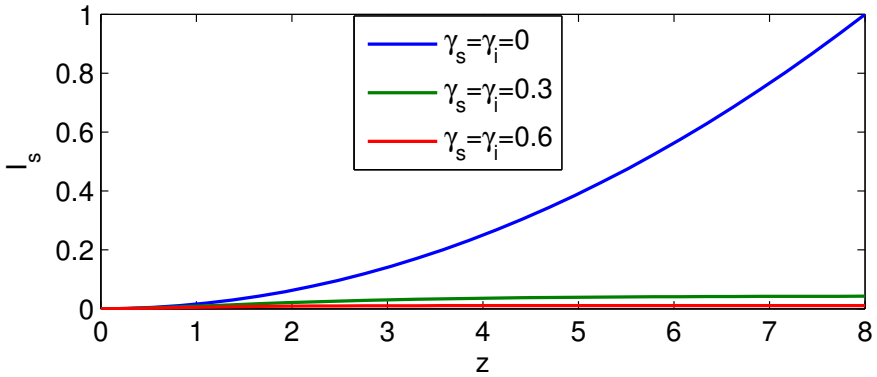

Figure 2.6: Total signal mode intensity I_s vs. the propagation distance in a single waveguide for different signal and idler losses $\gamma_s = \gamma_i = \gamma = \{0, 0.3, 0.6\}$. Parameters are $A = 1$, $\Delta\beta^{(0)} = 0$, $\gamma_p = 0$.

Figure 2.6 shows the behavior of the total signal intensity vs. the propagation distance for different losses in the regime of phase-matching. Total signal intensity exhibits fast growth in the absence of losses. However when moderate of high losses are present, the total signal intensity I_s approaches a fixed value at large distances, see Eq. (2.16).

2.2 Spatial entanglement in waveguide array

It was shown that nonlinear WGAs can serve as a reconfigurable on-chip source of spatially entangled photon pairs [56–59]. Since internal generation of photon pairs in nonlinear waveguide arrays solves the problem of input losses, it is important to understand the effect of internal losses on photon-pair propagation and resulting entanglement and correlations.

For the theoretical analysis, we combine the one-waveguide Hamiltonians introduced in the previous section, and the linear coupling between the waveguides through the Hamiltonian $\hat{H}_c$. If the waveguide parameters are identical across

the whole array, then the Hamiltonian is:

$$\begin{aligned}
\hat{H}(z) &= \hat{H}_{nl}(z) + \hat{H}_{bs}(z) + \hat{H}_{c}(z), && (2.22)\\
\hat{H}_{nl}(z) &= \sum_{n_s} \beta_s^{(0)} a_s^\dagger(n_s) a_s(n_s) + \sum_{n_i} \beta_i^{(0)} a_i^\dagger(n_i) a_i(n_i) && (2.23)\\
&+ \sum_{n_p} \left[E_p(z, n_p) a_s^\dagger(n_p) a_i^\dagger(n_p) + E_p^*(z, n_p) a_s(n_p) a_i(n_p) \right],\\
\hat{H}_{bs}(z) &= \sum_{n_s} \sqrt{2\gamma_s} \left[a_s(n_s) b_s^\dagger(z, n_s) + a_s^\dagger(n_s) b_s(z, n_s) \right] && (2.24)\\
&+ \sum_{n_i} \sqrt{2\gamma_i} \left[a_i(n_i) b_i^\dagger(z, n_i) + a_i^\dagger(n_i) b_i(z, n_i) \right],\\
\hat{H}_{c}(z) &= \sum_{n_s} C_s \left[a_s(n_s) a_s^\dagger(n_s + 1) + a_s^\dagger(n_s) a_s(n_s + 1) \right] && (2.25)\\
&+ \sum_{n_i} C_i \left[a_i(n_s) a_i^\dagger(n_i + 1) + a_i^\dagger(n_i) a_i(n_i + 1) \right]. && (2.26)
\end{aligned}$$

Here n_s and n_i are the waveguide numbers for the signal and idler photons, $a_{s,i}^\dagger(n)$ and $a_{s,i}(n)$ are the creation and annihilation operators for the signal and idler photons in a waveguide number n, $b_{s,i}^\dagger(z, n)$ describe creation of photons which are lost from a waveguide number n at a coordinate z, $C_{s,i}$ are the coupling constants between the neighboring waveguides, $E_p(z, n_p)$ is proportional to pump amplitude in waveguide n_p. Then, we seek a solution for a biphoton state as:

$$\begin{aligned}
|\Psi(z)\rangle &= \sum_{n_s} \sum_{n_i} \Phi_{n_s,n_i}(z) a_s^\dagger(n_s) a_i^\dagger(n_i) |0\rangle\\
&+ \sum_{n_s} \sum_{n_i} \int_0^z dz_l \tilde{\Phi}_{n_s,n_i}^{(s)}(z, z_l) a_s^\dagger(n_s) b_i^\dagger(z_l, n_i) |0\rangle\\
&+ \sum_{n_s} \sum_{n_i} \int_0^z dz_l \tilde{\Phi}_{n_s,n_i}^{(i)}(z, z_l) b_s^\dagger(z_l, n_s) a_i^\dagger(n_i) |0\rangle \qquad (2.27)\\
&+ \sum_{n_s} \sum_{n_i} \int_0^z dz_{l_s} \int_0^z dz_{l_i} \tilde{\Phi}_{n_s,n_i}^{(si)}(z_{l_s}, z_{l_i}) b_s^\dagger(z_{l_s}, n_s) b_i^\dagger(z_{l_i}, n_i) |0\rangle.
\end{aligned}$$

The resulting set of equations for the evolution of the biphoton wave functions

is:

$$\Phi_{n_s,n_i}(z=0)=0,$$
$$\frac{\partial\Phi_{n_s,n_i}(z)}{\partial z}=-i\Delta\beta^{(0)}\Phi_{n_s,n_i}-(\gamma_s+\gamma_i)\Phi_{n_s,n_i}+A_{n_s}\delta_{n_s,n_i}e^{-\gamma_p z}$$
$$-iC_s(\Phi_{n_s-1,n_i}+\Phi_{n_s+1,n_i})-iC_i(\Phi_{n_s,n_i-1}+\Phi_{n_s,n_i+1}), \tag{2.28}$$
$$\frac{\partial\tilde{\Phi}^{(s)}_{n_s,n_i}(z,z_l)}{\partial z}=-(i\beta_s^{(0)}+\gamma_s)\tilde{\Phi}^{(s)}_{n_s,n_i}-iC_s(\tilde{\Phi}^{(s)}_{n_s-1,n_i}+\tilde{\Phi}^{(s)}_{n_s+1,n_i}),\ z\geq z_l, \tag{2.29}$$
$$\frac{\partial\tilde{\Phi}^{(i)}_{n_s,n_i}(z,z_l)}{\partial z}=-(i\beta_i^{(0)}+\gamma_i)\tilde{\Phi}^{(i)}_{n_s,n_i}-iC_i(\tilde{\Phi}^{(i)}_{n_s,n_i-1}+\tilde{\Phi}^{(i)}_{n_s,n_i+1}),\ z\geq z_l, \tag{2.30}$$
$$\tilde{\Phi}^{(s)}_{n_s,n_i}(z_l,z_l)=-i\sqrt{2\gamma_i}\Phi_{n_s,n_i}(z_l),\ \tilde{\Phi}^{(i)}_{n_s,n_i}(z_l,z_l)=-i\sqrt{2\gamma_s}\Phi_{n_s,n_i}(z_l), \tag{2.31}$$

where we do not consider the evolution of $\tilde{\Phi}^{(si)}$ wavefunction corresponding to both lost photons. The real-space representation can be Fourier-transformed into spatial k-space [58]:

$$\Phi_{k_s,k_i}=\sum_{n_s,n_i}\Phi_{n_s,n_i}e^{in_sk_s}e^{in_ik_i}. \tag{2.32}$$

Then the biphoton propagation equations in k-space can be written as follows:

$$\Phi_{k_s,k_i}(z=0)=0,$$
$$\frac{\partial\Phi_{k_s,k_i}(z)}{\partial z}=-(i\Delta\beta+\gamma_s+\gamma_i)\Phi_{k_s,k_i}+A_{k_s}\delta_{k_s,k_i}e^{-\gamma_p z}, \tag{2.33}$$
$$\frac{\partial\tilde{\Phi}^{(s)}_{n_s,n_i}(z,z_l)}{\partial z}=-(i\beta_s+\gamma_s)\tilde{\Phi}^{(s)}_{n_s,n_i},\ \frac{\partial\tilde{\Phi}^{(i)}_{n_s,n_i}(z,z_l)}{\partial z}=-(i\beta_i+\gamma_i)\tilde{\Phi}^{(s)}_{n_s,n_i}, \tag{2.34}$$
$$\tilde{\Phi}^{(s)}_{k_s,k_i}(z_l,z_l)=-i\sqrt{2\gamma_i}\Phi_{k_s,k_i}(z_l),\ \tilde{\Phi}^{(i)}_{k_s,k_i}(z_l,z_l)=-i\sqrt{2\gamma_s}\Phi_{k_s,k_i}(z_l), \tag{2.35}$$

where $\beta_s=\beta_s^{(0)}+2C_s\cos(k_s)$, $\beta_i=\beta_i^{(0)}+2C_i\cos(k_i)$, and $\Delta\beta=\beta_s+\beta_i$. These equations have the same form as Eqs. (2.6)-(2.9) for a single waveguide. Accordingly, a solution for the wave function Φ_{k_s,k_i} can be formulated analogous to Eq. (2.10).

Finally, the real-space wave functions can be calculated by applying the inverse Fourier transform:

$$\Phi_{n_s,n_i}=\frac{1}{(2\pi)^2}\int_{-\pi}^{\pi}\int_{-\pi}^{\pi}\mathrm{d}k_s\mathrm{d}k_i\Phi_{k_s,k_i}e^{-ik_sn_s}e^{-ik_in_i}, \tag{2.36}$$

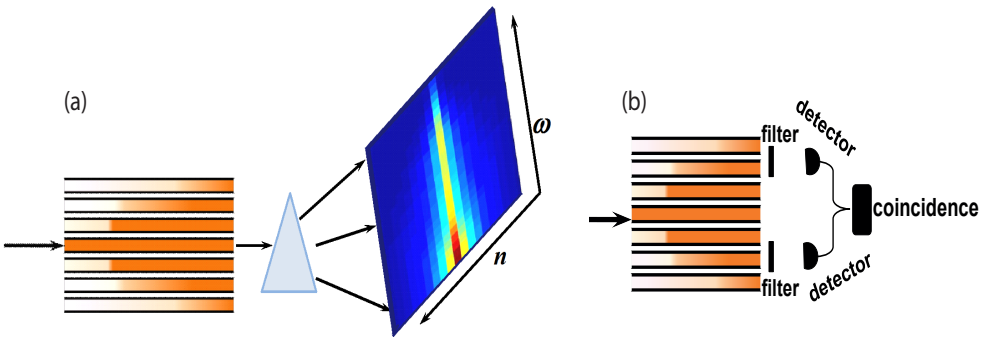

Figure 2.7: Scheme of the experimental setup designed to measure spectral and spatial distribution of the nonlinear WGA output photon-pair intensity. The pump beam generates photon pairs that suffer losses and couple to the neighboring waveguides. (a) The output intensity distribution can be characterised using a prism and a camera. Spectral filtering can be used to choose only a signal channel to measure the signal intensity I_s. (b) The photon-pair correlations can be characterised by measuring the coincidences from the two single photon detectors.

The dependence of the intensity for the signal mode on the propagation distance can be written in the following form for k-space:

$$I_s(k_s,z) = I_s^{(0)}(k_s,z) + \tilde{I}_s(k_s,z), \tag{2.37}$$

$$I_s^{(0)}(k_s,z) = \int_{-\pi}^{\pi} \mathrm{d}k_i |\Phi_{k_s,k_i}(z)|^2, \tag{2.38}$$

$$\tilde{I}_s(k_s,z) = \int_0^z \mathrm{d}z_l \int_{-\pi}^{\pi} \mathrm{d}k_i \left| \tilde{\Phi}^{(s)}_{k_s,k_i}(z,z_l) \right|^2, \tag{2.39}$$

and analogously for real space:

$$I_{n_s}(z) = I_s^{(0)}(n_s,z) + \tilde{I}_s(n_s,z), \tag{2.40}$$

$$I_s^{(0)}(n_s,z) = \sum_{n_i} |\Phi_{n_s,n_i}(z)|^2, \tag{2.41}$$

$$\tilde{I}_s(n_s,z) = \int_0^z \mathrm{d}z_l \sum_{n_i} \left| \tilde{\Phi}^{(s)}_{n_s,n_i}(z,z_l) \right|^2.$$

Here $I_s^{(0)}(n_s,z)$ is the contribution when both photons are not absorbed, and $\tilde{I}_s(n_s,z)$ is a contribution from the states with lost idler photons.

We analysed the properties of the generated photons in a narrow frequency

band while in experiment a broad band of frequencies is generated. Thus, in experiments one could use spectral filters or spatially resolving spectrometer [Fig. 2.7(a)], which allows one to measure the signal and idler intensity outputs from different waveguides at various frequencies. Additionally, a coincidence scheme at the WGA output [Fig. 2.7(b)] can be used to measure biphoton spatial correlations [51, 56], which normalized value is:

$$\Gamma_{n_s,n_i}(z) = |\Phi_{n_s,n_i}(z)|^2. \tag{2.42}$$

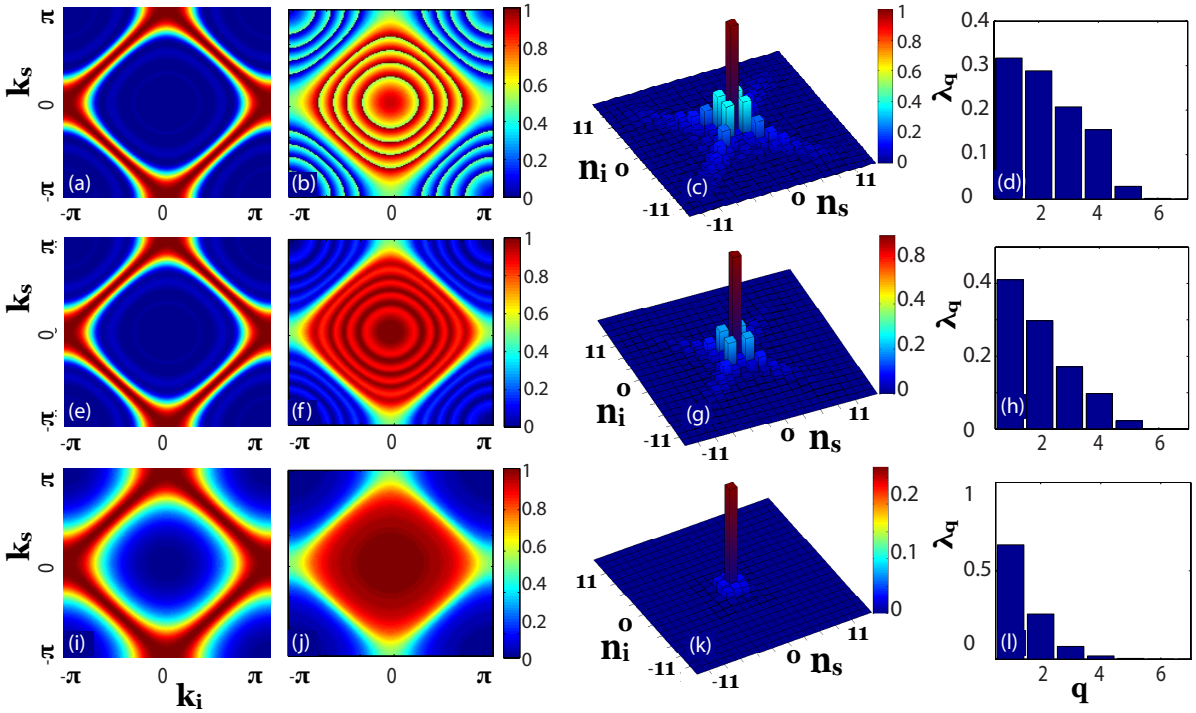

Figure 2.8: Photon-pair correlations in (a,e,i) k-space; (b,f,j) phase of photon-pair correlations in k-space; (c,g,k) real space correlations and (d,h,l) Schmidt decomposition depending on the mode number for different signal and idler loss, $\gamma_s = \gamma_i = \gamma/2$: (a,b,c,d) $\gamma = 0$, (e,f,g,h) $\gamma = 0.2$, (i,j,k,l) $\gamma = 0.6$. The pump is coupled to the central waveguide, $A(0) = 0$. Parameters are $z = 5$, $C_s = C_i = 1$, $\gamma_p = 0$, $\Delta\beta^{(0)} = 0$.

We present the plots of photon-pair correlations in k-space and real space for different values of losses in Fig. 2.8, considering the pump beam coupled to a single waveguide. In k-space [Fig. 2.8(a,e,i)] at different loss values the correlation profiles have a square shape corresponding to angular phase-matching in waveguide arrays [56, 59], however the square edges become broader for higher losses. The pase of photon-pair correlations in k-space [Fig. 2.8(b,f,j)] shows the less pronounced fringes with the increase of the losses, which contributes to

the change of spatial entanglement.. The real-space correlations in the absence of loss have a characteristic cross shape corresponding to the simultaneous bunching and anti-bunching [Fig. 2.8(c)], which is a signature of non-classicality [51, 56]. Importantly, these non-classical features are preserved even in presence of moderate loss [Fig. 2.8(g)]. Under strong loss, photons are only present in the central waveguide [Fig. 2.8(k)], as photons are absorbed before they can couple to the neighboring waveguides, and accordingly the non-classical spatial correlations are absent.

To exploit two photons as quantum resources it is necessary to know if they are entangled. This question can be answered by studying the Schmidt decomposition [121] of a biphoton wave function as follows:

$$\Phi_{k_s,k_i} = \sum_q \sqrt{\lambda_q}\phi_q(k_s)\varphi_q(k_i), \tag{2.43}$$

where λ_q are Schmidt coefficients ($\sum_q \lambda_q = 1$), and $\phi_q(k_s)$ and $\varphi_q(k_i)$ are Schmidt functions.

As mentioned previously, the generated photon pairs couple to a smaller number of neighboring waveguides with the increase of losses [Fig. 2.8(c,g,k)]. The same dynamics is also seen from the plots of Schmidt decomposition, where a single mode becomes dominating and the spatial entanglement decreases while losses increase [Fig. 2.8(d,h,l)]. The output photon statistics can be tailored by changing the pump profile and phase. When the pump beam is coupled with equal amplitudes and phases to two neighboring waveguides, $A(n) = 1$ for $n = 0, 1$, then the correlations are strongly modified (Fig. 2.9) compared to the single-waveguide pump excitation (Fig. 2.8). As losses increase, the photon-pair correlations are broadened in k-space [Fig. 2.9(a,d,g)] and gradually fade in real space [Fig. 2.9(b,e,h)]. An interesting point here is that with the increase of losses the real-space correlations transform from predominantly antibunching pattern (with the largest correlations on the anti-diagonal, $n_s = -n_i$) at low and moderate loss [Fig. 2.9(b,e)] to bunching pattern (with the largest correlations on the diagonal, $n_s = n_i$) at high loss [Fig. 2.9(h)]. The Schmidt decomposition in the case of pump in two neighbouring waveguides [Fig. 2.9(c,f,i)] shows the dynamics, which is similar to that in the case of pump in a single waveguide [Fig. 2.8(d,h,l)], although the Schmidt modes are distributed in pairs .

The amount of entanglement can be conveniently quantified by the cooperativity parameter – Schmidt number Q [122, 123], which is defined in terms of Schmidt eigenvalues as follows:

$$Q = \frac{1}{\sum_q \lambda_q^2}. \tag{2.44}$$

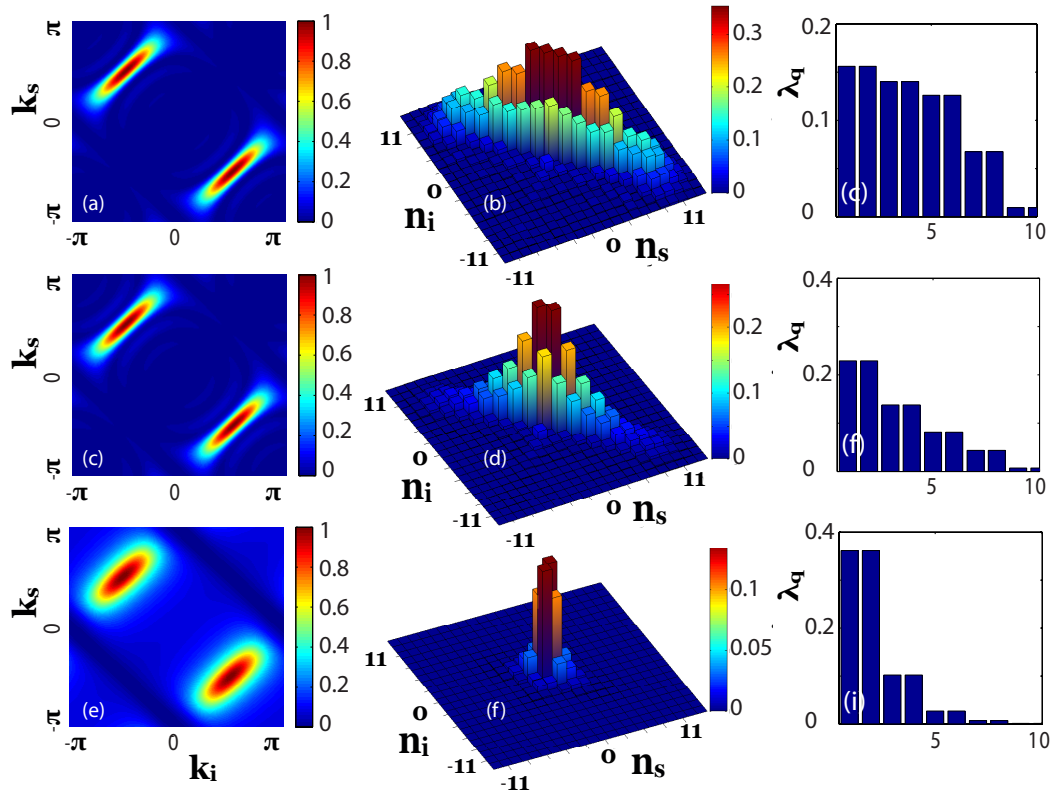

Figure 2.9: Photon-pair correlations in (a,d,g) k-space; (b,e,h) real space correlations and (c,f,i) Schmidt decomposition depending on the mode number (see, Eq. (2.43)) for different signal and idler loss, $\gamma_s = \gamma_i = \gamma/2$: (a,b,c) $\gamma = 0$, (d,e,f) $\gamma = 0.2$, (g,h,i) $\gamma = 0.6$. The pump is coupled in-phase to two neighboring waveguides in the centre, $A(0) = A(1) = 1$. Parameters are $z = 5$, $C_s = C_i = 1$, $\gamma_p = 0$, $\Delta\beta^{(0)} = 0$.

The lowest value of $Q = 1$ corresponds to a system with no quantum entanglement.

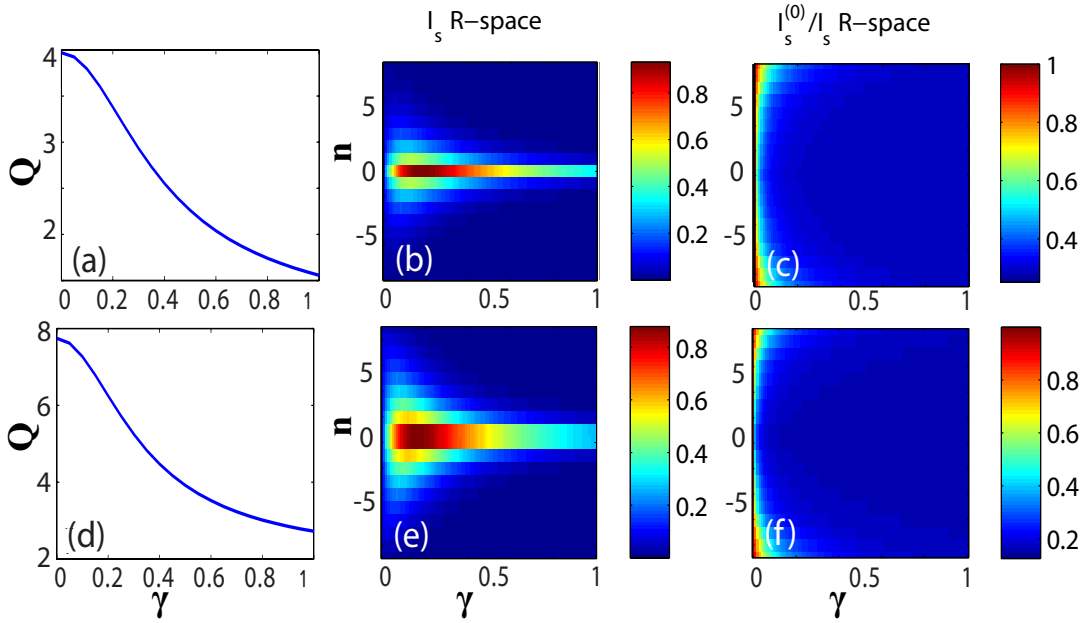

Figure 2.10: (a,d) Schmidt number, (b,e) the signal mode full intensity in real space and (c,f) fraction of signal photons coupled with idler photons to all signal photons in real space vs. the signal and idler loss γ ($\gamma_i = \gamma_s = \gamma/2$) for different pump profiles: (a-c) pump coupled to the central waveguide, $A(0) = 1$, (d-f) pump coupled in-phase to two neighboring waveguides, $A(0) = A(1) = 1$. Parameters are $z = 5$, $C_s = C_i = 1$, $\gamma_p = 0$, $\Delta\beta^{(0)} = 0$.

We show the dynamics of the Schmidt number [Fig. 2.10(a,d)] as well as full signal intensity in real space [Fig. 2.10(b,e)] and the ratio $I_s^{(0)}/I_s$ defining the fraction of signal photons coupled with the idler photon to all signal photons [Fig. 2.10(c,f)] for different values of loss γ ($\gamma_s = \gamma_i = \gamma/2$) and two different pump excitations. We see that both in the case when pump is coupled to the central waveguide and in the case when pump is coupled to two neighboring waveguides, the total signal intensity I_s first increases and then starts to decrease with the increase of losses, while the Schmidt number and the ratio $I_s^{(0)}/I_s$ always decrease with the increase of losses. Signal photons with lost idlers do not interfere, thus their counts always add up. This is in contrast with signal photons paired with idler, which can interfere destructively. It is this loss-induced suppression of destructive interference which can lead to an increase in the total photon counts.

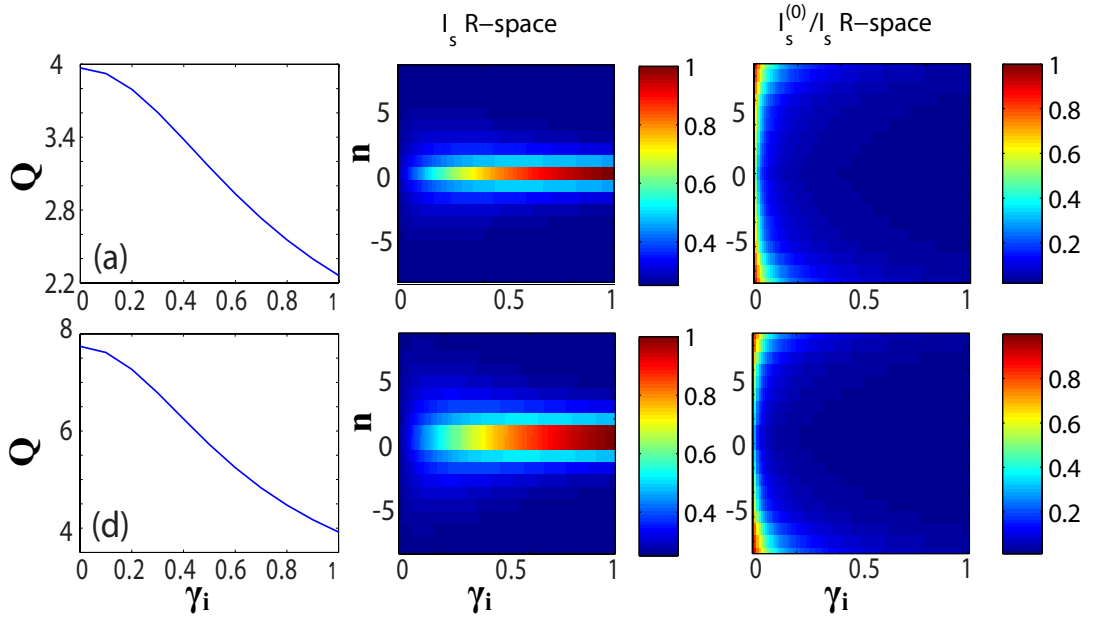

Figure 2.11: (a,d) Schmidt number, (b,e) the signal mode full intensity in real space and (c,f) fraction of signal photons coupled with idler photons to all signal photons in real space vs. the idler loss γ_i for different pump profiles: (a-c) pump coupled to the central waveguide, $A(0) = 1$, (d-f) pump coupled in-phase to two neighboring waveguides, $A(0) = A(1) = 1$. Parameters are $z = 5$, $C_s = C_i = 1$, $\gamma_p = \gamma_s = 0$, $\Delta\beta^{(0)} = 0$.

It is also interesting to consider the case of non-degenerate SPDC, when there is no signal loss ($\gamma_s = 0$), and only the idler loss is present ($\gamma_i > 0$). We show the corresponding Schmidt number, the total signal intensity I_s and signal intensity ratio $I_s^{(0)}/I_s$ in Fig. 2.11. In this case while the Schmidt number [Fig. 2.11(a,d)] and the ratio $I_s^{(0)}/I_s$ [Fig. 2.10(c,f)] decrease, total signal intensity I_s [Fig. 2.11(b,e)] always increases with the increase of idler losses. These trends are in agreement with the single waveguide case [c.f. Fig. 2.4], however in a waveguide array we additionally observe loss-influenced reshaping of spatial intensity profiles.

In this work we have performed analytical and numerical analysis of the effect of linear losses on spontaneous parametric down-conversion in quadratic nonlinear waveguide and waveguide arrays, considering in detail biphoton and single-photon outputs under a variety of conditions. We have shown that idler losses can lead to increase of signal intensity and stabilisation of signal output in relation to the waveguide length. We have also demonstrated that signal and idler losses lead to the transformation of common sinc-shaped photon-pair correlation spectrum into a Lorenzian shape, and that this transformation can be fully reversed by specific increase in pump losses. Finally we have shown that nonlinear waveguide arrays can serve as a robust integrated platform for the generation of entangled pho-

ton states with non-classical spatial correlations, and that the operation of such quantum circuit is tolerant even to relatively high losses. Specifically, we show that if the loss is not strong enough to prevent the coupling between the waveguides, then the spatial non-classical behavior is at least qualitatively preserved. We expect that this work will open new opportunities in developing loss-tolerant quantum integrated circuits.

Chapter 3

Linear optical emulation of photon-pair generation in nonlinear lossy waveguides

In this chapter we establish theoretically and demonstrate experimentally that photon-pair generation through spontaneous parametric down-conversion in a nonlinear waveguide with scattering or material losses can be effectively emulated by classical laser light propagation through a specially designed linear waveguide circuit. This platform can represent arbitrary photon and pump losses, with potential for the emulation of non-Markovian decay. We characterize the photon-pair correlation spectrum and observe its characteristic transformation from the well known sinc-shape in lossless waveguides towards a Lorentzian shape in the presence of photon loss. The research on the establishment of quantum-classical analogies is a hot topic, because the same quantum electromagnetic field is responsible for both processes [97]. Recent examples including simulated quantum walks of entangled photons [58] and development of classical characterization methods to predict quantum device performance [98, 99]. In this chapter, we suggest and experimentally demonstrate that photon-pair generation through SPDC in a nonlinear lossy waveguide can be emulated in a specially designed linear lossless waveguide lattice. One of the most practical and promising approaches in the integrated-optic area seems to be to construct optical circuits based on low-loss glass waveguides. Coupled waveguide structures can be implemented using the femtosecond (fs) laser direct writing approach with high accuracy, which allow fabricate complex and elongated devices. Whereas we focus on a common case of Markovian losses, the developed waveguide platform can be further applied to optically emulate the effects of non-Markovian (non-exponential) decay and quantum decoherence phenomena [91], which can occur in nano-plasmonic circuits [124].

3.1 Theory of classical emulation

This section presents theoretical results on the possibility to emulate quantum nonlinear, lossy system by classical lossless circuit [Fig. 3.1]. Lattices of weakly coupled optical waveguides have provided to be a useful tool for simulating various coherent quantum phenomena (see [91] and references therein). In the optical emulator, a classical complex optical mode amplitude evolution along a waveguide directly matches the complex biphoton wavefunction dynamics. The full theory on the process of SPDC in a lossy $\chi^{(2)}$ nonlinear waveguide pumped by a quasi-CW laser is presented in Sec. 2.1. It has been obtained the analytical solution for the nonunitary evolution of biphoton wave functions (see, Eq. (2.10)). There are analytical results for the normalized intensity of photons generated through SPDC (see, Eqs. (2.11) and (2.13)).

The emulating circuit should represent the biphoton wavefuction evolution according to the Hamiltonian that contains nonlinear and loss terms as in Eq. (2.1). Interestingly, the nonlinear part describing the biphoton generation in a lossless waveguide can be emulated by directionally coupled waveguides [58]. Furthermore, Markovian losses can be emulated through the coupling between one waveguide and a semi-infinite waveguide array [91].

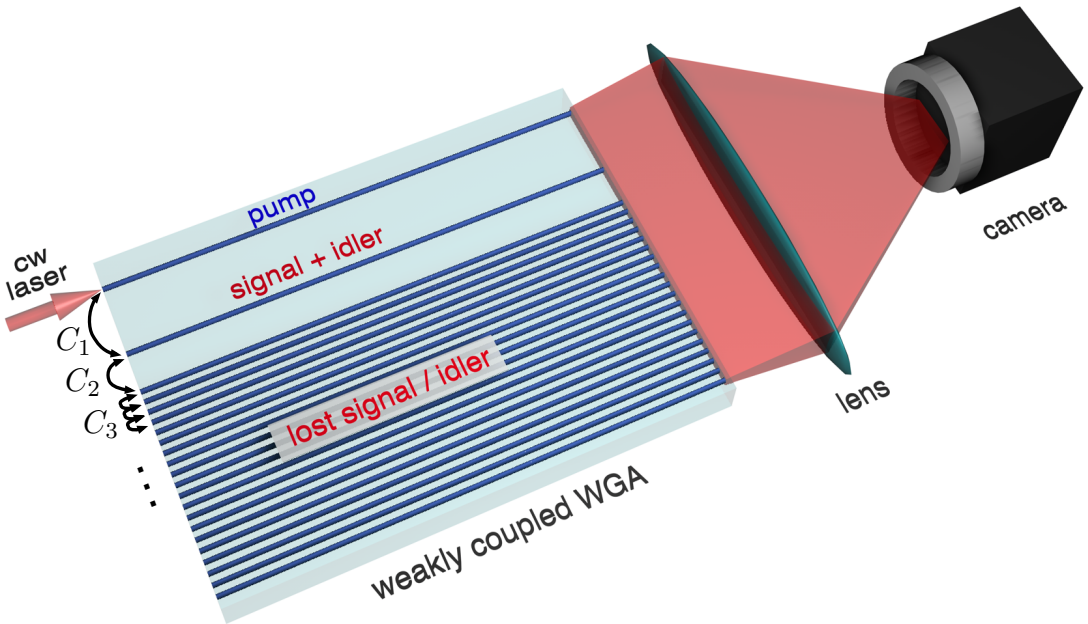

Figure 3.1: Sketch of the experimental setup with the classical optical emulator circuit based on coupled linear waveguides. Laser light is launched into the the first waveguide and the output intensities are imaged on a CCD camera.

We initially consider the case of a lossless pump propagation with $\gamma_p = 0$, and accordingly, in Eq. (2.3) $E(z) = A(0)$. Laser light is launched into the first

waveguide representing the pump. Weak coupling of the first to the second waveguide (C_1) emulates the generation of biphotons. Accordingly, the light amplitude in the second waveguide emulates the biphoton wavefunction. Additionally, the propagation constant in the first waveguide is detuned with respect to the other one's in order to account for the phase mismatch $\Delta\beta$. The photon losses are emulated by light coupling out of the second to the third waveguide (C_2), followed by the propagation through an array of waveguides (waveguide number $n \geq 3$) with high coupling rate $C_3 > C_2 > C_1$. We consider the array to be semi-infinite, or in practice, sufficiently wide to avoid reflections from the edge.

We now establish the mathematical correspondence between the biphoton wavefunction evolution and the light propagation in the linear waveguide circuit. The laser light propagation in the circuit is described by the coupled mode equations

$$i\frac{\partial \psi_n}{\partial z} - \beta_n \psi_n + C_{n-1}\psi_{n-1} + C_n \psi_{n+1} = 0, \tag{3.1}$$

where $n \geq 1$ are the waveguide numbers, ψ_n are the complex classical mode amplitudes, C_n are the coupling coefficients proportional to the mode overlaps in the neighboring waveguides, and β_n are the waveguide propagation constants. We set $C_0 \equiv 0$, and in the loss-emulating section $C_{n\geq 4} = C_3$ as well as $\beta_{n\geq 3} = \beta_2$.

We introduce the Fourier representation,

$$\psi_n(z) = \int_{-\infty}^{\infty} \mathrm{e}^{i\beta z} f_n(\beta)\mathrm{d}\beta. \tag{3.2}$$

For the analysis, the structure can be considered infinite, extending over all z. We apply inverse transform to Eq. (3.1) to obtain the corresponding coupled algebraic equations for the Fourier coefficients,

$$-\beta f_n + C_{n-1} f_{n-1} + C_n f_{n+1} - \beta_n f_n = 0. \tag{3.3}$$

The solution of Eq. (3.3) in the semi-infinite section with the homogeneous coupling C_3 for $n \geq 3$ has the form of a discrete Bloch wave [125],

$$f_n = f_3 \exp[\imath k\,(n-3)] \tag{3.4}$$

The wavenumber k satisfies the spatial dispersion relation $-\beta + 2C_3\cos(k) - \beta_2 = 0$, following from Eq. (3.3). Next we assume that for $n > 3$ the coupling between the loss emulating waveguides is much larger than the propagation constant, $C_3 \gg |\beta, \Delta\beta^{(0)}|$, which means that $\cos(k) \ll 1$, and thus, $k = \kappa + \pi/2$, with

$|\kappa| \ll 1$. Therefore, we can rewrite the dispersion relation as

$$\beta = -\Delta\beta^{(0)} - 2C_3 \sin(\kappa) \approx -\Delta\beta^{(0)} - 2C_3\kappa, \tag{3.5}$$

where $\Delta\beta^{(0)} = \beta_s^{(0)} + \beta_i^{(0)}$, $\beta_{s,i}^{(0)}$ are the signal and idler propagation constants relative to the pump. Employing this dispersion, we find from Eq. (3.3) a relation between the modes in the second and the third waveguides

$$f_3 = (C_2/C_3)\exp(ik) f_2 \approx (C_2/C_3) i f_2, \tag{3.6}$$

and accordingly in real space the Fourier transform of Eq. (3.6) will give us the following result

$$\psi_3(z) \approx (C_2/C_3) i \psi_2(z). \tag{3.7}$$

Now we can express the modes at $n \geq 3$ through the mode propagating in the second waveguide

$$f_n = \frac{C_2}{C_3} f_2 i^{n-2} \mathrm{e}^{\kappa(n-2)}, \quad n \geq 3. \tag{3.8}$$

We substitute Eq. (3.7)in the expression Eq. (3.1) for $n = 2$ and obtain

$$i\frac{\partial \psi_2}{\partial z} - \left(\beta_2 - i\frac{C_2^2}{C_3}\right)\psi_2 + C_1\psi_1 = 0. \tag{3.9}$$

Further, we consider the undepleted pump regime with $C_1 z \ll 1$, and in particular, $\psi_1(z) \approx \psi_1(0)\exp(i\beta_1 z)$. We next determine wrote the mode profiles in real space by substituting Eq. (3.8) in Eq. (3.2)

$$\begin{aligned}
&\psi_n(z) = \frac{C_2}{C_3}\int \mathrm{e}^{i\beta z} f_2(\beta) i^{(n-2)} \mathrm{e}^{\kappa(n-2)} \mathrm{d}\beta = \\
&\frac{C_2}{C_3} i^{(n-2)} \mathrm{e}^{-\frac{i(n-2)}{2C_3}\Delta\beta^{(0)}} \int \mathrm{d}\beta f_2(\beta) \mathrm{e}^{i\beta\left(z - \frac{(n-2)}{2C_3}\right)} = \\
&\frac{C_2}{C_3} i^{(n-2)} \mathrm{e}^{-\frac{i(n-2)}{2C_3}\Delta\beta^{(0)}} \psi_2\left(z - \frac{n-2}{2C_3}\right), \; n \geq 3.
\end{aligned} \tag{3.10}$$

Finally, comparison of Eq. (2.6) for the biphoton state and Eq. (3.9) for classical light evolution in the second waveguide unambiguously shows their equivalence (for $\gamma_{s,i,p} \equiv 0$). We require that $\psi_2(z) \equiv \Phi(z)$, and obtain the following relations:

$$\gamma = \frac{C_2^2}{C_3}, \quad \psi_1(0) = -\frac{A\chi}{C_1}, \quad \beta_1 = 0, \quad \beta_2 = \Delta\beta^{(0)}. \tag{3.11}$$

The last step is to find relation between the biphoton state $\tilde{\Phi}^{(s)}$, which corre-

sponds to a mixed state with the lost idler photon, and the modes propagating in the loss simulating waveguides $\psi_n, (n \geq 3)$. Since $|\psi_2(z)|^2 = |\Phi(z)|^2$ we can rewrite Eq. (2.9) as follows:

$$|\tilde{\Phi}^{(s)}(z_l, z_l)|^2 = 2\gamma\,|\psi_2(z_l)|^2 = 2\gamma\left(\frac{C_3}{C_2}\right)^2\left|\psi_n\left(z_l + \frac{n-2}{2C_3}\right)\right|^2 = 2C_3\left|\psi_n\left(z_l + \frac{n-2}{2C_3}\right)\right|^2, \tag{3.12}$$

where we used the relation between the loss and the coupling coefficients from (3.11).

In this vein, the considered waveguide lattice shown in Fig. 3.1 effectively emulates the SPDC in a nonlinear lossy waveguide. Specifically, the intensity in waveguide $n = 2$ represents the probability of the signal-idler biphoton generation at the output.

3.2 Experimental results and analysis

In order to perform an experimental analysis of the emulation of the SPDC in single nonlinear waveguide with losses through the linear waveguide array our collaborators form Friedrich-Schiller-University, Jena, Germany fabricated waveguide structures using the femtosecond laser direct writing technique [34, 126].

Modern communication technology is based on integrated optical devices which control the properties of light in all-optical networks. Key elements within these networks are active and passive waveguides, splitters, connectors, and filters. The optical function of these elements is based on a spatial refractive-index modification [127]. The effects of radiation damage in high-silica glasses have been performed with the objective of producing optical devices. Use of ultra-short laser pulses for the direct writing of photonic structures has been demonstrated [126, 127]. When intense ultra-short laser pulses are focused inside transparent materials nonlinear absorption will occur in the focal volume leading to optical breakdown and the formation of a microplasma. This localized energy deposition induces permanent structural and refractive index changes [126, 128]. By moving the sample with respect to the focus of the laser beam waveguides can be written along arbitrary paths. Since the material is transparent for the processing laser beam this technology is applicable like no other for the fabrication of three-dimensional integrated optical devices [127]. The direct laser writing approach has been used to fabricate a variety of photonic devices like waveguides [129], 3D-couplers [130], and evanescently coupled waveguide arrays [131, 132].

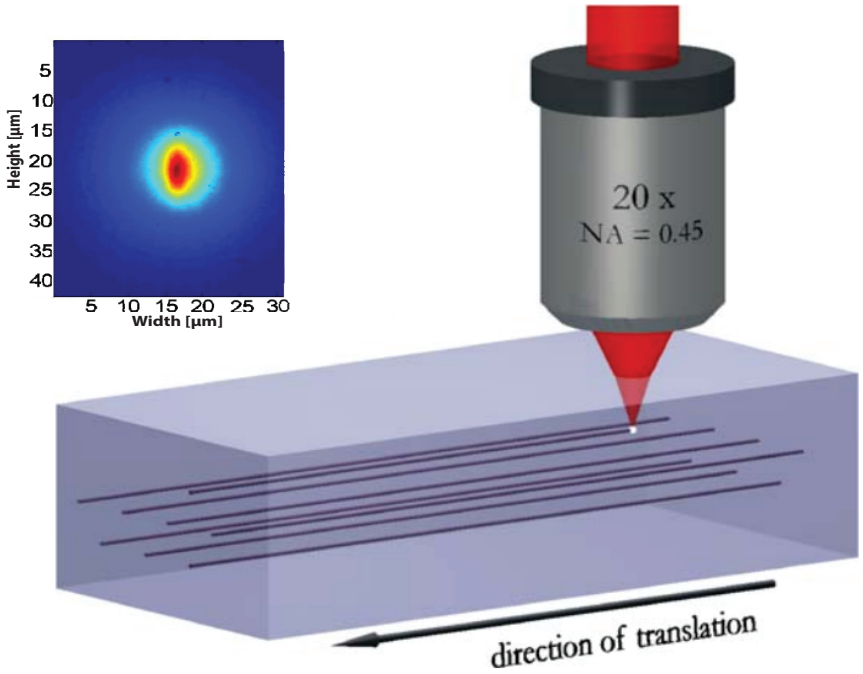

Figure 3.2: Schematic of the writing process in transparent bulk material using fs-laser pulses [128, 132] with measured near-field profile at $\lambda = 800nm$ for a waveguide written at $500\mu m/s$ and. Translating the substrate with respect to the laser focus permits the fabrication of 3D waveguide circuits.

It has been shown that specific pulse energy, repetition rate and writing speed should be taken into account in order to fabricate low loss positive index guiding waveguide devices in a specific type of glass. The high extraction efficiency of photons from glass waveguide circuits has made them the most practical method for exploring a range of quantum photonic devices and concepts. The waveguides formed through femtosecond laser direct write (FLDW) can be fabricated the minimal insertion losses [34]. Unlike planar lightwave circuit (PLC) fabrication the FLDW technique is a one step process, which doesn't require masking procedure or clean room environment. This means that prototypes can be produced rapidly and iterative fabrication methods can be engaged. Furthermore the laser is easily focused at multiple depths inside the material enabling three dimensional waveguide circuits which are extremely challenging to produce using lithographic methods. This allows the production of vertically coupled waveguide arrays for the study of photon correlations and novel 3D integrated waveguide circuits [34]. A visionary image of the fabrication process is shown in Fig. 3.2 where three dimensional waveguides are drown inside a block of glass at the point of laser focus. The use of fs laser written waveguide structures provides a flexible technique to fabricate permanent structures for linear and nonlinear applications. It has been demonstrated the possibility of fabrication of large three dimensional waveguide structures with high accuracy.

In the experiment carried at Friedrich-Schiller-University, Jena the propagation constant detuning of the pump guide was controlled via the inscription velocity. A set of samples were fabricated corresponding to different propagation constants $\Delta\beta^{(0)}$. The waveguides' length is 7.6 cm, and their transverse separation determines the coupling coefficient between them. While the structures emulate different mismatch and loss regimes, the coupling between the first and the second waveguide stays constant at $C_1 = 0.0575$ cm^{-1}. Thus, the effective pump amplitude A is kept constant for all experiments at the same laser power ($|\psi_1|^2$) according to Eq. (3.11). For the classical-optical emulation laser light of 633 nm was injected into the first waveguide and the output intensity of the complete structure was observed via a CCD camera, as illustrated in Fig. 3.1.

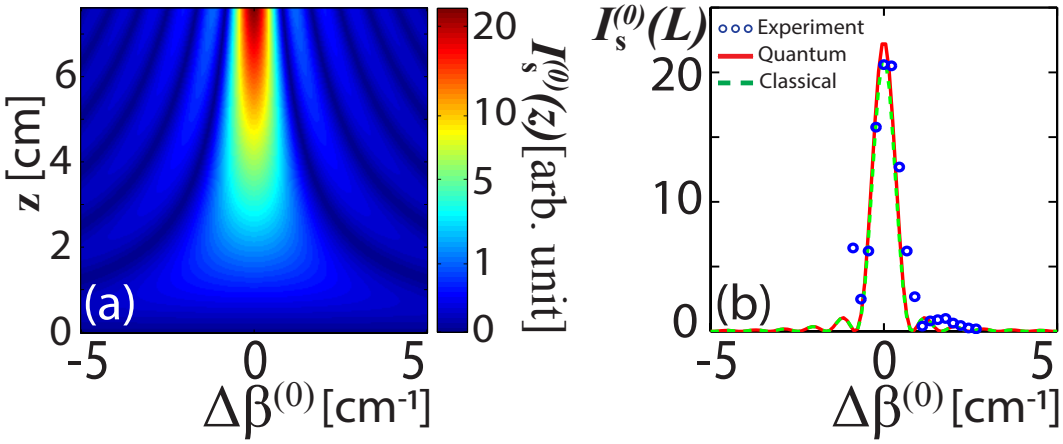

Figure 3.3: Emulation of photon-pair generation in a lossless waveguide ($\gamma = 0$). (a) Quantum solution for biphoton intensity evolution in a nonlinear waveguide according to Eq. (3.13). (b) Output intensity vs the phase mismatch: experimental measurements (blue circles), quantum solution by Eq. (3.13) (solid red line), and numerical solution of the emulating linear system Eqs. (3.1) (dashed green line). The length of the waveguides is $L = 7.6$ cm, the coupling coefficient between first and second waveguides is $C_1 = 0.0575$ cm^{-1}, and $C_2 = 0$. Fabrication deviations of the laser written waveguides result in an uncertainty of the phase mismatch (difference in propagation constants) but is within the marker size.

As a first step we analyze the simplest case without loss ($\gamma = 0$). Then the intensity for the signal-idler biphoton provided by Eq. (2.11) exhibits a characteristic sinc-shape,

$$I_s^{(0)}(z) = A^2 z^2 \mathrm{sinc}^2\left(\frac{\Delta\beta^{(0)} z}{2}\right). \tag{3.13}$$

Fig. 3.3(a) shows this biphoton intensity evolution along a nonlinear waveguide for different phase mismatches. The emulation of SPDC in a nonlinear lossless

waveguide is realized by just two linear coupled waveguides ($n = 1, 2$). In accordance with Eq. (3.11) $C_2 = 0$ represents the lossless case, such that there is no coupling to the loss emulating array with $n \geq 3$. The corresponding experimental results are presented in Fig. 3.3(b) as blue circles, when we insert losses the figure shows transformation from sinc form to Lorentz form.

For comparison we plot the quantum solution with a solid red line and the numerical solution of the coupled-mode equations representing the emulating circuit with a dashed green line. In the theoretical simulations the pump amplitude is normalized according to the experimental results and is constant for the lossless and the loss-emulating case at $A\chi = 0.6238$. The data shows excellent agreement between both theoretical curves and the experimental measurements across a wide range of phase mismatches.

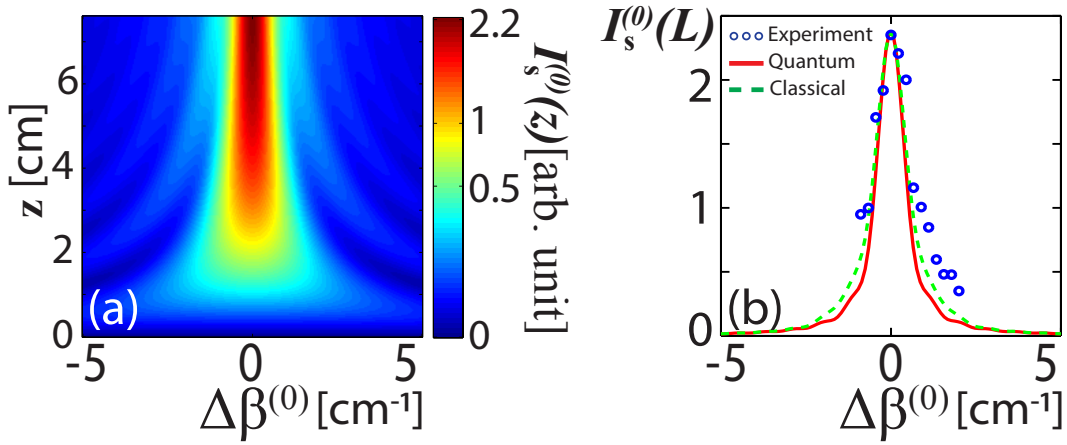

Figure 3.4: Emulation of photon-pair generation in a waveguide with loss ($\gamma = 0.397$ cm^{-1}). The corresponding experimental couplings are $C_2 = 0.63$ cm^{-1} and $C_3 = 1.0$ cm^{-1}. Other parameters and notations are the same as in Fig. 3.3.

Next, we investigate the SPDC in a nonlinear lossy waveguide and its classical emulation. In the presence of loss the biphoton intensity dependence on the phase mismatch transforms from a sinc-shape to a Lorentzian shape [63, 65], as described by Eq. (2.11), which is imaged in Fig. 3.4(a). The emulating system now includes the loss-emulating array with waveguide couplings that determine the loss coefficient, see Eq. (3.11). The array consists of 20 waveguides ($n = 3 \ldots 22$), which is sufficient to avoid reflections from the boundary. Both the experimental and theoretical (quantum calculation and coupled mode analysis) results are shown in Fig. 3.4(b). Again, a nice agreement of the data can by noted and the Lorentzian shape is clearly verified by our experiments.

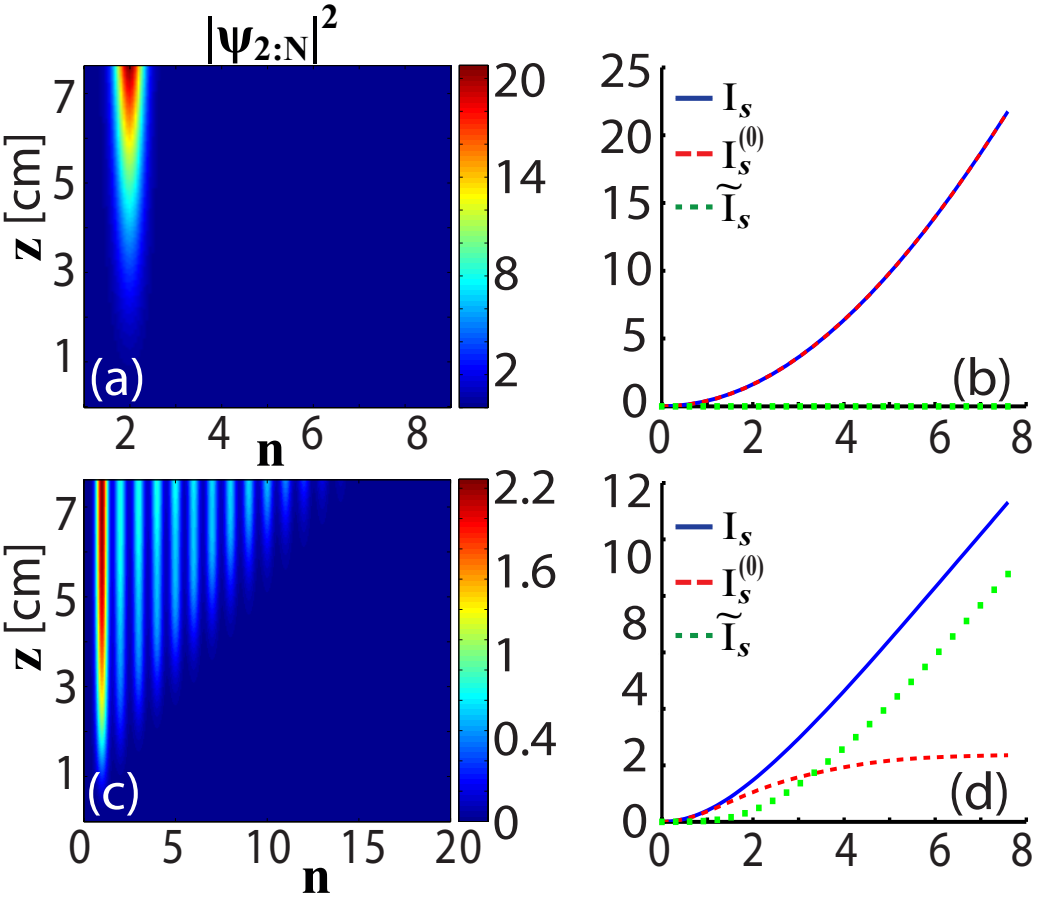

Figure 3.5: Theoretical simulation of the intensities at the output of the coupled waveguide array and the nonlinear lossy waveguide ($\Delta\beta^{(0)} = 0$). (a,c) Distribution of the output intensity in the waveguide array depending on the number of waveguides and the propagation distance; (b,d) Intensities: total (I_s), biphoton related ($I_s^{(0)}$) and contribution from the states with lost idler photons ($\widetilde{I}_s$). (a,b) $C_1 = 0.0575$ cm^{-1}, $C_2 = C_3 = 0$ (corresponding loss $\gamma = 0$), (c,d) we neglect losses on the sum frequency ($\gamma_p = 0$) and $C_1 = 0.0575$ cm^{-1}, $C_2 = 0.63$ cm^{-1}, $C_3 = 1.0$ cm^{-1} (corresponding loss is $\gamma = 0.397$ cm^{-1}).

We discuss behavior of the intensities at the output of the coupled waveguide array and the nonlinear lossy waveguide depending on the propagation distance for different loss values. It is easy to notice form Fig. 3.5(b) that in case of lossless system the total intensity coincide with biphoton related intensity ($I_s^{(0)}$), we have the same picture in the waveguide array all intensity is concentrated in the second waveguide and the intensity in the loss simulating waveguides ($n > 2$) is equal to zero [see Fig. 3.5(a)]. Fig. 3.5(d) shows that if we introduce losses in the system the contribution from the states with lost idler photons ($\widetilde{I}_s$) increases and the total intensity decreases. Similarly the intensities at the output of loss emulating waveguides differ from zero [see, Fig. 3.5(c)].

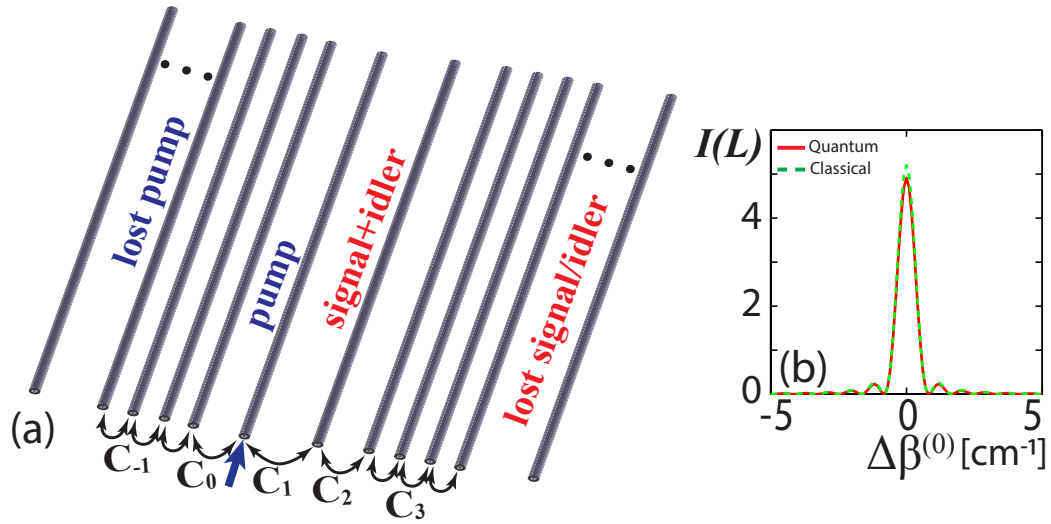

Figure 3.6: Emulation of photon-pair generation in a waveguide with photon and pump losses. (a) Design of the corresponding linear circuit with an additional array at $n \leq 0$ emulating the pump-loss. (b) Output intensity vs the phase mismatch: quantum solution by Eq. (3.13) (solid red line) and numerical solution of the emulating linear system by Eq. (3.1) (dashed green line). The pump and photon losses are matched, $\gamma_\mathrm{p} = \gamma = 0.1$ cm^{-1}, $C_0 = C_2 = 0.3162$ cm^{-1}, and $C_{-1} = C_3 = 1$ cm^{-1}. Other parameters are the same as in Fig. 3.4.

Unfortunately the experimental results for the intensity which corresponds to a contribution from the states with lost idler photons $\tilde{I}_s(z)$ didn't match perfectly with the theoretical results. The issue is that the intensity at the output of the waveguides emulating the losses is very low and is impossible to completely detect by the available camera.

This chapter presents results on the possibility to emulate quantum nonlinear, lossy system by classical lossless lattices of weakly coupled optical waveguides. We discussed only the scenario when signal and idler photons are generated and localised in the same waveguide, meaning have approximately the same frequency and the propagation constants. The case when we have photons in different waveguides is a very interesting and open problem. It is not that trivial to predict the outcome because of large diminutions of Hilbert space.

Additionally, we point out that the circuit can be designed to emulate the effect of pump losses as well. This can be achieved by placing a second loss-emulating array on the left of the pump waveguide, as illustrated in Fig. 3.6(a). The corresponding coupling coefficients are found analogous to Eq. (3.11) as $\gamma_\mathrm{p} = C_0^2/C_{-1}$. We also set $C_{n\leq -2} = C_{-1}$ and $\beta_{n\leq 0} = 0$. A particularly interesting situation arises when the pump loss is equal to the combined signal and idler losses, such that $\gamma_\mathrm{p} = \gamma$. Then, the biphoton dependence of mismatch recovers a sinc-shape, just like in the lossless case, which is depicted in Fig. 3.6(b). Finally, we note that by altering the arrangement of loss-emulating guides, the developed

waveguide platform can be tailored to emulate the effects of non-Markovian (non-exponential) decay and quantum decoherence phenomena [91].

In conclusion, we present the theoretical concept and the experimental realization of a classical optical emulator of quantum photon-pair generation in a lossy quadratic nonlinear waveguide. The transformation of a common sinc-shaped photon-pair correlation spectrum into a Lorenzian shape in the presence of signal and idler photon losses was demonstrated. Furthermore, the pump losses can be emulated as well, in particular when the pump and photon losses are matched a restoration of the sinc-shaped dependence of the output on the phase mismatch is observed. Our approach based on a linear waveguide lattice is very flexible, and can further enable emulations of non-Markovian processes, which are a common feature in photonic nanostructures including plasmonic circuits.

Chapter 4

Spatially inhomogeneous losses and parity time symmetry

Integrated photon sources based on nonlinear waveguide arrays have applications in the development of on-chip quantum communication and computation devices [20, 32, 33, 36, 37]. These chips are perfect for the generation and shaping of spatial modes [45, 109–112]. The classical characterization of quantum device performance [97] is an active research topic. We present theoretical results on possibilities to characterize spontaneous parametric down conversion (SPDC) through classical sum frequency generation in nonlinear lossy waveguide array. We call this technique stimulated multimode tomography.

Nowadays, the development of new generation of devices for efficient generation of nonlinear processes for use in emerging quantum technologies is under intense investigation [133–135]. Waveguide SPDC sources are becoming more widely used [48, 136, 137] for improvements in the fabrication of quantum technologies and lead to the disposition of more and more devices on the same chip. The relationship between quantum processes and optical classical processes has recently become of practical importance for characterizing photon sources based on spontaneous quantum nonlinear optical processes [98, 99]. This relation could allow direct but slow coincidence detection measurements of a spontaneous process to be replaced by faster and more convenient optical power measurements of the corresponding classical process. Recent examples include simulated quantum walks of entangled photons [58] and development of classical characterization methods to predict quantum device performance [98, 99].

One application of such an analogy between quantum and classical emissions is the light propagation in parity-time- (PT-) symmetric optical systems with balanced gain and loss. Photonic structures consisting of coupled waveguides with regions of gain and loss offer many novel possibilities for shaping optical beams. The beam dynamics in this case may demonstrate properties qualitatively

different from those usually observed in conservative systems. Among them are power oscillations, nonmonotonous dependence of the transmission on absorption, unidirectional invisibility [89, 138], conical diffraction, and unusual switching regimes [90, 138, 139] and formation of spatial and temporal solitons [140] in nonlinear structures.

In optics, such complex PT-symmetric structures can be realized in nonlinear couplers within the context of the paraxial theory of diffraction by involving symmetric index guiding and an antisymmetric gain/loss profile [80, 84, 85]. This structure is PT-symmetric around its central axis. Below the critical gain/loss value, the modal intensity is equally divided between the two sites and illustrate oscillatory coupling between the two modes. As the non-Hermitian PT potential strength is increased beyond the PT-symmetry breaking point, the two modes become isolated in each site, oscillatory coupling between the two modes disappears and is replaced by a hyperbolic behaviour (one mode decays and the other grows). It is important to note that PT-symmetry breaking can also occur in entirely passive dual systems where one channel exhibits loss [81]. In this new configuration the PT phase transition point is now shifted.

In Sec. 4.1 we describe photon-pair generation through spontaneous parametric down-conversion (SPDC) in quadratic nonlinear waveguide array with different linear absorption in all waveguides. Direct coincidence detection measurements of a spontaneous process are very slow. A new measurement technique has enabled previously unobtainable resolution in the spectral characterization of two-photon states from various waveguides which enable faster and more convenient optical power measurements of the corresponding classical process. A useful connection between SPDC and SFG has been shown in nonlinear one mode optical waveguides with arbitrary scattering loss [99], as well quantum and classical processes analogy in multimode system without losses [141]. Section 4.2 is devoted to sum frequency generation (SFG) in nonlinear lossy, multimode waveguide array and the analysis of the correspondence of the results with ones for the SPDC. Sections 4.3 and 4.4 discuss the results due to the PT-symmetry breaking threshold in nonlinear PT-symmetric coupler, which consists of one lossy and one conservative waveguide.

4.1 SPDC in a lossy waveguide array: eigenmode solution

The process of SPDC can occur in a $\chi^{(2)}$ nonlinear waveguide pumped by a laser, where a pump photon at frequency ω_3 can be spontaneously split into signal and idler photons with corresponding frequencies ω_1 and ω_2, where $\omega_3 = \omega_1 + \omega_2$ (see, Fig. 4.1). The effect of linear losses on SPDC was previously considered in various contexts [62–64] and was analysed in detail in Chapter 2 [65] and

Appendix A. We take the main concept for description of the biphoton function evolution from Chapter 2 but now generalize if for the case of spatially inhomogeneous losses. We consider that losses are different in each waveguide. According to the general principles the photon dynamics is governed by a Hamiltonian Eq. (2.1) and the solution for a two-photon state at distance z is given by Eq. (2.5).

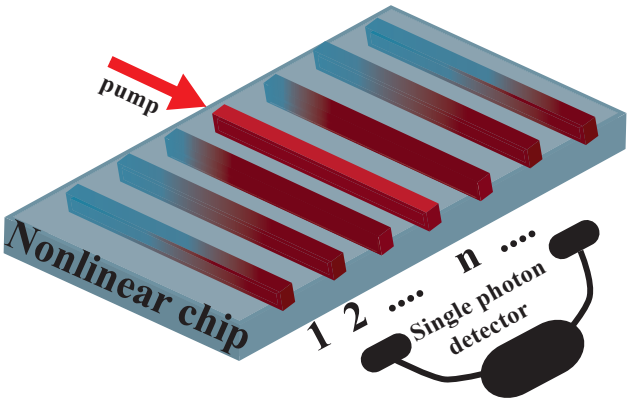

Figure 4.1: Scheme of spontaneous parametric down-conversion in nonlinear waveguide array with spatial inhomogeneous losses.

Taking into account the detailed derivation of biphoton wave function evolution Eq. (2.28) and considering spatially inhomogeneous losses, we derive Schrödinger-type equations for the photon pair amplitudes Φ_{n_1,n_2} (n_1, n_2, are waveguide numbers for signal and idler photons) as follows,

$$\frac{\partial \Phi_{n_1,n_2}(z)}{\partial z} = -i\Delta\beta\Phi_{n_1,n_2} - (\gamma_s(n_1) + \gamma_i(n_2))\Phi_{n_1,n_2} - iC_s(\Phi_{n_1-1,n_2} + \Phi_{n_1+1,n_2}) - iC_i(\Phi_{n_1,n_2-1} + \Phi_{n_1,n_2+1}) + A_{n_1}\delta_{n_1,n_2}. \quad (4.1)$$

We also write the propagation equation for the undepleted pump amplitude. We consider the low conversion efficiency regime which means we neglect the probability of recombination of photon pairs into pump photon and write the propagation of the pump field in the following form,

$$\frac{\partial A_{n_3}(z)}{\partial z} = (-i\beta_p - \gamma_p(n_3))\, A_{n_3} - iC_p(A_{n_3-1} + A_{n_3+1}). \quad (4.2)$$

where $\Delta\beta = \beta_s + \beta_i$ is the pump and photon-pair phase velocity mismatch in a single waveguide, $C_{s,i}$ are frequency-independent coupling constants between the neighboring waveguides for signal and idler photons, C_p is a coupling coefficient for the pump field, $\gamma_{s,i,p}(n)$ are loss coefficients of signal, idler photons and the pump in the n_jth waveguide ($j = 1, 2, 3$), correspondingly. A_n is proportional to

the normalized pump amplitude at frequency ω_p and to the quadratic nonlinearity χ.

We search for the solution of the inhomogeneous equations as

$$\Phi_{n_1,n_2}(z) = \sum_{m_1 m_2} u_{n_1,m_1} v_{n_2,m_2} B_{m_1,m_2}(z) \tag{4.3}$$

where $u_{n_1,m_1} v_{n_2,m_2}$ are eigenmode solutions of homogeneous Schrödinger equation and $B_{m_1,m_2}(z)$ is the z dependent coefficient of the expansion. The solution of the eigenmode problem for the signal u_{n_1,m_1} and the idler v_{n_2,m_2} which could be written in the matrix form as follows

$$\frac{\partial}{\partial z}\begin{pmatrix} u_1 \\ u_2 \\ ... \\ u_m \end{pmatrix} = \tilde{H}\begin{pmatrix} u_1 \\ u_2 \\ ... \\ u_m \end{pmatrix}, \tag{4.4}$$

where

$$\tilde{H} = \begin{pmatrix} -\frac{i\Delta\beta}{2} - \gamma_s(n_1) & -iC_s & 0 & ... & 0 \\ -iC_s & -\frac{i\Delta\beta}{2} - \gamma_s(n_1) & -iC_s & ... & 0 \\ .. & .. & .. & .. & .. \\ 0 & 0 & ... & -iC_s & -\frac{i\Delta\beta}{2} - \gamma_s(n_1) \end{pmatrix} \tag{4.5}$$

is the homogeneous transformation Hamiltonian of the signal mode. We have the similar formula for the idler photon. u_{n_1,m_1} and the v_{n_2,m_2} can be represented through $U_1(n_1,m_1)$ and $U_2(n_2,m_2)$, respectively, where $U_1(n_1,m_1)$ is the eigenvector for the signal photon with eigenvalues $\lambda^s_{1(2)}$ and $U_2(n_2,m_2)$ is the eigenvector for the idler photon with eigenvalues $\lambda^i_{1(2)}$. In general $U_j(n,m)$, where $j=1$ corresponds to the frequency $\omega_s \equiv \omega_1$, $j=2$ for $\omega_i \equiv \omega_2$, and $j=3$ corresponds to the pump frequency $\omega_p \equiv \omega_3$, n_j are indexes over the waveguide numbers and m_j are indexes for the modes.

The detailed mathematical analysis of SPDC in the waveguide array with spatially inhomogeneous losses and the eigenmode solutions of Eqs. (4.1) and (4.2) are presented in Appendix B.1. Homogeneous Schrödinger equation for the signal and idler modes is presented in Hamiltonian form in Eq. (4.4). It is seen from Eq. (4.5) that Hamiltonian describing evolution of signal (idler) eigenmodes has a form of symmetric matrix: $\tilde{\mathbf{H}} = \tilde{\mathbf{H}}^{\mathbf{T}}$ with complex elements. It has been shown [142] that the eigenmodes of the transpose matrices satisfy the following orthogonality relation: $\sum_n U_j(n,m_j)U_j(n,m_k) = 0$ if $m_j \neq m_k$. This orthogonality relation leads to following expression; $\mathbf{U_j^T U_j} = \mathbf{\Pi_j}$, where $\Pi_j = diag_m\left(\sum_n U_j^2(n,m)\right)$. We can write inverse matrix as $\mathbf{U_j^{-1}} = \mathbf{U_j^{-1} U_j U_j^T \Pi_j^{-1}} =$

$\mathbf{U_j^T \Pi_j^{-1}}$, which means we can write the relation more explicitly as,

$$U_1^{-1}(m_2, n_1) = \frac{U_1(n_1, m_2)}{\sum_q U_1^2(q, m_2)}. \tag{4.6}$$

The detailed derivation of the results for the z dependent coefficient of the expansion and the two-photon function is presented in Appendix B. Here we present only the final results for the z dependent coefficient and the two photon amplitude,

$$\begin{aligned} B_{m_1,m_2}(z) = & \frac{iz}{\det(U_1)\det(U_2)\det(U_3)} \sum_{m_3,n_3} \mathrm{e}^{\frac{\left(\lambda^p_{m_3}-\lambda^s_{m_1}-\lambda^i_{m_2}\right)z}{2}} \times \\ & \operatorname{sinc}\left(\frac{\left(\lambda^p_{m_3}-\lambda^s_{m_1}-\lambda^i_{m_2}\right)z}{2}\right) \times \\ & \left\{\frac{U_1(n_3,m_1)}{\sum_q U_1^2(q,m_1)} U_3(n_3,m_3) \frac{U_3(n_3,m_3)}{\sum_l U_3^2(l,m_3)} A_{n_3,n_3}(0) \frac{U_2(n_3,m_2)}{\sum_p U_2^2(p,m_2)}\right\}, \end{aligned} \tag{4.7}$$

Now we consider that we have pump in the n_3th waveguide $\Phi_{n_1,n_2} = \sum_{n_3} A_{n_3} \Phi^{n_3}_{n_1,n_2}$ and write results for the two photon amplitude as follows,

$$\begin{aligned} \Phi^{n_3}_{n_1,n_2} = & \frac{iz}{\det(U_1)\det(U_2)\det(U_3)} \times \\ & \sum_{m_3,m_2,m_1} \mathrm{e}^{\frac{\left(\lambda^p_{m_3}+\lambda^s_{m_1}+\lambda^i_{m_2}\right)z}{2}} \operatorname{sinc}\left(\frac{\left(\lambda^p_{m_3}-\lambda^s_{m_1}-\lambda^i_{m_2}\right)z}{2}\right) \times \\ & \left\{U_1(n_1,m_1) \frac{U_1(n_3,m_1)}{\sum_q U_1^2(q,m_1)} U_3(n_3,m_3) \frac{U_3(n_3,m_3)}{\sum_k U_3^2(k,m_3)} \times \right. \\ & \left. A_{n_3,n_3}(0) \frac{U_2(n_3,m_2)}{\sum_l U_2^2(l,m_2)} U_2(n_2,m_2)\right\}. \end{aligned} \tag{4.8}$$

4.2 Sum Frequency Generation: Eigenmode solution

Nowadays there are many structures that could potentially be used for the generation of quantum nonlinear optical processes, but to check the efficiency of these sources is still time consuming process. Thus the relationship between quantum processes and optical classical processes has recently become of practical importance for characterizing photon sources. The technique will only become

more valuable as improvements in fabrication technology lead to more and more devices on the same chip.

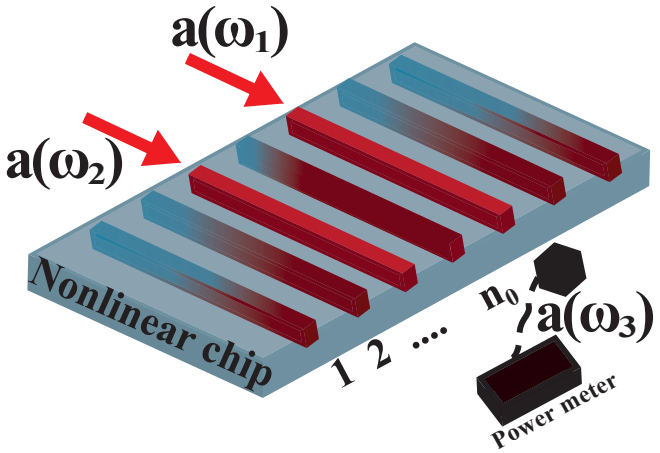

Figure 4.2: Scheme of sum frequency generation in nonlinear waveguide array with spatially inhomogeneous losses.

Here we present the theory of the SFG which occur in $\chi^{(2)}$ nonlinear lossy waveguide array pumped by two pulses on the ω_1 and ω_2 frequencies, which sum into a mode with the frequency ω_3: $\omega_1 + \omega_2 = \omega_3$ (see Fig. 4.2). The full coupled mode equations for SFG are written in the following form [2, 131, 143]

$$\frac{\partial a_{n_1}(\omega_1)}{\partial z} = (-i\beta_s - \gamma_s(n_1))\, a_{n_1}(\omega_1) - iC_s\Big(a_{n_1-1}(\omega_1) + a_{n_1+1}(\omega_1)\Big) + a_{n_3}(\omega_3)a^*_{n_2}(\omega_2), \tag{4.9}$$

$$\frac{\partial a_{n_2}(\omega_2)}{\partial z} = (-i\beta_i - \gamma_i(n_2))\, a_{n_2}(\omega_2) - iC_i\Big(a_{n_2-1}(\omega_2) + a_{n_2+1}(\omega_2)\Big) + a_{n_3}(\omega_3)a^*_{n_1}(\omega_1), \tag{4.10}$$

$$\frac{\partial a_{n_3}(\omega_3)}{\partial z} = (-i\beta_p - \gamma_p(n_3))\, a_{n_3}(\omega_3) - iC_p\Big(a_{n_3-1}(\omega_3) + a_{n_3+1}(\omega_3)\Big) + a_{n_3}(\omega_1)a_{n_3}(\omega_2). \tag{4.11}$$

We consider low conversion efficiency $a_1(\omega_3) \ll 1$ and $a_2(\omega_3) \ll 1$ to compare the results with the photon pair amplitude of the SPDC process. The coupled mode equations for SFG are rewritten in the following form

$$\frac{\partial a_{n_1}(\omega_1)}{\partial z} = (-i\beta_s - \gamma_s(n_1))\, a_{n_1}(\omega_1) - iC_s\Big(a_{n_1-1}(\omega_1) + a_{n_1+1}(\omega_1)\Big), \quad (4.12)$$

$$\frac{\partial a_{n_2}(\omega_2)}{\partial z} = (-i\beta_i - \gamma_i(n_2))\, a_{n_2}(\omega_2) - iC_i\Big(a_{n_2-1}(\omega_2) + a_{n_2+1}(\omega_2)\Big), \quad (4.13)$$

$$\frac{\partial a_{n_3}(\omega_3)}{\partial z} = (-i\beta_p - \gamma_p(n_3))\, a_{n_3}(\omega_3) - iC_p\Big(a_{n_3-1}(\omega_3) + a_{n_3+1}(\omega_3)\Big) + a_{n_3}(\omega_1)a_{n_3}(\omega_2). \quad (4.14)$$

where $a_{n_i}(\omega_i)$ is a mode amplitude in the n_ith waveguide with the ω_ith frequency $(i = 1, 2, 3)$.

It is easy to notice from the Eqs. (4.12), (4.13) that we can solve the eigenvalue-eigenmode problem for each mode i $(i = 1, 2)$ separately. We found the eigenmode problem for the signal/idler modes very similar to the one for the quantum process in Eq. (4.4). The full derivation of the eigenmode solution for the sum frequency generation in waveguide array with inhomogeneous losses is presented in Appendix B.2.

We search for the solution of the inhomogeneous array of equations for the output mode as

$$a_{n_3}(z) = \sum_{m_3} U_3\left(n_3, m_3\right) \mathrm{e}^{\lambda^p_{Cm_3} z} \Upsilon^{m_3}(z). \quad (4.15)$$

Here we present the final results for the $\Upsilon^{m_3}(z)$ which is the z dependent expansion function

$$\Upsilon^{m_3}_{n_1,n_2} = \frac{iz}{\det(U_1)\det(U_2)\det(U_3)} \times \sum_{m_1,m_2}\sum_{n_3} \mathrm{e}^{\frac{\left(\lambda^p_{Cm_3} - \lambda^s_{Cm_1} - \lambda^i_{Cm_2}\right)z}{2}} \mathrm{sinc}\left(\frac{\left(\lambda^p_{Cm_3} - \lambda^s_{Cm_1} - \lambda^i_{Cm_2}\right) z}{2}\right) \times \frac{U_3\left(n_3, m_3\right)}{\sum_q U_3^2\left(q, m_3\right)} U_1\left(n_3, m_1\right) \frac{U_1\left(n_1, m_1\right)}{\sum_l U_1^2\left(l, m_1\right)} U_2\left(n_3, m_2\right) \frac{U_2\left(n_2, m_2\right)}{\sum_p U_2^2\left(p, m_2\right)} \times E^s_{n_1} E^i_{n_2}, \quad (4.16)$$

$\tilde{\Phi}^{n_3}_{n_1,n_2}(\omega_3, z) = a_{n_3}(\omega_3, z; n_1, n_2)$ is the mode at the sum frequency at the output of the waveguide n_3, when we have input signal mode in the n_1 and idler mode in the n_2 waveguides, correspondingly. We receive the final results for the

mode propagating on the sum frequency as,

$$\tilde{\Phi}^{n_3}_{n_1,n_2}(\omega_3,z)=\frac{iz}{\det(U_1)\det(U_2)\det(U_3)}\times \sum_{m_3,m_2,m_1} \mathrm{e}^{\frac{\left(\lambda^p_{Cm_3}+\lambda^s_{Cm_1}+\lambda^i_{Cm_2}\right)z}{2}}\operatorname{sinc}\left(\frac{\left(\lambda^p_{Cm_3}-\lambda^s_{Cm_1}-\lambda^i_{Cm_2}\right)z}{2}\right)\times U_3\left(n_3,m_3\right)\frac{U_3\left(n_3,m_3\right)}{\sum\limits_k U_3^2\left(k,m_3\right)}U_1\left(n_3,m_1\right)\frac{U_1\left(n_1,m_1\right)}{\sum\limits_q U_1^2\left(q,m_1\right)}U_2\left(n_3,m_2\right)\frac{U_2\left(n_2,m_2\right)}{\sum\limits_l U_2^2\left(l,m_2\right)}\times E^s_{n_1}E^i_{n_2}. \tag{4.17}$$

It is easy to see that Eq. (4.17) and Eq. (4.8) express the three mode interaction which have very similar forms in terms of eigenmodes. Both quantum wave function $\Phi^{n_3}_{n_1,n_2}$ and the classical amplitude $\tilde{\Phi}^{n_3}_{n_1,n_2}$ depend on the number of the waveguides of the input and output modes and expressed through the same eigenmodes. The only difference is, that in case of SPDC the input is pump amplitude and outputs are signal and idler modes, while in the case of SFG the inputs are signal and idler modes and the output is the mode with the sum frequency, for better understanding the correspondence see Fig. 4.3.

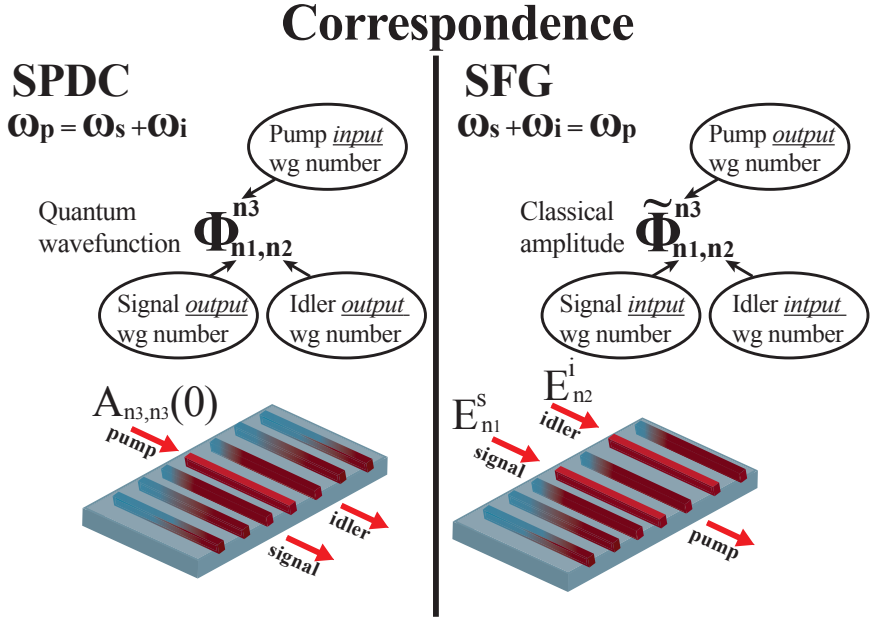

Figure 4.3: Scheme of correspondence between quantum wave function generated through spontaneous parametric down-conversion and classical amplitude from sum frequency generation.

4.3 SPDC in PT-coupler

Photonic structures consisting of coupled waveguides with regions of gain and loss offer many novel possibilities for shaping optical beams. PT-symmetry effect predictions are confirmed in experiments with light propagation in couplers with gains and losses [144]. One of the most interesting effects associated with this class of Hamiltonians is the emergence of a phase transition behavior arising from a spontaneous breakdown of PT-symmetry, after which the spectrum becomes complex [145, 146]. In this section we describe photon-pair generation through spontaneous parametric down-conversion (SPDC) in quadratic nonlinear couplers with linear absorption in one waveguide (see, Fig. 4.4(a)).

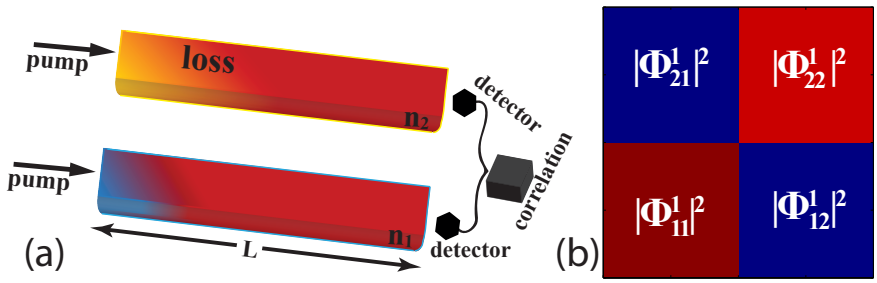

Figure 4.4: (a) Scheme of generation of photon pairs through the spontaneous parametric down-conversion in passive PT-symmetric nonlinear coupler with linear absorption in one waveguide. (b) Scheme of biphoton correlation function. Upper index n_3 of $|\Phi^{n_3}_{n_1,n_2}|^2$ stands for the input field waveguide number, while the bottom indices n_1 and n_2 show the waveguide number of signal and idler modes, respectively. We consider case where losses for signal and idler modes are equal $\gamma_s = \gamma_i$ which lead to the symmetry where anti-diagonal elements are equal $|\Phi_{1,2}|^2 = \Phi_{2,1}|^2$.

We discuss Schrödinger-type equations for the photon pair amplitudes Φ_{n_1,n_2} in the coupler (special case of Eq. (4.1)). Firstly we solve the homogenised array of equations and write Schrödinger-type equations for the for signal and idler modes in the coupler, which are the simplified forms of Eqs. (4.4)

$$\frac{\partial}{\partial z}\begin{pmatrix} u_1 \\ u_2 \end{pmatrix} = \begin{pmatrix} -\frac{i\Delta\beta}{2} & -iC_s \\ -iC_s & -\frac{i\Delta\beta}{2} - \gamma_s \end{pmatrix}\begin{pmatrix} u_1 \\ u_2 \end{pmatrix}. \tag{4.18}$$

$$\frac{\partial}{\partial z}\begin{pmatrix} v_1 \\ v_2 \end{pmatrix} = \begin{pmatrix} -\frac{i\Delta\beta}{2} & -iC_i \\ -iC_i & -\frac{i\Delta\beta}{2} - \gamma_i \end{pmatrix}\begin{pmatrix} v_1 \\ v_2 \end{pmatrix}. \tag{4.19}$$

We find eigenvalues and eigenmodes as it was done in Sec. 4.1 and find analytical expressions for the eigenvalues and eigenfunctions (Eq. (B.5)). The eigen-

values, for instance, of signal modes are found as

$$\lambda_1^s = \frac{1}{2}\left(-\gamma_s - \xi_1\right) - \frac{i}{2}\Delta\beta;$$
$$\lambda_2^s = \frac{1}{2}\left(-\gamma_s + \xi_1\right) - \frac{i}{2}\Delta\beta \tag{4.20}$$

where $\xi_1 = \sqrt{-4C_s^2 + \gamma_s^2}$ and $\xi_2 = \sqrt{-4C_i^2 + \gamma_i^2}$. It is easy to notice that the phase shift will happen if $-4C_s^2 + \gamma_s^2 < 0$, which means the symmetry breaking condition for the SPDC in the passive coupler is $\gamma > 2C$.

Eigenmodes of signal and idler modes are found as:

$$U_1 = \begin{pmatrix} 2iC_s & \gamma_s + \xi_1 \\ \gamma_s + \xi_1 & -2iC_s \end{pmatrix} \times \frac{1}{\sqrt{4C_s^2 + \gamma_s^2 + \xi_1\xi_1^* + \gamma_s(\xi_1 + \xi_1^*)}}, \tag{4.21}$$

$$U_2 = \begin{pmatrix} 2iC_i & \gamma_i + \xi_2 \\ \gamma_i + \xi_2 & -2iC_i \end{pmatrix} \times \frac{1}{\sqrt{4C_i^2 + \gamma_i^2 + \xi_2\xi_2^* + \gamma_2(\xi_2 + \xi_2^*)}}. \tag{4.22}$$

Here are presented the analytical results for the forms of the z dependent biphoton coefficients of the expansion in the mode space $B_{m_1,m_2}(z)$ at $z = L(m_1, m_2 = 1, 2$ are mode numbers) substituting Eq. (4.21) in Eq. (4.7)

$$B_{1,1}(L) = -\frac{L}{4}\left[\frac{-4A_1C_iC_s}{\xi_s\xi_i\left(\xi_s + \gamma_s\right)\left(\xi_i + \gamma_i\right)} + \frac{A_2}{\xi_s\xi_i}\right] e^{\left(\frac{iL(4\Delta\beta - i(\gamma_i + \gamma_s + \xi_i + \xi_s))}{4}\right)} \times \operatorname{sinc}\left(\frac{L(4\Delta\beta - i(\gamma_i + \gamma_s + \xi_i + \xi_s))}{4}\right),$$

$$B_{1,2}(L) = \frac{iL}{2}\left[\frac{A_1C_s}{\xi_i\xi_s\left(\xi_s + \gamma_s\right)} - \frac{A_2C_i}{\xi_s\xi_i\left(\xi_i + \gamma_i\right)}\right] e^{\left(\frac{iL(4\Delta\beta - i(\gamma_i + \gamma_s - \xi_i + \xi_s))}{4}\right)} \times \operatorname{sinc}\left(\frac{L(4\Delta\beta - i(\gamma_i + \gamma_s - \xi_i + \xi_s))}{4}\right),$$

$$B_{2,1}(L) = -\frac{iL}{2}\left[\frac{A_2C_s}{\xi_i\xi_s\left(\xi_s + \gamma_s\right)} - \frac{A_1C_i}{\xi_s\xi_i\left(\xi_i + \gamma_i\right)}\right] e^{\left(\frac{iL(4\Delta\beta - i(\gamma_i + \gamma_s + \xi_i - \xi_s))}{4}\right)} \times \operatorname{sinc}\left(\frac{L(4\Delta\beta - i(\gamma_i + \gamma_s + \xi_i - \xi_s))}{4}\right),$$

$$B_{2,2}(L) = \frac{L}{4}\left[\frac{-4A_2C_iC_s}{\xi_s\xi_i\left(\xi_s + \gamma_s\right)\left(\xi_i + \gamma_i\right)} + \frac{A_1}{\xi_s\xi_i}\right] e^{\left(\frac{iL(4\Delta\beta - i(\gamma_i + \gamma_s - \xi_i - \xi_s))}{4}\right)} \times \operatorname{sinc}\left(\frac{L(4\Delta\beta - i(\gamma_i + \gamma_s - \xi_i - \xi_s))}{4}\right). \tag{4.23}$$

We look at the dynamics of the biphoton functions along the waveguides below and above the PT-symmetric breaking threshold Fig. (4.5).

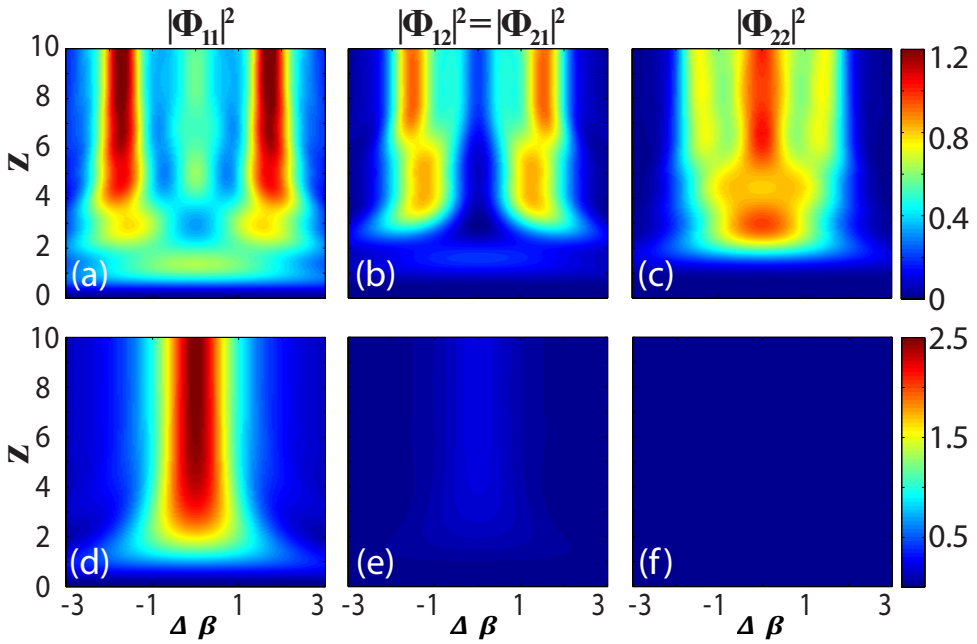

Figure 4.5: Behavior of the module square of biphoton function depending on the propagation direction and phase-mismatch. The coupling coefficients for signal and idler modes are $C_s = C_i = 1$. The pump is only in the first waveguide. $A_1 = 1, A_2 = 0$ and $L = 10$. (a,b,c) $\gamma_s = \gamma_i = 0.5$ losses are below the symmetry breaking threshold. (d,e,f) The PT-symmetry is broken as $\gamma_s = \gamma_i = 3$ over the symmetry breaking threshold. (a,d) Biphoton function when both photons are in the first waveguide. (b,e) Biphoton function with one photon in first waveguide and the another one in the second and (c,f) both photons are in the second lossy waveguide.

We assume that losses of signal (γ_s) and idler photons (γ_i) are equal to each other and equal γ and the corresponding coupling constants are equal, too ($C_s = C_i = C$). It is easy to notice that for the losses below PT-Symmetry breaking threshold ($\gamma < 2C$) there are efficient quantum walks in the system [see Fig. 4.5(a,b,c)]. Situation changes for losses over the threshold and quantum walks are suppressed [Fig. 4.5(d,e,f)].

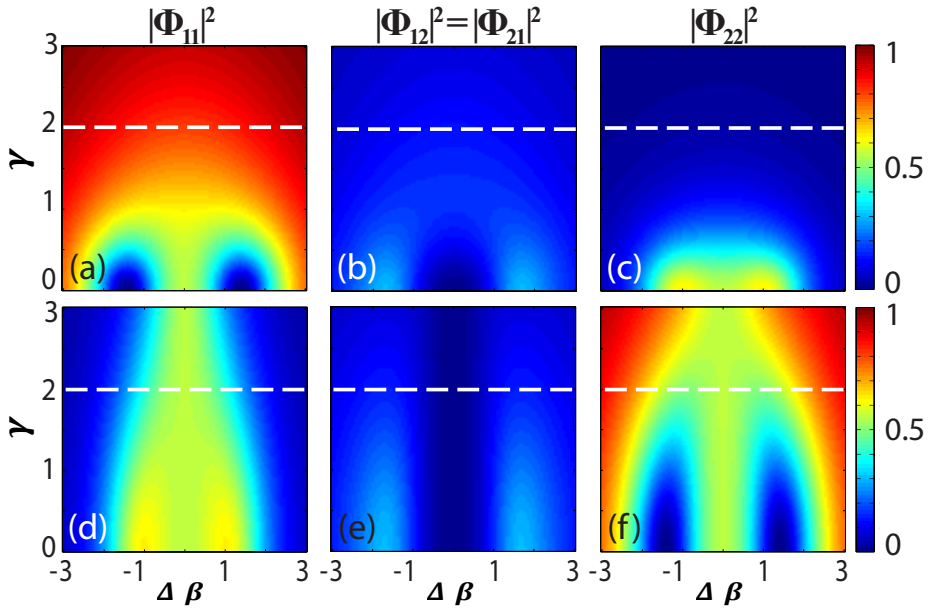

Figure 4.6: Biphoton function depending on losses and phase-mismatch in stationary regime ($z \to \infty$). (a,b,c) Pump is coupled to the waveguide without losses ($A_1 = 1, A_2 = 0$). (b,d,e) Pump is only in the waveguide with losses ($A_1 = 0, A_2 = 1$).

$\gamma = 2C$ appears to be a PT-symmetry breaking threshold for efficient quantum walks even in stationary regime. The photon pair correlations of biphotons in the waveguide without losses $\Gamma(1,1) = |\Phi_{1,1}|^2$ exhibits no dependence on losses when the pump is coupled to the same waveguide [Fig. 4.6(a)], but we see a drop in the amplitude for the other photon pair correlations $|\Phi_{1,2}|^2 = |\Phi_{2,1}|^2$ [Fig. 4.6(b)] and $|\Phi_{2,2}|^2$ [Fig. 4.6(c)]. Similar dynamics are observed in the system where the pump is coupled to the waveguide with losses [Fig. 4.6(d,e,f)].

4.4 SFG in PT-coupler

Here we discuss a specific case of the process presented in Sec. 4.2, namely, SFG in the PT-coupler consisting of one conservative and one lossy waveguide (see, Fig. 4.7(a)). We rewrite the coupled mode equations Eqs. (B.13) explicitly for the coupler in the matrix form for each mode as follows

$$\frac{\partial}{\partial z}\begin{pmatrix} a_1(\omega_1) \\ a_2(\omega_1) \end{pmatrix} = \begin{pmatrix} -i\beta_s & -iC_s \\ -iC_s & -i\beta_s - \gamma_s \end{pmatrix}\begin{pmatrix} a_1(\omega_1) \\ a_2(\omega_1) \end{pmatrix}. \tag{4.24}$$

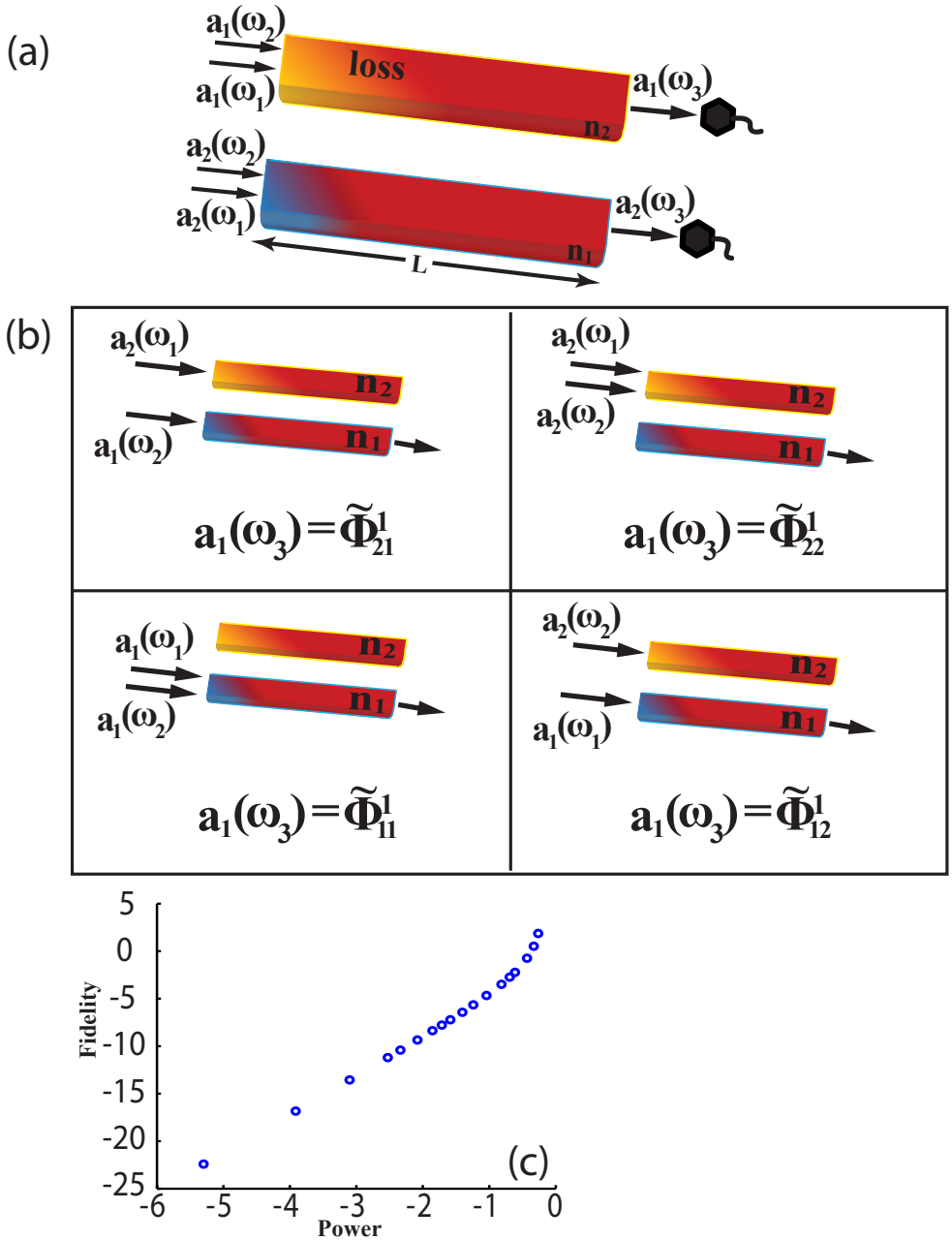

Figure 4.7: (a) Scheme of sum frequency generation in passive PT-symmetric nonlinear coupler with linear absorption in one waveguide. (b) Schematic correspondence between biphoton function and the mode at sum frequency generated through SFG ($\tilde{\Phi}^{n_3}_{n_1,n_2}(\omega_3, z) = a_{n_3}(\omega_3, z; n_1, n_2)$ see Appendix B.2 for details). (c) Fidelity of the SPDC and SFG correlation depending on the input power. Both Fidelity and the power are on a logarithmic scale with base 10.

We solve an eigenmode problem as in the previous section and find corre-

sponding eigenvalues as,

$$\lambda^s_{C1} = \frac{1}{2}\left(-2i\beta_s - \gamma_s - \xi_1\right),$$
$$\lambda^s_{C2} = \frac{1}{2}\left(-2i\beta_s - \gamma_s + \xi_1\right). \tag{4.25}$$

The form of the eigenvectors for the SFG is coinside with the ones for SPDC in Eq. (4.21).

Fig. 4.7(b) illustrates correspondence between the mode generated through SFG at the output of first waveguide and the biphoton function generated in SPDC pumped in the first waveguide (see Fig. 4.4(b)), with precision up to the input pump field amplitudes. We looked at the normalized fidelity of the SPDC conversion predicted by SFG depending on the input power [see Fig. 4.7(c)]. We define the power of the SFG as $P^{n_1,n_2} = |E^s_{n_1}|^2 + |E^i_{n_2}|^2$ where $E^{s,i}$ are the input pump amplitudes for the signal and idler modes and the fidelity is $\sum_{n_1,n_2,n_3} |\tilde{\Phi}^{n_3}_{n_1,n_2} - \Phi^{n_3}_{n_1,n_2}|^2$, where $\tilde{\Phi}^{n_3}_{n_1,n_2}$ is a solution of the full coupled mode equations (4.9-4.11).

In Sec. 4.2 we have shown the exact matching of the bi-photon function generated SPDC and the modes at the sum frequency generated in SFG in the low conversion approximation Eqs. (4.17) and (4.8). Fig. 4.7(c) shows the possibility to predict the conversion efficiency of SPDC through the SFG with very good precision if the pump amplitudes are not very strong.

In this chapter we have performed analytical and numerical analysis of the quantum spontaneous parametric down-conversion and sum frequency generation in nonlinear lossy waveguide arrays. We have analysed the behaviour of the SPDC and SFG in the passive PT-symmetric coupler and compared the results. We have shown that the PT-symmetry breaking threshold significantly affects the quantum walks of the signal and idler photon pairs generated trough SPDC.

Our results can be used for the further research of phenomena in PT-symmetric plasmonic [147, 148] and metamaterial [147] structures, which have attracted interest in recent years. Metamaterials allow considerable control over the electric and magnetic fields of light, so that permittivities, permeabilities, and refractive indices can be tuned to have positive, negative, and near-zero values. Metamaterials have enabled negative refraction perfect optical lensing [149, 150] and invisibility cloaking [151, 152]. Complementarily, PT -symmetric media allow control over electromagnetic field distributions in loss and gain media, so that light propagation can be asymmetric and even unidirectional. Metamaterials, whose optical properties are determined both by their subwavelength building blocks and a reasonable choice of their loss/gain profile would enable unprecedented control over electric and magnetic optical fields across wavelength and subwavelength scales, and may enable an entirely new class of bulk synthetic

photonic media [147].

Chapter 5

Optical parametric amplification in parity-time symmetric couplers

Parametric amplifiers are commonly used as an integral part of optical setups enabling flexible wavelength conversion and tunable signal gain, extending the range of lasers where gain media are limited to particular wavelengths. Wave amplification is efficiently realized in the regime of difference-frequency generation in media with quadratic optical nonlinearity [2]. Importantly, the amplification rate is determined by the pump, enabling ultrafast all-optical tunability. In this work, we reveal the potential of PT-symmetric systems for optical parametric amplification, and identify a new regime of spectral PT anti-symmetry in such devices. Such devices can, on one hand, realize ultrafast spatial signal switching through pump-controlled breaking of PT symmetry, and on the other hand enable spectrally-selective mode amplification in analogy with PT lasers.

In the linear regime, at low light intensities, such coupler realizes PT-symmetric optical system [81]. However at higher intensities the effect of quadratic nonlinear interactions becomes important. It was predicted that in the regime of second-harmonic generation, when the signal and idler waves have identical spectra at half of the pump frequency, parametric interactions in PT couplers can support a rich variety of nonlinear modes [153]. Furthermore, formation of quadratic solitons in spatially extended PT-symmetric structures was analyzed in detail [154, 155]. However, the fundamentally important regime of parametric amplification in PT systems remained unexplored.

This chapter is devoted to detailed analysis of parametric amplification in PT systems. It has been identified a distinct spectral parity time anti-symmetry associated with optical parametric interaction, and has been shown that pump-controlled symmetry breaking can facilitate spectrally selective mode amplification in analogy with PT lasers. It has been also establish a connection between breaking of spectral and spatial mode symmetries, revealing the potential to

implement unconventional regimes of spatial light switching through ultrafast control of PT breaking by pump pulses.

5.1 Spectral anti-PT symmetry

We analyze the process of optical parametric amplification based on nonlinear mixing between a strong pump, and signal and idler waves, as illustrated in Fig. 5.1. We model the wave propagation using coupled-mode equations [2] in the regime of narrowband and undepleted pump,

$$\begin{aligned}
i\frac{\partial E_{s1}}{\partial z} &= -\beta_{s1}E_{s1} - i\gamma_{s1}E_{s1} - C_sE_{s2} + i\chi_1E_{p1}E_{i1}^*,\\
i\frac{\partial E_{s2}}{\partial z} &= -\beta_{s2}E_{s2} - i\gamma_{s2}E_{s2} - C_sE_{s1} + i\chi_2E_{p2}E_{i2}^*,\\
i\frac{\partial E_{i1}}{\partial z} &= -\beta_{i1}E_{i1} - i\gamma_{i1}E_{i1} - C_iE_{i2} + i\chi_1E_{p1}E_{s1}^*,\\
i\frac{\partial E_{i2}}{\partial z} &= -\beta_{i2}E_{i2} - i\gamma_{i2}E_{i2} - C_iE_{i1} + i\chi_2E_{p2}E_{s2}^*,\\
i\frac{\partial E_{p1}}{\partial z} &= -\beta_{p1}E_{p1} - i\gamma_{p1}E_{p1} - C_pE_{p2},\\
i\frac{\partial E_{p2}}{\partial z} &= -\beta_{p2}E_{p2} - i\gamma_{p2}E_{p2} - C_pE_{p1}.
\end{aligned} \tag{5.1}$$

Here the subscripts stand for signal ('s'), idler ('i'), and pump ('p') waves in the two waveguides ('1' and '2'), E are the mode amplitudes, z is the propagation distance along the waveguides, β are the propagation constants (for the pump mode, the propagation constant is adjusted to account for quasi-phase-matching through periodic waveguide poling [2]), γ are the linear loss coefficients, C are the mode coupling coefficients between the waveguides, and χ are effective quadratic nonlinear coefficients. Here we also assume that fundamental pump mode does not couple between the waveguides [48].

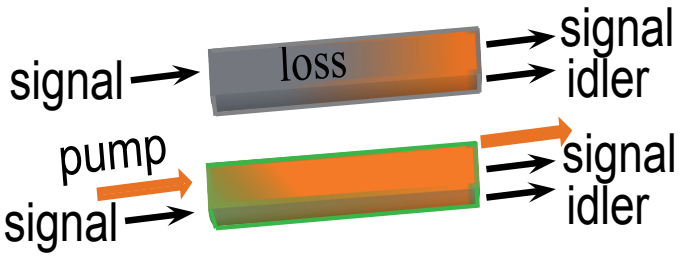

Figure 5.1: Scheme of PT-symmetric nonlinear coupler with linear absorption in one waveguide.

We find that PT-symmetry in the regime of parametric amplification can be achieved in a near-degenerate case when the waveguide parameters are practically

the same at signal and idler frequencies, i.e. $\gamma_{i1} = \gamma_{s1} = \gamma_1$, $\gamma_{i2} = \gamma_{s2} = \gamma_2$, and $C_s = C_i = C$. We assume that the waveguides are engineered such that $\beta_{s1} = \beta_{s2} = \beta_s$ and $\beta_{i1} = \beta_{i2} = \beta_i$, which is the regime required for linear PT-symmetry as demonstrated experimentally [81, 82]. Under usual experimental conditions the mode at higher pump frequency is much stronger localized compared to signal an idler [48], leading to suppressed coupling between the waveguides and also very small sensitivity to metal deposited on top of waveguides, meaning that $C_p \equiv 0$ and $\gamma_{p1} = \gamma_{p2} = 0$. We further consider a case of equal QPM-adjusted pump propagation constants in two waveguides, $\beta_{p1} = \beta_{p2} = \beta_p$, which can be achieved by designed the waveguide parameters or poling the waveguides with different periods. The latter condition does not need to be satisfied if pump is coupled to one waveguide, which already enables full range of mode switching and amplification control as we demonstrate in the following.

To reveal the PT-symmetry properties of Eqs. (5.1), we represent the equations for signal and idler waves in the Schredinger type equation,

$$i\frac{\mathrm{d}\mathbf{a}}{\mathrm{d}z} = \mathcal{H}\mathbf{a}, \tag{5.2}$$

where

$$\mathbf{a}(z) = \begin{pmatrix} a_{s1}(z) \\ a_{s2}(z) \\ a^*_{i1}(z) \\ a^*_{i2}(z) \end{pmatrix} = \begin{pmatrix} E_{s1}(z)e^{-i(\beta+\beta_s)z} \\ E_{s2}(z)e^{-i(\beta+\beta_s)z} \\ E^*_{i1}(z)e^{i(\beta+\beta_i)z} \\ E^*_{i2}(z)e^{i(\beta+\beta_i)z} \end{pmatrix}, \tag{5.3}$$

and

$$\mathcal{H} = \begin{pmatrix} \beta - i\gamma_1 & -C & iA_1 & 0 \\ -C & \beta - i\gamma_2 & 0 & iA_2 \\ iA_1^* & 0 & -\beta - i\gamma_1 & C \\ 0 & iA_2^* & C & -\beta - i\gamma_2 \end{pmatrix}, \tag{5.4}$$

where $\beta = (\beta_p - \beta_s - \beta_i)/2$ defines the phase mismatch of parametric wave mixing, and $A_{1,2}$ are the normalized input pump amplitudes, $A_1 = \chi_1 E_{p1}(z = 0)$ and $A_2 = \chi_1 E_{p2}(z = 0)$.

A key result of our analysis is that the Hamiltonian $\mathcal{H}$ possesses a *spectral anti-PT symmetry*, corresponding to a negative sign on the right-hand side of the following equality,

$$\mathcal{P}_{1,+}\mathcal{P}_{2,+}\mathcal{T}\mathcal{H} = -\mathcal{H}\mathcal{P}_{1,+}\mathcal{P}_{2,+}\mathcal{T}. \tag{5.5}$$

The term anti-PT symmetry was used to underline the sign difference between the general commutation relation for PT symmetric Hamiltonian presented in Eq. (1.9) and Eq. (5.5). Here $\mathcal{T}$ is a time-reversal operator which changes $z \to -z$ and performs a complex conjugation. The *parity operators operate in spectral*

domain, interchanging the signal and idler waves,

$$\mathcal{P}_{1,\pm} = \{a_{s1} \leftrightarrow \pm a_{i1}^*\}\,,\ \mathcal{P}_{2,\pm} = \{a_{s2} \leftrightarrow \pm a_{i2}^*\}\,. \tag{5.6}$$

We define the parity operators with both symmetric ('+') and antisymmetric ('-') transformations, since the latter will be useful in the following analysis. We note that such unusual symmetry is fundamentally different from the previously studied antisymmetric PT-metamaterials with modulated dielectric and magnetic properties [156].

Since the Hamiltonian is linear in the undepleted pump regime, the dynamics of signal and idler waves is defined by the eigenmode solutions,

$$\mathbf{a}(z) = \widetilde{\mathbf{a}}(\sigma)\exp(i\sigma z), \tag{5.7}$$

where σ is an eigenvalue. The real part, $\mathrm{Re}\,(\sigma)$, defines the phase velocity, whereas the imaginary part determines the modal gain, $\Gamma = -\mathrm{Im}(\sigma)$.

We now determine the effect of spectral anti-PT symmetry on the eigenmode properties by substituting Eq. (5.7) into Eq. (5.2) and applying PT operator. We obtain that if $\widetilde{\mathbf{a}}(\sigma)$ is an eigenmode, then $\widetilde{\mathbf{a}}(-\sigma^*) = \mathcal{P}_{1,+}\mathcal{P}_{2,+}\mathcal{T}\widetilde{\mathbf{a}}(\sigma)$ is also an eigenmode. There are two possibilities how these relations can be satisfied. First, the mode can be PT-symmetric, when PT transformation maps the mode profile to itself (up to an overall phase), which happens if $-\sigma^* = \sigma$, and accordingly $\mathrm{Re}(\sigma) = 0$. Such *spectrally PT-symmetric modes would generally experience gain/loss different from other modes*, since there are no specific relations for the value of $\mathrm{Im}(\sigma)$. Second, if the mode profile has broken PT-symmetry, the PT transformation relates two different modes with eigenvalues $\sigma_2 = -\sigma_1^*$. It follows that *a pair of spectrally PT-broken modes experience the same loss or gain*, $\mathrm{Im}(\sigma_1) = \mathrm{Im}(\sigma_2)$, but they have different phase velocities, $\mathrm{Re}(\sigma_1) = -\mathrm{Re}(\sigma_2)$. Remarkably, the established relations of mode symmetry and gain/loss are reversed in comparison to previously studied spatial PT-symmetry in directional couplers [81, 82], due to the spectral anti-PT symmetry of parametric wave mixing.

We now demonstrate that the modal PT-breaking can be controlled by the pump beam. Due to the electronic nature of quadratic nonlinearity, such tuning can be ultrafast, directly following the pump profile in real time [2]. Overall, there are four eigenmodes of the Hamiltonian. Accordingly, there can be three possible symmetry regimes: (i) there are two mode pairs with broken PT-symmetry, (ii) one pair of PT-broken modes and a pair of PT-symmetric modes, or (iii) two pairs of PT-symmetric modes. The eigenvalues which are solutions of quartic equations from Hamiltonian (5.4) are cumbersome to analyze. That is why as an example, we present numerical analysis of the mode properties in a coupler with loss in the second waveguide, and pump coupled to the first waveguide. We

show the largest mode gain $\Gamma = \mathrm{Max}[-\mathrm{Im}(\sigma)]$ in Figs. 5.2(a,b) and the number of PT-symmetric mode pairs in Figs. 5.2(c,d), depending on the pump amplitude A_1 and the phase-mismatch, for different values of linear loss.

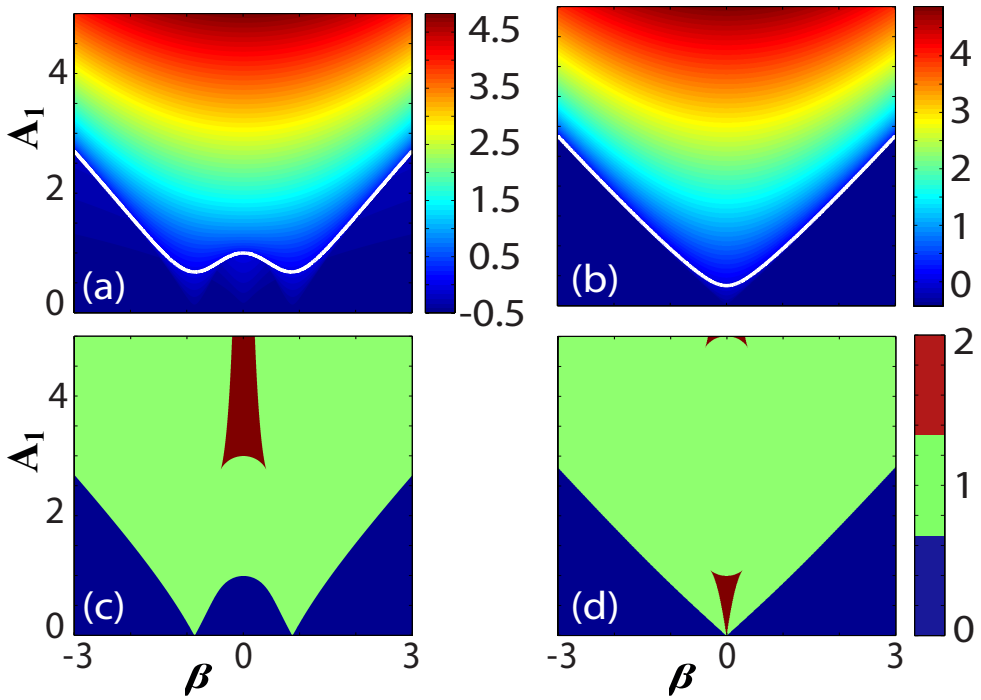

Figure 5.2: a,b) The largest mode gain (white line marks a zero gain level) and (c,d) number of PT-symmetric mode pairs vs. the input pump and the phase-mismatch. The linear losses are (a,c) $\gamma_{2s} = \gamma_{2i} = 1$, (b,d) $\gamma_{2s} = \gamma_{2i} = 3$. For all the plots $\gamma_{1s} = \gamma_{1i} = 0$, $C = 1$ and $A_2 = 0$.

We observe that in the regime when all modes have broken spectral PT symmetry [blue shaded regions in Figs. 5.2(c,d)], the modes experience negative gain [c.f. Figs. 5.2(a,b)]. This happens because pairs of eigenmodes exhibit the same amount of gain/loss, and effectively the amounts of gain and loss are averaged out between the eigenmodes. However upon transition to the region with spectrally PT-symmetric modes [green and red shaded regions in Figs. 5.2(c,d)], there appears an unequal redistribution of gain and loss between the modes. One PT-symmetric eigenmode exhibits gain much larger then all other modes, while the latter experience stronger loss. Such sensitivity of amplification to PT-breaking threshold could be used to discriminate between multiple spectral modes, analogous to the concept of PT-lasers [87, 88].

5.2 Spatial symmetries and switching

We now establish a connection between the spectral PT-symmetry identified above, and the spatial wave dynamics due to waveguide coupling. We first con-

sider a special case which can be treated analytically, corresponding to perfect phase-matching, $\beta = 0$, and additionally $\mathrm{Im}(A_1^* A_2) = 0$. The latter condition can be transformed to $\mathrm{Im}(A_1) = \mathrm{Im}(A_2) = 0$ under a substitution

$$\begin{pmatrix} a_{s1}(z) \\ a_{s2}(z) \\ a_{i1}(z) \\ a_{i2}(z) \end{pmatrix} = \exp(i\varphi) \begin{pmatrix} a_{s1}(z) \\ a_{s2}(z) \\ a_{i1}(z) \\ a_{i2}(z) \end{pmatrix}, \tag{5.8}$$

with appropriately chosen constant phase φ Then, we find that

$$\mathcal{P}_{1,+}\mathcal{P}_{2,-}\mathcal{H} = \mathcal{H}\mathcal{P}_{1,+}\mathcal{P}_{2,-}, \tag{5.9}$$

$$\mathcal{P}_{1,-}\mathcal{P}_{2,+}\mathcal{H} = \mathcal{H}\mathcal{P}_{1,-}\mathcal{P}_{2,+}. \tag{5.10}$$

Accordingly, there appear two pairs of eigenmodes which profiles satisfy the first or second symmetry, respectively. Remarkably, the signal dynamics is governed by equations resembles those for a linear PT-symmetric coupler [81, 82]:

$$i\frac{\mathrm{d}\mathbf{a}_s}{\mathrm{d}z} = \mathcal{H}_r \mathbf{a}_s,\ \mathcal{H}_r = \begin{pmatrix} i(\eta A_1 - \gamma_1) & -C \\ -C & i(-\eta A_2 - \gamma_2) \end{pmatrix}, \tag{5.11}$$

where $\mathbf{a}_s = (a_{s1}; a_{s2})$, $\eta = +1$ or $\eta = -1$ for the modes with symmetries according to Eq. (5.9) or (5.10), respectively. If $\mathcal{H}$ is exactly PT symmetric, then its eigenmodes $\mathbf{a}$ are simultaneously the eigenstates of the corresponding $\mathcal{P}_{1(2),+(-)}$ symmetry operators. Therefore we require $a_{i1}^* = \eta a_{s1}$ and $a_{i2}^* = -\eta a_{s2}$, which reduces Hamiltonian (5.4). We see that the linear loss is modified due to the parametric gain determined by the pump amplitudes. The coupler Eqs. ((5.11)) are symmetric with respect to *spatial PT-symmetry*, up to a gauge transformation [81] expressed through the identity matrix ($\mathcal{I}$) in the following relation,

$$\mathcal{P}_{12}\mathcal{T}(\mathcal{H}_r - \bar{\rho}\,\mathcal{I}) = (\mathcal{H}_r - \bar{\rho}\,\mathcal{I})\mathcal{P}_{12}\mathcal{T}, \tag{5.12}$$

where the *spatial parity operator* $\mathbf{P}_{12}$ swaps the mode amplitudes between the waveguides, $a_{s1} \leftrightarrow a_{s2}$ and $a_{i1} \leftrightarrow a_{i2}$. The coefficient $\bar{\rho} = (\eta A_1 - \gamma_1)/2 + (-\eta A_2 - \gamma_2)/2$ defines the average gain or loss between the two waveguides, which depends on the pump amplitudes and signal/idler mode symmetries corresponding to the different sign 'η'. The mode eigenvalues are

$$\sigma = -i\bar{\rho} \pm (1/2)\sqrt{4C^2 - [\gamma_1 - \gamma_2 - \eta(A_1 + A_2)]^2}. \tag{5.13}$$

We present characteristic dependencies of the eigenvalues on the pump amplitude in the first waveguide in Fig. 5.3. Both *spatial and spectral PT-symmetry breaking occurs simultaneously* at the threshold $|\gamma_1 - \gamma_2 - \eta(A_1 + A_2)| = 2C$. For the

parameter values in Figs. 5.4(a,b), the threshold amplitude is $A_1 = 1$ for $\eta = +1$ and $A_1 = 3$ for $\eta = -1$. However, the spatial and spectral symmetries are opposite: a mode pair is spatially PT-symmetric and has spectrally broken symmetry below threshold, whereas the situation is reversed above the threshold.

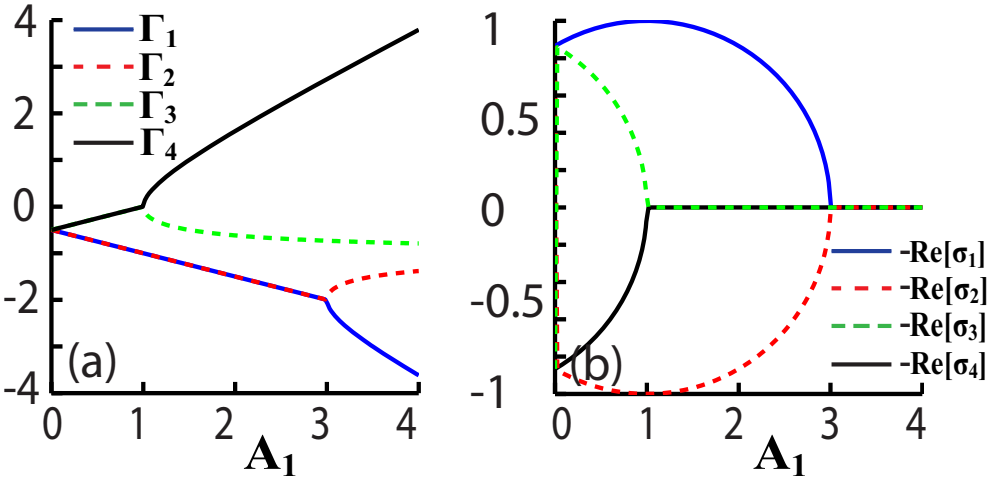

Figure 5.3: Mode eigenvalues vs. the pump amplitude in the first waveguide ($A_2 = 0$): a) Negative imaginary part defining mode amplification, $\Gamma = -\mathrm{Im}(\sigma)$, and (b) Real part defining propagation constant, $Re(\sigma)$. Parameters are $\gamma_{1s} = \gamma_{1i} = 0$, $\gamma_{2s} = \gamma_{2i} = 1$, $C = 1$, and $\beta = 0$.

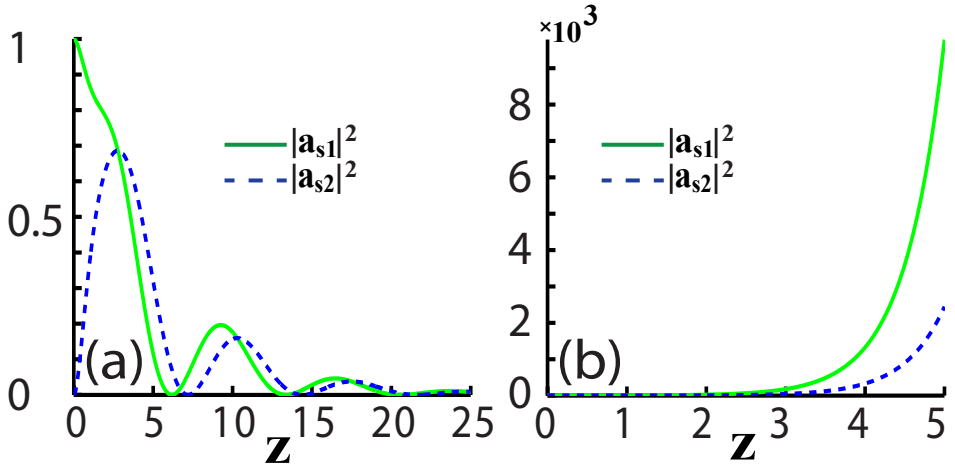

Figure 5.4: Evolution of the signal mode intensity along the waveguides: solid (green) lines — the first waveguide without loss, dashed (blue) line — the second waveguide with loss. The pump amplitude is (a) below PT-symmetry breaking threshold ($A_1 = 0.5$) and (b) above threshold ($A_1 = 1.5$). Parameters are $\gamma_{1s} = \gamma_{1i} = 0$, $\gamma_{2s} = \gamma_{2i} = 1$, $C = 1$, and $\beta = 0$.

We show the evolution of the signal and idler intensities along the waveguides in Fig. 5.4. At lower pump powers [Figs. 5.4(a)] signal and idler periodically switch between the waveguides due to a beating between two modes exhibiting the same (negative) gain. However for stronger pump above the PT threshold [Figs. 5.4(b)], only one supermode with the strongest gain dominates and accordingly oscillations are suppressed.

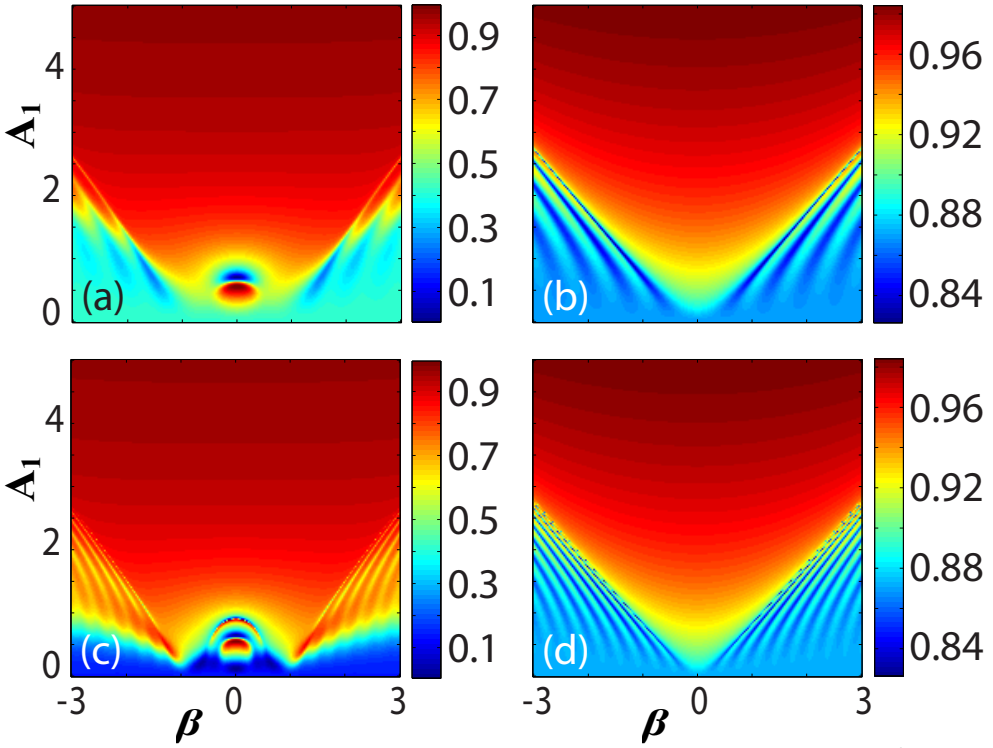

Figure 5.5: Fraction of signal intensity in the first waveguide, $|a_{s1}|^2/(|a_{s1}|^2 + |a_{s2}|^2)$, vs. the pump amplitude in the first waveguide and the phase-mismatch. Propagation distances are (a,b) $L = 5C$ and (c,d) $L = 10C$. Parameters correspond to (a,c) Figs. 5.2(a,c) and (b,d) Figs. 5.2(b,d).

Finally, we investigate numerically a connection between spectral PT-breaking and spatial mode dynamics in a general case of non-zero phase mismatch. We present in Fig. 5.5 the fraction of signal intensity in the first waveguide depending on the phase-mismatch and the pump amplitude for different propagation distances. We find that spatial dynamics strongly depends on the spatial PT-symmetry of modes in the linear regime (at low pump amplitudes $A_j \to 0$). The linear modes are PT-symmetric if $|\gamma_1 - \gamma_2| < 2C$, and then the pump amplitude can control the period of mode coupling between the waveguides, while the oscillations get suppressed close to the spectral PT threshold, see Figs. 5.5(a,c) and Fig. 5.2(c). However if the linear modes are PT-broken for $|\gamma_1 - \gamma_2| > 2C$, then mode beating between the waveguides still occurs below the spectral PT

threshold, but with very small modulation amplitude, see Figs. 5.5(b,d) and Fig. 5.2(d). In all cases, the mode beating changes faster with pump amplitude at longer distances.

In conclusion, we have identified an anti-PT spectral symmetry of a parametric amplifier based on a quadratically nonlinear coupler with different losses in two waveguides. For pump powers below a threshold the modes form pairs with broken PT symmetry and same gain/loss, whereas above the threshold one PT-symmetric mode experiences the largest gain. This can facilitate spectrally-selective mode amplification, and we expect that this effect will become even more pronounced in resonator structures in analogy with single-mode operation of PT microring lasers [87, 88]. We have established an underlying connection between spectral anti-PT and conventional spatial PT mode symmetries, which reveals the possibility to control spatial light switching and amplification through parametric gain. Accordingly, the suggested platform can implement various unconventional regimes of light control previously suggested for PT-symmetric structures, such as unidirectional [79] and nonreciprocal [157] operation, but with the advantage of ultrafast all-optical control of PT-symmetry regimes by pump pulses. We anticipate that, due to the universality of parametric amplification processes, these concepts will be extended to different physical mechanisms including Kerr-type optical nonlinearity.

Chapter 6

Single-photon down-conversion in nonlinear waveguide arrays

All the previous chapters analyse behaviour of the quantum and classical processes described by the non-Hermitian Hamiltonian. In this chapter, we describe SPDC in a nonlinear WGA for a single-photon pump, applying quantum pump description and taking into account possible pump depletion. It was suggested that on-chip generation of entangled photons is possible with nonlinear waveguide arrays (WGAs), which can efficiently produce entangled photon pairs and simultaneously shape their spatial correlations through quantum walks [56]. So far, only the regime of a strong classical pump coupled to a nonlinear WGA was studied [47, 56, 57, 158]. However, investigation of nonlinear effects in a few-photon regime can lead to fundamental and ultimately technological advances. All processes described in the current chapter are characterized by the Hermitian Hamiltonian, we didn't include any losses in the system but important experimental results include two-photon sum-frequency generation [159, 160] and SPDC with a single-photon pump [161]. Generation of photon triplets using cascaded spontaneous parametric down-conversion detected rate of triplets as 4.7±0.6 counts per hour. Recently, coherent single-photon conversion has been demonstrated based on a four-wave-mixing interaction which mimicked SPDC process in a quadratic crystals [162], which can lead to optically switchable quantum circuits with a complete control over individual photons. The coherent photon conversion corresponds to a pair detection rate (for $4.8\mu W$ of effective power in the 710-nm input) of 1.45±0.02 pairs per second per milliwatt of 532-nm pump power.

In this chapter we discuss the dynamics of pump and generated photons and find very interesting behavior of compression of Rabi-like oscillations. The Rabi cycle is defined initially for the two-level quantum system. When light interacts with a two-level system this can lead to a periodic exchange of energy between the light field and the two-level system. Rabi oscillation is a cyclic process of emitting

and re-absorbing of light photon, which an atom exhibits with the application of a coherent beam at resonant frequency. Then the atom undergoes Rabi flipping between upper and lower states and consequently the population in each state will oscillate in time with the Rabi frequency which is independent of the frequency of the applied electromagnetic field, rather depends linearly on the strength of the field and the dipole matrix element of transition. These are oscillations of the quantum mechanical expectation values of level populations and photon numbers. Coupled waveguides/arrays mimic and visualize dynamical features of discrete quantum systems with similar structures in their physical behaviour and mathematical formalism. The possibility of Rabi oscillations is exhibited theoretically in the waveguide array on the basis of intra-band Flocuet - Bloch modes oscillation [163], by considering adiabatic transitions between confined modes in properly modulated waveguide structure [164], and on the basis of specially modulated and alternately coupled linear waveguide array [165].

6.1 Rabi-like oscillations compression and spectral dispersion

First we study the properties of the SPDC process in a single nonlinear waveguide [Fig. 6.1(a)]. The Hamiltonian of the system can then be written as follows [7, 62]:

$$\begin{aligned}\hat{H} = &\int d\omega_p \int d\omega_s \int d\omega_i \left[\chi a_p(\omega_p) a_s^\dagger(\omega_s) a_i^\dagger(\omega_i) + \chi^* a_p^\dagger(\omega_p) a_s(\omega_s) a_i(\omega_i)\right] \\ &+ \int d\omega_p \beta_p(\omega_p) a^\dagger(\omega_p) a_p(\omega_p) + \int d\omega_s \beta_s(\omega_s) a_s^\dagger(\omega_s) a_s(\omega_s) \\ &+ \int d\omega_i \beta_i(\omega_i) a_i^\dagger(\omega_i) a_i(\omega_i),\end{aligned} \tag{6.1}$$

where a_j ($a_j^\dagger$) are annihilation (creation) operators for pump, signal and idler modes ($j = p, s, i$), ω_j and β_j are the corresponding frequencies and mode propagation constants in a waveguide, and χ is the effective nonlinear susceptibility coefficient.

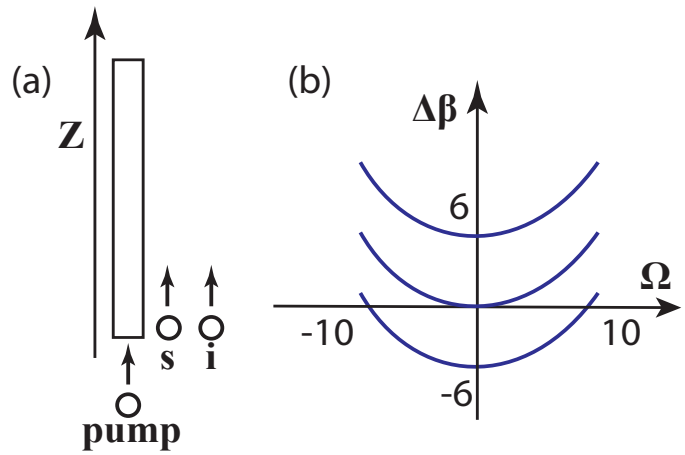

Figure 6.1: (a) Scheme of SPDC for single-photon pump in a quadratic nonlinear waveguide. At the input we have singe "pump" photon represented by circle titled as pump and the arrow shows its propagation direction. The circles titled s and i are signal and idler photons generated through SPDC and arrows again show their propagation direction. (b) Three kinds of possible phase-matching conditions : (1) $\Delta\beta_0 = -6$, non-degenerate SPDC favoring $\omega_s \neq \omega_i$, (2) $\Delta\beta_0 = 0$, degenerate SPDC favoring $\omega_s \simeq \omega_i$, and (3) $\Delta\beta_0 = 6$, phase-mismatched SPDC.

We analyze the process when a single pump photon is converted into a signal photon and an idler photons. We consider the case of a pump photon with long temporal duration, and accordingly narrow spectrum. However, the spectra of signal and idler photons can be much broader. Then, we seek the wave function describing the evolution of photon states in a form similar to Refs. [162, 166], but accounting for spectra of photons:

$$\begin{aligned} |\psi\rangle =& e^{i\beta_U z}\int_{-\infty}^{\infty} d\omega_p \Big[U(z)S(\omega_p)a_p^\dagger(\omega_p) + \int_{-\infty}^{\infty} d\Omega V(\Omega,z) \\ &\times S(\omega_p)a_s^\dagger(\omega_p/2+\Omega)a_i^\dagger(\omega_p/2-\Omega)\Big]|0\rangle, \end{aligned} \tag{6.2}$$

Here U is the pump amplitude, V is the biphoton amplitude, $S(\omega_p)$ is the pump spectral distribution that is normalized as $\int d\omega_p |S(\omega_p)|^2 = 1$, Ω is the detuning of signal and idler photons as $\omega_s = \omega_p/2 + \Omega$ and $\omega_i = \omega_p/2 - \Omega$, $\beta_U = \beta_p$ at the central pump frequency, and $|0\rangle$ is the vacuum state. Note that U and V are considered to be independent on ω_p for a narrowband single-photon pump. According to the field quantization [9], the integration should be performed over positive frequencies. Then, the integration limits in Eq. (6.2) are from 0 to ∞ for ω_p. We assume that $V(\Omega, z)$ is non-zero only for $|\Omega \ll \omega_p|$, and formally consider integration over Ω for the whole interval $(-\infty, \infty)$ to simplify mathematical notations.

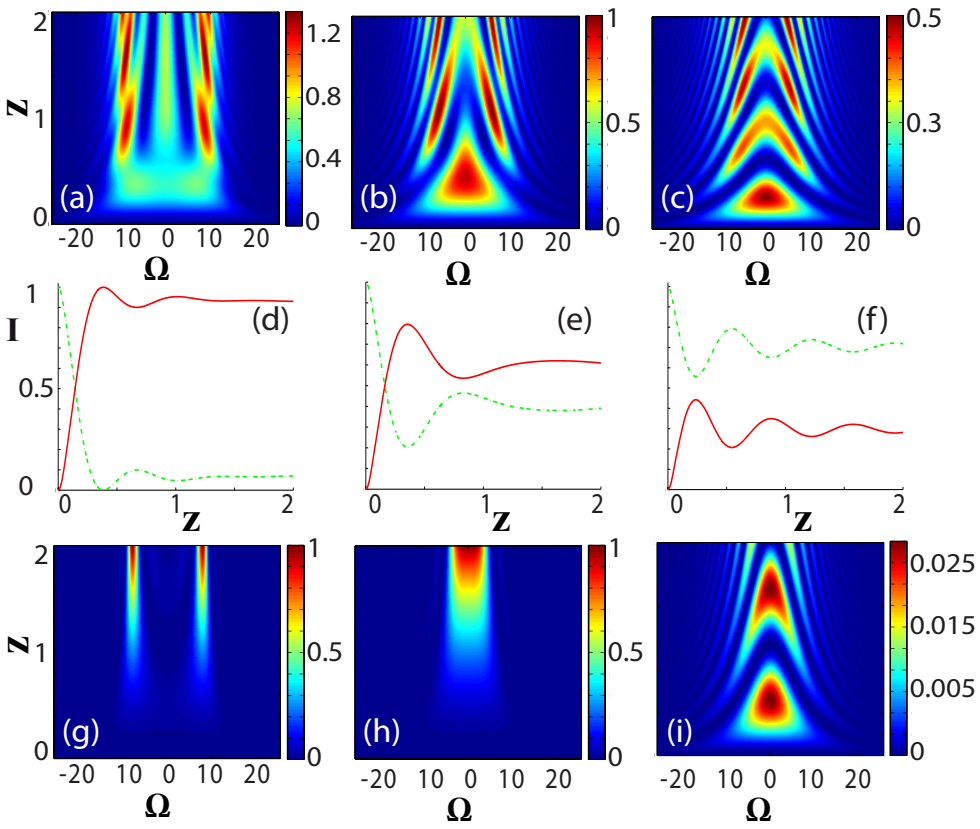

Figure 6.2: (a,b,c) Biphoton intensity I_V depending on propagation distance and frequency for different phase-matching conditions; (d,e,f) Pump intensity I_p (dashed line) and signal (or idler) intensity $\tilde{I}_V$ (solid line); (g,h,i) Biphoton intensities depending on propagation distance and frequency for classical undepleted pump $U(z) \equiv$ const. The phase-matching parameters are (a,d,g) $\Delta\beta_0 = -6$; (b,e,h) $\Delta\beta_0 = 0$ and (c,f,i) $\Delta\beta_0 = 6$.

The wavefunction $|\psi\rangle$ for the SPDC obeys the Schrödinger equation for a traveling wave [7]:

$$i\frac{\mathrm{d}|\psi\rangle}{\mathrm{d}z} = \hat{H}|\psi\rangle. \tag{6.3}$$

We substitute Eq. (6.2) into Eq. (6.3), and obtain the coupled-mode equations while neglecting the dependence of mismatches β_j on ω_p for a narrowband pump photon:

$$\begin{aligned} \frac{dU(z)}{dz} &= -\chi \int_{-\infty}^{\infty} d\Omega V(\Omega, z), \\ \frac{dV(\Omega, z)}{dz} &= \chi^* U(z) + i\Delta\beta(\Omega) V(\Omega, z), \end{aligned} \tag{6.4}$$

where $\Delta\beta = \beta_s(\omega_p, \omega_p/2+\Omega) + \beta_i(\omega_p, \omega_p/2-\Omega) - \beta_U$ we take Taylor expansion of it. As the first order differentiation will have opposite signs and, as it is mentioned

in the text, we consider the signal and idler photons corresponding to the same waveguide mode the first order terms cancel each other, thus the mismatch can be approximated by a quadratic dependence,

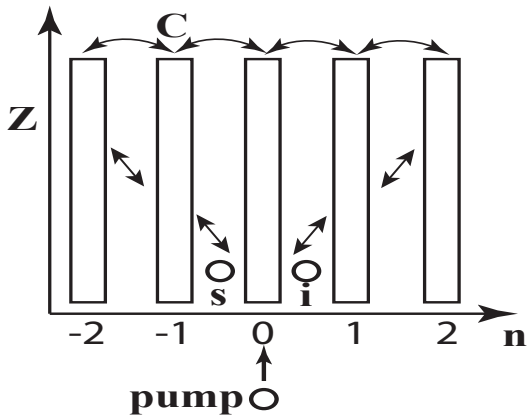

Figure 6.3: Scheme of SPDC and quantum walks for single-photon pump in the waveguide array with the coupling C between the waveguides. Singe pump photon represented by circle titled as "pump" is the input, two circles represent signal and idler photons. The arrows show that they can move in both directions: forward or backwards

$$\Delta\beta \approx \Delta\beta_0 + K_0\Omega^2. \tag{6.5}$$

The absolute values of parameters χ and K_0 can be rescaled to arbitrary values by appropriate normalization of the propagation distance (z) and the frequency detuning (Ω). To be specific, we present numerical simulations for $\chi = 1$, $K_0 = 0.1$, and analyze three generic cases of positive, zero, or negative mismatches $\Delta\beta_0$. For different values of $\Delta\beta_0$, the SPDC process can be phase-matched in either degenerate (if $\Delta\beta_0 = 0$, $\Delta\beta(\Omega = 0) = 0$) or non-degenerate (if $\Delta\beta_0 < 0$, $\Delta\beta(\Omega \neq 0) = 0$) regime, or have no phase-matching for any signal and idler frequencies within the considered frequency band if $\Delta\beta_0 > 0$, see Fig. 6.1(b). It is interesting to mention that even in case of degenerate regime we have $\omega_s \simeq \omega_i$ because the process is spontaneous thus there is always some distribution around each frequency.

We calculate the signal (or idler) intensity spectra $I_V = |V(\Omega, z)|^2$ depending on propagation distance and frequency for different phase mismatches [Figs. 6.2(a,b,c)], using the initial conditions corresponding to a single-photon pump: $U(0) = 1$ and $V(\Omega, z = 0) = 0$. In Figs. 6.2(b,c) the intensity is mostly concentrated in the degenerate spectral region, while in Fig. 6.2(a) the signal (idler) intensity is shifted towards the frequency side bands, in agreement with Fig. 6.1(b). This behavior leads to interesting interplay between the overall pump intensity $I_p = |U|^2$ and the overall signal (idler) intensity $\tilde{I}_V = \int d\Omega |V(\Omega, z)|^2$

[Figs. 6.2(d,e,f)]. In the case of non-degenerate phase mismatch most of pump energy is converted to signal and idler energy [Fig. 6.2(d)], while in the case of degenerate phase-matching we see partial transformation [Fig. 6.2(e)]. In case of positive phase mismatch there is no efficient generation of signal and idler photon pairs [Fig. 6.2(f)]. Remarkably in all three cases there is almost no overall back-conversion from biphotons to pump, since the Rabi-like oscillations of different signal (idler) frequency components are not synchronized due to a frequency-dependent phase mismatch. For comparison, we show in Figs. 6.2(g,h,i) the spectral intensities of signal (idler) photons in the case of a strong classical pump. We see that compared to the classical pump regime, the biphoton spectra in a single-photon-pumped regime [Figs. 6.2(a,b,c)] have more complex structure with extra periodical modulation along the propagation direction. This modulation is attributed to partial back-conversion from a biphoton back to a pump photon.

6.2 Biphoton generation efficiency and dispersion

In this section we extend the analysis from a single waveguide to a periodic array of coupled waveguides. We study the behavior of the SPDC when a single pump photon is coupled to a waveguide in the center of the array [Fig. 6.3]. We assume zero coupling between waveguides at the pump frequency and constant coupling between the neighboring waveguides at the signal and idler frequencies, which is typical for $LiNbO_3$ waveguide arrays [56]. The Hamiltonian of such system has the following form:

$$\begin{aligned}
\hat{H} = &\sum_{n_p} \int d\omega_p \int d\omega_s \int d\omega_i \Big[\chi a_p(n_p,\omega_p) a_s^\dagger(n_p,\omega_s) a_i^\dagger(n_p,\omega_i) \\
&+ \chi^* a_p^\dagger(n_p,\omega_p) a_s(n_p,\omega_s) a_i(n_p,\omega_i) \Big] \\
&+ \int d\omega_p \sum_{n_p} \beta_p(\omega_p) a_p^\dagger(n_p,\omega_p) a_p(n_p,\omega_p) + \int d\omega_s \sum_{n_s} \beta_s(\omega_s) a_s^\dagger(n_s,\omega_s) a_s(n_s,\omega_s) \\
&+ \int d\omega_i \sum_{n_i} \beta_i(\omega_i) a_i^\dagger(n_i,\omega_i) a_i(n_i,\omega_i) \\
&+ C \int d\omega_s \sum_{n_s} \Big[a_s(n_s,\omega_s) a_s^\dagger(n_s+1,\omega_s) + a_s^\dagger(n_s,\omega_s) a_s(n_s+1,\omega_s) \Big] \\
&+ C \int d\omega_i \sum_{n_i} \Big[a_i(n_i,\omega_i) a_i^\dagger(n_i+1,\omega_i) + a_i^\dagger(n_i,\omega_i) a_i(n_i+1,\omega_i) \Big].
\end{aligned} \tag{6.6}$$

Here C is a coupling coefficient in a homogenous waveguide array, and n_j ($j = p, s, i$) are the numbers of the waveguides for the corresponding pump, signal and idler photons. We now assume that the pump photon spectrum is narrow, similar to the preceding analysis for a single waveguide, and then the wavefunction describing the photon dynamics in the system can be formulated in the following form:

$$|\psi\rangle = e^{i\beta_U z}\int d\omega_p\Big[\sum_{n_p} U_{n_p}(z)S(\omega_p)a_p^\dagger(n_p,\omega_p) + \sum_{n_s,n_i}\int d\omega_p\int d\Omega V_{n_s,n_i}(\Omega,z)S(\omega_p)a_s^\dagger(n_s,\omega_p/2+\Omega)a_i^\dagger(n_i,\omega_p/2-\Omega)\Big]|0\rangle. \quad (6.7)$$

The coupled-mode equations can be derived by substituting the wavefunction from Eq. (6.7) into Eq. (6.3) for the Hamiltonian from Eq. (6.6):

$$\begin{aligned}
&\frac{dU_{n_p}(z)}{dz} = -\chi\int_{-\infty}^{\infty} d\Omega V_{n_p,n_p}(\Omega,z),\\
&\frac{dV_{n_s,n_i}(\Omega,z)}{dz} = \chi^*\delta_{n_s,n_i}U_{n_s}(z) + i\Delta\beta(\Omega)V_{n_s,n_i}(\Omega,z)\\
&+iC\Big[V_{n_s-1,n_i}(\Omega,z) + V_{n_s+1,n_i}(\Omega,z) + V_{n_s,n_i-1}(\Omega,z) + V_{n_s,n_i+1}(\Omega,z)\Big]. \quad (6.8)
\end{aligned}$$

We seek a solution of Eq. (6.8) for initial conditions $U_{n_p=0}(z=0)=1$, $U_{n_p\neq 0}(z=0)=0$ and $V_{n_s,n_i}(\Omega,z=0)=0$ and parameters $C=1$, $\chi=1$ and $K_0=0.1$.

We analyze the evolution of the pump and signal photon intensities along the propagation distance for three different phase-matching conditions. Figures 6.4(a,b,c) show the pump intensities $W_p(n_p) = |U_{n_p}(z)|^2$ across the array, Figs. 6.4(d,e,f) show the signal intensities $W_V(n_s) = \int d\Omega \sum_{n_i} |V_{n_s,n_i}(\Omega,z)|^2$, and Figs. 6.4(g,h,i) show the total signal and idler intensities integrated over all waveguides vs. the frequency $W_\Omega = \sum_{n_s}\sum_{n_i}|V_{n_s,n_i}(\Omega,z)|^2$. We notice that for the non-degenerate phase-matching condition ($\Delta\beta_0 = -6$) the pump mode inserted in the central waveguide [Fig. 6.4(a)] transforms into two biphoton modes, which propagate in different waveguides [Fig. 6.4(d)] with different frequencies [Fig. 6.4(g)] and don't recombine during the propagation. The degenerate phase-matching condition corresponds to efficient SPDC and continuous conversion between pump and biphoton modes during the propagation [Figs. 6.4(b,e,h)]. We observe non-efficient biphoton generation in case of the positive phase mismatch ($\Delta\beta_0 = 6$) as the pump mode remains approximately unchanged during its propagation [Fig. 6.4(c)] and the intensity of the generated biphotons remains comparatively small [Figs. 6.4(f,i)].

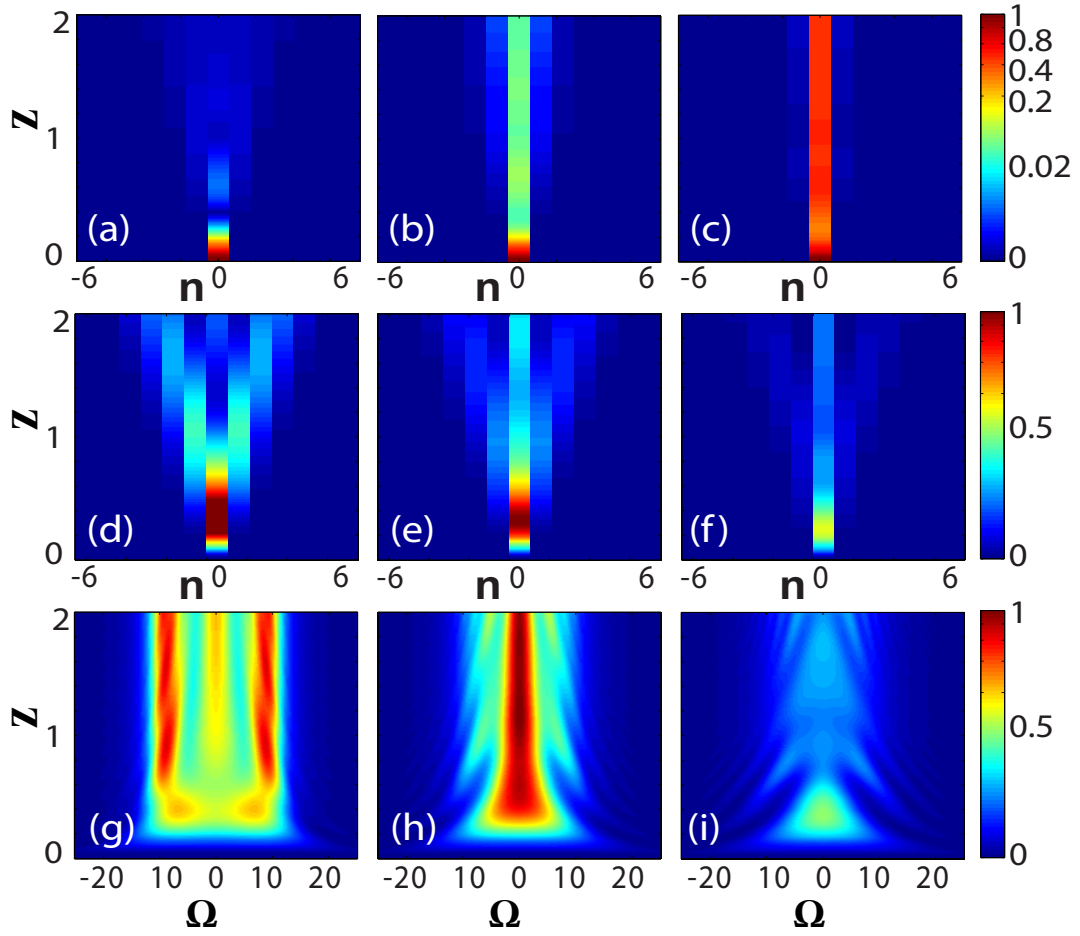

Figure 6.4: (a,b,c) Pump intensity $W_p(n)$ and (d,e,f) biphoton intensity $W_V(n)$ vs. the propagation distance and waveguide number; (g,h,i) Biphoton intensities depending on propagation distance and frequency Ω for different phase-matching conditions (a,d,g) $\Delta\beta_0 = -6$; (b,e,h) $\Delta\beta_0 = 0$, and (c,f,i) $\Delta\beta_0 = 6$.

Next we analyze spatial biphoton correlations $\Gamma_{n_s,n_i}(L) = \int d\Omega |V_{n_s,n_i}(\Omega, L)|^2$ with single-photon pump for three phase-matching regimes [Figs. 6.5(a,b,c)]. For a strong classical pump and degenerate phase-matching, the correlations feature a cross shape, corresponding to the simultaneous bunching and anti-bunching of photon pairs [56]. However, the biphoton spatial correlations arising from a single-photon pump with degenerate phase-matching [Fig. 6.5(b)] have a more complex structures, where the bunching branch is preserved only close to the central waveguide, while additional areas of bunching and antibunching appear further away from the center.

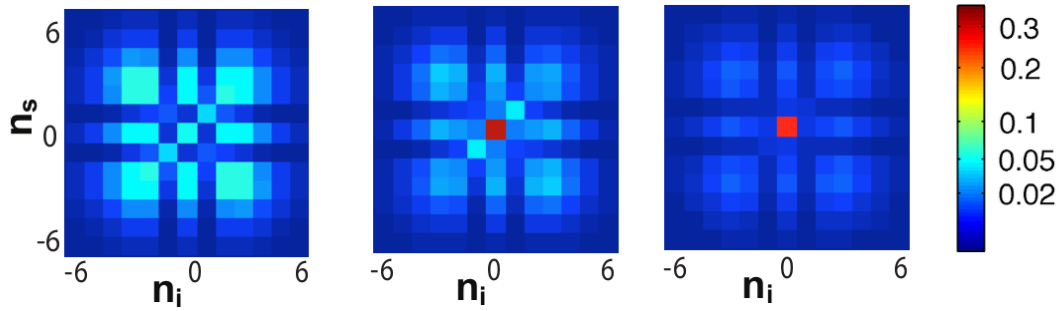

Figure 6.5: Spatial biphoton correlations Γ_{n_s,n_i} at the propagation distance $z = 2$ for different phase-matching conditions (a) $\Delta\beta_0 = -6$; (b) $\Delta\beta_0 = 0$ and (c) $\Delta\beta_0 = 6$.

The spatial biphoton correlations in a WGA are less pronounced in the case of positive phase mismatch [Fig. 6.5(c)] and more pronounced in the case of negative phase mismatch [Fig. 6.5(c)]. The non-trivial shape of the spatial correlations arises due to a complex interplay of photon conversion and frequency dispersion.

To conclude, this chapter has described spontaneous parametric down-conversion of a single-photon pump in nonlinear waveguide array. A number of non-trivial phenomena related to generation of a broad spectrum of signal and idler photons by a narrow-band pump have been demonstrated. These include the absence of back-conversion in a single waveguide due to effective suppression of Rabi-like oscillations and unusual photon-pair correlations in waveguide arrays. These results suggest new possibilities for photon path control and engineering of multi-photon states, which could be beneficial for further development of integrated quantum photonics.

Chapter 7

Conclusion and outlook

Quantum and classical properties of light propagating in the nonlinear optical waveguides spark significant of research driven by fundamental interest and applications. Nonlinear waveguide arrays can be used to efficiently generate entangled photon pairs and simultaneously shape their spatial correlations through quantum walks. Such integrated photon sources can find applications in the development of on-chip quantum communication and computation devices. In recent years the quantum optics of attenuating media was developed. Firstly, because quantum information protocols are inevitably affected by noise, secondly photonic structures composed of coupled waveguides with lossy regions offer new possibilities for shaping optical beams and pulses. Finally, there has been increased interest in nonlinear hybrid plasmonic waveguide as surface plasmon polaritons offer increased field confirmation and minituisation.

In this thesis we address an important problem of the effect of losses on the generation and propagation of both quantum and classical light in nonlinear waveguide structure.

We describe photon-pair generation through spontaneous parametric down-conversion in quadratic nonlinear waveguide arrays, and determine the tolerance to loss when quantum features in spatial correlations are preserved. We demonstrate that photon-pair generation through SPDC in a nonlinear lossy waveguide can be simulated by classical linear light propagation in a semi-infinite array of weakly coupled single-mode optical waveguides with the different coupling coefficients controlled by waveguide spacing. The demonstrated waveguide platform can be further applied to optically simulate the effects of non-Markovian losses and quantum decoherence phenomena. In the thesis we perform analytical and numerical analysis of the quantum spontaneous parametric down-conversion and sum frequency generation and presented theoretical results on possibilities to characterize SPDC through classical sum frequency generation in nonlinear lossy waveguide array. This technique is called stimulated multimode tomogra-

phy. In the last chapter in contrast to whole thesis we discuss the system which is described by a Hermitian Hamiltonian. We describe spontaneous parametric down-conversion of a single-photon pump, which can be presented as pump depletion, in nonlinear waveguide arrays. The results suggest new possibilities for photon path control and engineering of multi-photon states, which could be beneficial for further development of integrated quantum photonics.

Some of the effects predicted in this thesis were observed in experiment, with good agreement to my theory. However, we believe that more can be done in the research of generation and propagation of quantum and classical light in non-Hermitian integrated photonics both from theoretical and experimental points of view.

In Chapter 3 we discuss SPDC in a single lossy waveguide, where we take into account only losses of the signal and idler photons. We present not only theoretical but also experimental emulation of SPDC in the system which includes the loss-emulating array with waveguide couplings. We point out theoretically that the circuit can be designed to emulate the effect of pump losses as well, and it will be very interesting to conduct experiment and see the correlations with the theory.

Our preliminary studies suggest that finite number of loss emulating waveguides can be a perfect platform for description of non-Markovian losses. Non-Markovian behavior is detected in radiation modes of subwavelength plasmonic nanostructures and in analysis of spontaneous emission of excited two-level atoms. It will be interesting to discuss the theoretical model of a quantum system which displays non-Markovian behavior and show the possibility to simulate it in linear coupled waveguide arrays.

Most recently there has been a growing excitement among researchers about the prospects for building plasmonic devices, which enable strong, coherent interactions between quantum emitter system and photons which is essential for quantum communication and quantum information science. Unlike in classical optics, the possible benefits of metamaterials and plasmonic structures in quantum optics have not been widely explored so far. It is an important and still open question whether the similar effective-medium parameters describe the propagation of quantum states of light in metamaterials and plasmonic structures. From this perspective the research direction to follow would be to study photon generation and control in structures with loss, such as hybrid plasmonic waveguides and metamaterials.

Appendix A

Derivation of two-photon state in lossy waveguide arrays

In this Appendix, we detail the derivation procedure of Eqs. (2.6)-(2.9). As discussed in Sec. 2.1, the photon state evolution is governed by a sum of Hamiltonian operators provided by the Eqs. (2.2),(2.4):

$$\hat{H}(z) = \hat{H}_{nl}(z) + \hat{H}_{bs}(z). \tag{A.1}$$

Accordingly, the evolution of a photon state ($|\ominus(z)\rangle$) is governed by the Schrödinger equation in the undepleted classical pump approximation [40, 48, 167]:

$$\frac{\partial|\ominus(z)\rangle}{\partial z} = -i\hat{H}(z)|\ominus(z)\rangle. \tag{A.2}$$

It is pretty common in optics to write Schreodinger equation in terms of propagation coordinate z. The transition from conventional formulation in time (t) to the propagation coordinate (z) works in a quasi-monochromatic and one-directional propagation regime. Then one can assume $z = vt$, where v is a fixed phase velocity [50, 51, 58, 168].

We consider the case of sufficiently weak pump, such that multiple photon pairs are not generated simultaneously, i.e. we neglect cascading processes. Then, the photon state can be approximately represented as a sum of the unperturbed vacuum state ($|0\rangle$) and the biphoton state ($|\Psi(z)\rangle$) (see Eq. (2.5) and in Ref. [59]). Under such assumptions, the approximate Schrödinger equation for the biphoton wavefunction is:

$$\frac{\partial|\Psi(z)\rangle}{\partial z} \simeq -i\hat{H}(z)\left(|\Psi(z)\rangle + |0\rangle\right). \tag{A.3}$$

We now seek the solution for the two-photon state in the form of Eq. (2.5), which we specially choose to obtain a solution of Eq. (A.3), taking into account

all possible two-photon states. We consider a vacuum input state, with zero photon pairs:

$$\begin{aligned}&\Phi(z=0)=0,\\&\tilde{\Phi}^{(s)}(z=0,z_l)=\tilde{\Phi}^{(i)}(z=0,z_l)=0,\\&\tilde{\Phi}^{(si)}(z_s=0,z_l=0)=0.\end{aligned}\tag{A.4}$$

First, we calculate the action of $\hat{H}_{nl}$ on the biphoton state $|\Psi(z)\rangle$, which describes the photon evolution inside a quadratically nonlinear waveguide:

$$\begin{aligned}\hat{H}_{nl}|\Psi(z)\rangle &= \Bigg[\beta_s\Phi(z)a_s^\dagger a_i^\dagger|0\rangle+\beta_s\int_0^z dz_l\tilde{\Phi}^{(s)}(z,z_l)a_s^\dagger b_i^\dagger(z_l)|0\rangle\\&+\beta_i\Phi(z)a_s^\dagger a_i^\dagger|0\rangle+\beta_i\int_0^z dz_l\tilde{\Phi}^{(i)}(z,z_l)b_s^\dagger(z_l)a_i^\dagger|0\rangle\Bigg]+E_p^*\Phi(z)|0\rangle\\&+E_p\Bigg[\Phi(z)a_s^{\dagger2}a_i^{\dagger2}|0\rangle+\int_0^z dz_l\tilde{\Phi}^{(s)}(z,z_l)a_s^{\dagger2}a_i^\dagger b_i^\dagger(z_l)|0\rangle\\&+\int_0^z dz_l\tilde{\Phi}^{(i)}(z,z_l)a_s^\dagger a_i^{\dagger2}b_s^\dagger(z_l)|0\rangle\\&+\int_0^z dz_{l_s}\int_0^z dz_{l_i}\tilde{\Phi}^{(si)}(z_{l_s},z_{l_i})a_s^\dagger b_s^\dagger(z_{l_s})a_i^\dagger b_i^\dagger(z_{l_i})|0\rangle\Bigg].\end{aligned}\tag{A.5}$$

In the following we assume that higher order terms in Eq. (A.5) that correspond to cascaded processes are negligible in comparison to the first order ones. Specifically, we neglect the zero-photon state ($E_p^*\Phi(z)|0\rangle$), originating through cascading from vacuum to two-photons and back to vacuum; and four-photon state (the last square bracket term). Then, we calculate the action of the Hamiltonian $\hat{H}_{bs}$, which describes beam-splitters representing losses:

$$\begin{aligned}\hat{H}_{bs}|\Psi(z)\rangle &= \sqrt{2\gamma_s}\Phi(z)b_s^\dagger(z)a_i^\dagger|0\rangle+\sqrt{2\gamma_s}\int_0^z dz_l\tilde{\Phi}^{(s)}(z,z_l)b_s^\dagger(z)b_i^\dagger(z_l)|0\rangle\\&+\mathcal{H}(0)\sqrt{2\gamma_s}\tilde{\Phi}^{(i)}(z,z)a_s^\dagger a_i^\dagger|0\rangle\\&+\mathcal{H}(0)\sqrt{2\gamma_s}\int_0^z dz_{l_i}\tilde{\Phi}^{(si)}(z,z_{l_i})a_s^\dagger b_i^\dagger(z_{l_i})|0\rangle\\&+\sqrt{2\gamma_i}\Phi(z)a_s^\dagger b_i^\dagger(z)|0\rangle+\sqrt{2\gamma_i}\int_0^z dz_l\tilde{\Phi}^{(i)}(z,z_l)b_s^\dagger(z_l)b_i^\dagger(z)|0\rangle\\&+\mathcal{H}(0)\sqrt{2\gamma_i}\tilde{\Phi}^{(s)}(z,z)a_s^\dagger a_i^\dagger|0\rangle\\&+\mathcal{H}(0)\sqrt{2\gamma_i}\int_0^z dz_{l_s}\tilde{\Phi}^{(si)}(z_{l_s},z)a_i^\dagger b_s^\dagger(z_{l_s})|0\rangle.\end{aligned}\tag{A.6}$$

In these calculations, we use the standard properties of the creation and annihilation operators [114] and a Heaviside step function:

$$\mathcal{H}(z) = \int_{-\infty}^{z} \delta(t)dt = \begin{cases} 0, & z < 0, \\ \frac{1}{2}, & z = 0, \\ 1, & z > 0, \end{cases} \tag{A.7}$$

Finally, the action of the Hamiltonian operators on vacuum $|0\rangle$ is:

$$\hat{H}_{nl}|0\rangle = E_p a_s^\dagger a_i^\dagger |0\rangle, \quad \hat{H}_{bs}|0\rangle = 0. \tag{A.8}$$

As expected, the SPDC process described by $\hat{H}_{nl}$ leads to a generation of a photon pair from vacuum.

We now calculate the temporal derivative of the biphoton wavefunction $\Psi(z)$, which has the form of Eq. (2.5):

$$\begin{aligned} \frac{\partial|\Psi(z)\rangle}{\partial z} &= \frac{\partial\Phi(z)}{\partial z} a_s^\dagger a_i^\dagger|0\rangle + \tilde{\Phi}^{(s)}(z,z) a_s^\dagger b_i^\dagger(z)|0\rangle \\ &+ \int_0^z dz_l \frac{\partial\tilde{\Phi}^{(s)}(z,z_l)}{\partial z} a_s^\dagger b_i^\dagger(z_l)|0\rangle + \tilde{\Phi}^{(i)}(z,z) b_s^\dagger(z) a_i^\dagger|0\rangle \\ &+ \int_0^z dz_l \frac{\partial\tilde{\Phi}^{(i)}(z,z_l)}{\partial z} b_s^\dagger(z_l) a_i^\dagger|0\rangle + \int_0^z dz_l \tilde{\Phi}^{(si)}(z,z_l) b_s^\dagger(z) b_i^\dagger(z_l)|0\rangle \\ &+ \int_0^z dz_l \tilde{\Phi}^{(si)}(z_{l_s},z) b_s^\dagger(z_l) b_i^\dagger(z)|0\rangle. \end{aligned} \tag{A.9}$$

We substitute Eqs. (A.5)-(A.9) into Eq. (A.3), and collect terms representing different photon states. The state of both photons in the waveguide (i.e. the photons that are not lost through the beamsplitters) is $a_s^\dagger a_i^\dagger|0\rangle$. Multiplying both sides of Eq. (A.3) by Hermitian conjugate of the state expression, i.e. $\langle 0|a_s a_i$, and taking into account Eqs. (A.5)-(A.9), we obtain:

$$\frac{\partial\Phi(z)}{\partial z} = -i\left[(\beta_s+\beta_i)\,\Phi(z) + E_p + \tfrac{1}{2}\sqrt{2\gamma_s}\tilde{\Phi}^{(i)}(z,z) + \tfrac{1}{2}\sqrt{2\gamma_i}\tilde{\Phi}^{(s)}(z,z)\right]. \tag{A.10}$$

Then we determine the evolution of states where either idler or signal photon is lost at a propagation distance z_l by multiplying both sides of Eq. (A.3) by the Hermitian conjugates of $a_s^\dagger b_i^\dagger(z_l)|0\rangle$ and $b_s^\dagger(z_l)a_i^\dagger|0\rangle$, respectively:

$$\begin{aligned} \frac{\partial\tilde{\Phi}^{(s)}(z,z_l)}{\partial z}\mathcal{H}(z-z_l) &= -i\left[\beta_s\tilde{\Phi}^{(s)}(z,z_l) + \frac{1}{2}\sqrt{2\gamma_s}\tilde{\Phi}^{(si)}(z,z_l)\right]\mathcal{H}(z-z_l) \\ &\quad -i\sqrt{2\gamma_i}\Phi(z)\delta(z-z_l) - \tilde{\Phi}^{(s)}(z,z)\delta(z-z_l), \end{aligned} \tag{A.11}$$

$$\frac{\partial\tilde{\Phi}^{(i)}(z,z_l)}{\partial z}\mathcal{H}(z-z_l) = -i\left[\beta_i\tilde{\Phi}^{(i)}(z,z_l)+\frac{1}{2}\sqrt{2\gamma_i}\tilde{\Phi}^{(si)}(z_l,z)\right]\mathcal{H}(z-z_l) -i\sqrt{2\gamma_s}\Phi(z)\delta(z-z_l)-\tilde{\Phi}^{(i)}(z,z)\delta(z-z_l). \quad \text{(A.12)}$$

To find the state where both photons are lost, i.e. signal photon is lost at a coordinate z_{l_s} and idler photon is lost at a coordinate z_{l_i}, we multiply Eq. (A.3) by the Hermitian conjugate of $b_s^\dagger(z_{l_s})b_i^\dagger(z_{l_i})|0\rangle$:

$$\tilde{\Phi}^{(si)}(z,z_{l_i})\delta(z-z_{l_s})\mathcal{H}(z-z_{l_i})+\tilde{\Phi}^{(si)}(z_{l_s},z)\delta(z-z_{l_i})\mathcal{H}(z-z_{l_s}) = -i\frac{1}{2}\sqrt{2\gamma_s}\tilde{\Phi}^{(s)}(z,z_{l_i})\delta(z-z_{l_s})\mathcal{H}(z-z_{l_i}) -i\frac{1}{2}\sqrt{2\gamma_i}\tilde{\Phi}^{(i)}(z,z_{l_s})\delta(z-z_{l_i})\mathcal{H}(z-z_{l_s}). \quad \text{(A.13)}$$

Afterwards we solve Eqs. (A.13) taking into account the initial conditions in Eq. (A.4):

$$\begin{aligned}\tilde{\Phi}^{(si)}(z_{l_s},z_{l_i}) &= -i\frac{1}{2}\sqrt{2\gamma_s}\tilde{\Phi}^{(s)}(z_{l_s},z_{l_i}),\ z_{l_s}\geq z_{l_i},\\ \tilde{\Phi}^{(si)}(z_{l_s},z_{l_i}) &= -i\frac{1}{2}\sqrt{2\gamma_i}\tilde{\Phi}^{(i)}(z_{l_i},z_{l_s}),\ z_{l_s}\leq z_{l_i}.\end{aligned} \quad \text{(A.14)}$$

Then we calculate $\tilde{\Phi}^{(s)}(z_l,z_l)$ and $\tilde{\Phi}^{(i)}(z_l,z_l)$ by integrating the Eqs. (A.11) and A.12 for $z_l-\epsilon<z<z_l+\epsilon$ in the limit $\epsilon\to 0$:

$$\begin{aligned}&\tilde{\Phi}^{(s)}(z_l,z_l)=-i\sqrt{2\gamma_i}\Phi(z_l),\ \tilde{\Phi}^{(s)}(z<z_l,z_l)=0,\\ &\tilde{\Phi}^{(i)}(z_l,z_l)=-i\sqrt{2\gamma_s}\Phi(z_l),\ \tilde{\Phi}^{(i)}(z<z_l,z_l)=0.\end{aligned} \quad \text{(A.15)}$$

Finally we substitute Eqs. (A.14) and (A.15) into Eqs. (A.10)-(A.12) and obtain the relations for the evolution of the biphoton wave function, as written in Eqs. (2.6)-(2.8):

$$\frac{\partial\Phi(z)}{\partial z}=-(i\Delta\beta^{(0)}+\gamma_s+\gamma_i)\Phi(z)+Ae^{-\gamma_p z}, \quad \text{(A.16)}$$

$$\frac{\partial\tilde{\Phi}^{(s)}(z,z_l)}{\partial z}=-(i\beta_s^{(0)}+\gamma_s)\tilde{\Phi}^{(s)}(z,z_l),\ z\geq z_l, \quad \text{(A.17)}$$

$$\frac{\partial\tilde{\Phi}^{(i)}(z,z_l)}{\partial z}=-(i\beta_i^{(0)}+\gamma_i)\tilde{\Phi}^{(i)}(z,z_l),\ z\geq z_l. \quad \text{(A.18)}$$

Appendix B

Eigenmode solution of SPDC and SFG

B.1 Eigenmode solution of SPDC in a lossy waveguide array

In this Appendix, we detail the eigenmode solution of Eqs. (4.1) and (4.2). We have found results for the SPDC in the waveguide array with spatially inhomogeneous losses Eqs. (4.7) and (4.8) as discussed in Sec. 4.1.

Firstly we find eigenmode solution for the pump field from Eq. (4.2). The solution is given through the fundamental matrix solution $\mathcal{M}$ as follows

$$\mathbf{A}(z) = \mathcal{M}(\mathbf{z})\left(\mathcal{M}(\mathbf{0})\right)^{-\mathbf{1}}\mathbf{A}(\mathbf{0}), \tag{B.1}$$

where

$$\mathcal{M}^{n_3}(z) = \sum_{m_3} U_3\left(n_3, m_3\right) \mathrm{e}^{\lambda^p_{m_3} z}. \tag{B.2}$$

where $U_3\left(n_3, m_3\right)$ is the eigenvector for the pump amplitude with eigenvalues $\lambda^p_{m_3}$ and $A(0)$ is the input field at $z = 0$, we assume that the pump is only in one of the waveguides and rewrite the input field in diagonal form as follows,

$$A(0) = \begin{pmatrix} A_1 & 0 & ... & 0 \\ ... & ... & ... & ... \\ 0 & ... & ... & A_{n_3} \end{pmatrix} \tag{B.3}$$

Substituting Eqs. (B.2) and (B.3) in the Eq. (B.1) we find the final result for the

pump field as

$$A_{n_3,n_3}(z) = \frac{1}{\det U_3} \sum_{m_3} U_3\left(n_3, m_3\right) \mathrm{e}^{\lambda^p_{m_3} z} \left(U_3\left(m_3, n_3\right) \right)^{-1} A_{n_3,n_3}(0). \tag{B.4}$$

The solution of the inhomogeneous differential equations is the sum of the solution of the homogeneous equation and the particular solution of the inhomogeneous one, thus we present the solution of Eq. (4.1) as $\Phi(z) = \Phi^0(z) + \Phi'(z)$. $\Phi^0(z) = 0$ as there are no input two photon states at $z = 0$, which means for SPDC $\Phi(z) = \Phi'(z)$. The solution of the homogeneous part of the Schrödinger-type equations for the photon pair amplitudes is presented as the product of solutions for the signal and idler modes. u_{n_1,m_1} and v_{n_2,m_2} are eigenmode solutions of homogeneous Schrödinger equation, which could be written in the matrix form as in Eq. (4.4)and Eq. (4.5). We present the solution of the eigenmode problem for the signal and the idler photons as follows:

$$\begin{aligned} u_{n_1,m_1} &= U_1\left(n_1, m_1\right) \mathrm{e}^{\lambda^s_{m_1} z}, \\ v_{n_2,m_2} &= U_2\left(n_2, m_2\right) \mathrm{e}^{\lambda^i_{m_2} z}. \end{aligned} \tag{B.5}$$

where $U_1\left(n_1, m_1\right)$ is the eigenvector for the signal photon with eigenvalues $\lambda^s_{1(2)}$ and $U_2\left(n_2, m_2\right)$ is the eigenvector for the idler photon with eigenvalues $\lambda^i_{1(2)}$.

Taking into account the seeking solution Eq. (4.3) $\Phi_{n_1,n_2}(z) = \sum_{m_1 m_2} u_{n_1,m_1} v_{n_2,m_2} B_{m_1,m_2}(z)$ for the inhomogeneous array of equations and substituting it in the Schrödinger Eq. (4.1) we find the equation for the z dependant expansion coefficient as follows,

$$\sum_{m_1 m_2} u_{n_1,m_1} v_{m_2,n_2} \frac{\partial B_{m_1,m_2}}{\partial z} = A_{n_3,n_3}(z). \tag{B.6}$$

Here we again assume that we have pump only in one of the waveguides with number n_3

$$B_{m_1,m_2} = \int_0^L \mathrm{d}z \left(\sum_{n_2} \left(\sum_{n_1} u^{-1}_{m_1,n_1} A_{n_3,n_3}(z) \right) v^{-1}_{n_2,m_2} \right), \tag{B.7}$$

We find the final result for two-photon amplitude as follows

$$\Phi_{n_1,n_2} = \sum_{m_2} \left(\sum_{m_1} u_{n_1,m_1} B_{m_1,m_2} \right) v_{n_2,m_2}. \tag{B.8}$$

Substituting Eqs. (B.5) and (B.4) in the Eq. (B.7) we can re-write the solution

for the z dependant expansion coefficient as

$$B_{m_1,m_2} = \frac{iz}{\det(U_1)\det(U_2)\det(U_3)} \sum_{m_3,n_3} \mathrm{e}^{\frac{\left(\lambda^p_{m_3}-\lambda^s_{m_1}-\lambda^i_{m_2}\right)z}{2}} \times \operatorname{sinc}\left(\frac{\left(\lambda^p_{m_3}-\lambda^s_{m_1}-\lambda^i_{m_2}\right)z}{2}\right) \times \left\{\frac{U_1\left(n_3,m_1,\right)}{\sum_q U_1^2\left(q,m_1\right)} U_3\left(n_3,m_3\right) \frac{U_3\left(n_3,m_3,\right)}{\sum_z U_3^2\left(l,m_3\right)} A_{n_3,n_3}(0) \frac{U_2\left(n_3,m_2,\right)}{\sum_p U_2^2\left(p,m_2\right)}\right\}, \quad \text{(B.9)}$$

Now we substitute Eq. (4.7) and (B.5) in the result for two-photon amplitude and taking into account the matrix symmetry relations (4.6) we get the following result

$$\begin{aligned}\Phi^{n_3}_{n_1,n_2} = {} & \frac{iz}{\det(U_1)\det(U_2)\det(U_3)} \times \\ & \sum_{m_3,m_2,m_1} \mathrm{e}^{\frac{\left(\lambda^p_{m_3}+\lambda^s_{m_1}+\lambda^i_{m_2}\right)z}{2}} \operatorname{sinc}\left(\frac{\left(\lambda^p_{m_3}-\lambda^s_{m_1}-\lambda^i_{m_2}\right)z}{2}\right) \times \\ & \left\{U_1\left(n_1,m_1\right) \frac{U_1\left(n_3,m_1\right)}{\sum_q U_1^2\left(q,m_1\right)} U_3\left(n_3,m_3\right) \frac{U_3\left(n_3,m_3\right)}{\sum_k U_3^2\left(k,m_3\right)} \times \right. \\ & \left. A_{n_3,n_3}(0) \frac{U_2\left(n_3,m_2\right)}{\sum_l U_2^2\left(l,m_2\right)} U_2\left(n_2,m_2\right)\right\}. \end{aligned} \quad \text{(B.10)}$$

Now let us assume that we can adjust our system to have single mode input, which means that we can write the input state as $A_{n_3} = A_{m_3} U_3\left(n_3,m_3\right) \mathrm{e}^{\lambda^p_{m_3} z}$ and substituting this in Eq. (4.7) we will have

$$\begin{aligned} B^{m_3}_{m_1,m_2} = {} & iz \mathrm{e}^{\frac{\left(\lambda^p_{m_3}-\lambda^s_{m_1}-\lambda^i_{m_2}\right)z}{2}} \operatorname{sinc}\left(\frac{\left(\lambda^p_{m_3}-\lambda^s_{m_1}-\lambda^i_{m_2}\right)z}{2}\right) \times \\ & \sum_{n_3} \frac{U_1\left(n_3,m_1,\right)}{\sum_q U_1^2\left(q,m_1\right)} A_{m_3,m_3}(0) U_3\left(n_3,m_3\right) \frac{U_2\left(n_3,m_2,\right)}{\sum_p U_2^2\left(p,m_2\right)}. \end{aligned} \quad \text{(B.11)}$$

Here for the simplicity of the registration we assume that our modes are normalized as follows $\sum_p U_j^2\left(p,m_i\right) = 1$.

$$B^{m_3}_{m_1,m_2} = ize^{\frac{\left(\lambda^p_{m_3}-\lambda^s_{m_1}-\lambda^i_{m_2}\right)z}{2}}\mathrm{sinc}\left(\frac{\left(\lambda^p_{m_3}-\lambda^s_{m_1}-\lambda^i_{m_2}\right)z}{2}\right)\times \sum_{n_3} U_1\left(n_3,m_1,\right)U_3\left(n_3,m_3\right)U_2\left(n_3,m_2,\right)A_{m_3,m_3}(0). \tag{B.12}$$

B.2 Eigenmode solution of SFG in a lossy waveguide array

In this section, we show the detailed derivation of the eigenmode solution of Eqs. (4.12-4.14) for sum frequency generation as discussed in Sec. 4.1.

$$\frac{\partial}{\partial z}\begin{pmatrix} a_1(\omega_1) \\ a_2(\omega_1) \\ ... \\ a_{n_1}(\omega_1)\end{pmatrix} = \begin{pmatrix} -i\beta_s-\gamma_s(n_1) & -iC_s & 0 & ... & 0 \\ -iC_s & -i\beta_s-\gamma_s(n_1) & -iC_s & ... & 0 \\ .. & .. & .. & .. & .. \\ 0 & 0 & ... & -iC_s & -i\beta_s-\gamma_s(n_1)\end{pmatrix} \times \begin{pmatrix} a_1(\omega_1) \\ a_2(\omega_1) \\ ... \\ a_{n_1}(\omega_1)\end{pmatrix}. \tag{B.13}$$

We solve the eigenvalue-eigenmode problem for the SFG process. We find $U_1\left(n_1,m_1\right)$ is the eigenvector for the modes with frequency ω_1 with eigenvalues $\lambda^s_{Cm_1}$ and $U_2\left(n_2,m_2\right)$ is the eigenvector for the mode with frequency ω_2 and eigenvalues $\lambda^i_{Cm_2}$. The solution of the propagating mode amplitudes a_s, a_i on each frequency ω_1, ω_2 is given through the fundamental matrix solution M as follows

$$\mathbf{a}_s(z,\omega_1) = \begin{pmatrix} a_1(\omega_1) \\ a_2(\omega_1) \\ ... \\ a_{n_1}(\omega_1)\end{pmatrix} = \mathbf{M}^s(z)\left(\mathbf{M}^s(0)\right)^{-1}\mathbf{E}^s \tag{B.14}$$

where $E^{s,i}_{n_{1,2}}$ are the input fields for the modes on the frequency $\omega_{1,2}$ in the mth

waveguide and

$$M^{s}_{n_1,m_1} = \sum_{m_1} U_1\left(n_1, m_1\right) \mathrm{e}^{\lambda^{s}_{Cm_1} z},$$
$$M^{i}_{n_2,m_2} = \sum_{m_2} U_1\left(n_2, m_2\right) \mathrm{e}^{\lambda^{i}_{Cm_2} z}. \tag{B.15}$$

Taking into account Eqs. (B.14,B.15) we find the following results for the mode amplitude on the frequencies ω_1 and ω_2 as follows:

$$\mathbf{a}_{n_3}(z,\omega_1) = \frac{1}{\det(U_1)} \left(\sum_{n_1,m_1} U_1\left(n_3, m_1\right) \mathrm{e}^{\lambda^{s}_{Cm_1} z} \frac{U_1\left(n_1, m_1\right)}{\sum_q U_1^2\left(q, m_1\right)} E^{s}_{n_1} \right) \tag{B.16}$$

and

$$\mathbf{a}_{n_3}(z,\omega_2) = \frac{1}{\det(U_2)} \left(\sum_{n_2,m_2} U_2\left(n_3, m_2\right) \mathrm{e}^{\lambda^{i}_{Cm_2} z} \frac{U_2\left(n_2, m_2\right)}{\sum_l U_2^2\left(l, m_2\right)} E^{i}_{n_2} \right) \tag{B.17}$$

Here we took into account the symmetry of the eigenmode matrixes defined in Eq. 4.6.

To find the eigenmode solution of the Eqs. (4.14) we firstly have to solve the homogenise equations without terms $\mathcal{F}(z,\omega_1,\omega_2) = a_{n_3}(z,\omega_1)a_{n_3}(z,\omega_2)$, $\mathcal{F}(z)$ is a product of signal (ω_1) and idler (ω_2) modes propagating in the waveguide where the pump mode is (in future some indexes or arguments could be skipped to keep the formulas).

We search solution of the inhomogeneous array of equations as

$$a_{n_3}(z) = \sum_{m_3} U_3\left(n_3, m_3\right) \mathrm{e}^{\lambda^{p}_{Cm_3} z} \Upsilon^{m_3}(z), \tag{B.18}$$

where U_3 - is the eigne mode for the mod on the sum frequency (ω_3) and $\Upsilon^{m_3}(z)$ - is the z dependant expansion function and λ^{p}_{C} - is the corresponding eigenvalue. We substitute the equation for the z dependant expansion function from the Eq. (4.14) as follows

$$\sum_{m_3} U_3\left(n_3, m_3\right) \mathrm{e}^{\lambda^{p}_{Cm_3} z} \frac{\partial \Upsilon^{m_3}}{\partial z} = \mathcal{F}_{n_3}(z). \tag{B.19}$$

Taking into account the results for the mode amplitudes for the frequencies ω_1 and ω_2 we will have the following equation for the z dependant expansion

function

$$\Upsilon^{m_3} = \frac{iz}{\det(U_1)\det(U_2)\det(U_3)} \times \sum_{m_1,m_2}\sum_{n_3} \mathrm{e}^{\frac{\left(\lambda^p_{Cm_3}-\lambda^s_{Cm_1}-\lambda^i_{Cm_2}\right)z}{2}} \mathrm{sinc}\left(\frac{\left(\lambda^p_{Cm_3}-\lambda^s_{Cm_1}-\lambda^i_{Cm_2}\right)z}{2}\right) \times \frac{U_3\left(n_3,m_3\right)}{\sum_q U_3^2\left(q,m_3\right)} U_1\left(n_3,m_1\right) \frac{U_1\left(n_1,m_1\right)}{\sum_l U_1^2\left(l,m_1\right)} U_2\left(n_3,m_2\right) \frac{U_2\left(n_2,m_2\right)}{\sum_p U_2^2\left(p,m_2\right)} E^s_{n_1} E^i_{n_2}. \quad \text{(B.20)}$$

We redefined the amplitude at the sum frequency $a_{n_3}(\omega_3, z; n_1, n_2)$ as new variable $\tilde{\Phi}^{n_3}_{n_1,n_2}(\omega_3)$ for the comparison of the results with the ones obtained for biphoton function Eq. (B.10),

$$\tilde{\Phi}^{n_3}_{n_1,n_2}(\omega_3, z) = a_{n_3}(\omega_3, z; n_1, n_2). \quad \text{(B.21)}$$

$\tilde{\Phi}^{n_3}_{n_1,n_2}(\omega_3)$ is the mode at the sum frequency at the output of the waveguide n_3, when we have input signal mode in the n_1 and idler mode in the n_2 waveguides, correspondingly.

Finally, substituting the results for the z dependant coefficient from Eq. (B.20) in Eq. (B.18) we will get the final results for the mode propagating on the sum frequency as,

$$\tilde{\Phi}^{n_3}_{n_1,n_2}(\omega_3, z) = \frac{iz}{\det(U_1)\det(U_2)\det(U_3)} \times \sum_{m_3,m_2,m_1} \mathrm{e}^{\frac{\left(\lambda^p_{Cm_3}+\lambda^s_{Cm_1}+\lambda^i_{Cm_2}\right)z}{2}} \mathrm{sinc}\left(\frac{\left(\lambda^p_{Cm_3}-\lambda^s_{Cm_1}-\lambda^i_{Cm_2}\right)z}{2}\right) \times U_3\left(n_3,m_3\right) \frac{U_3\left(n_3,m_3\right)}{\sum_k U_3^2\left(k,m_3\right)} U_1\left(n_3,m_1\right) \frac{U_1\left(n_1,m_1\right)}{\sum_q U_1^2\left(q,m_1\right)} U_2\left(n_3,m_2\right) \frac{U_2\left(n_2,m_2\right)}{\sum_l U_2^2\left(l,m_2\right)} \times E^s_{n_1} E^i_{n_2}. \quad \text{(B.22)}$$

We can imagine that we configure our system to have single mode signal and idler pumps in the mode space: $E^s_{n_1} = E^s_{m_1} U_1\left(n_1,m_1\right) \mathrm{e}^{\lambda^s_{Cm_1} z}$ and $E^i_{n_2} = E^i_{m_2} U_2\left(n_2,m_2\right) \mathrm{e}^{\lambda^i_{Cm_2} z}$ and substituting it in Eq. (B.20)

$$\Upsilon^{m_3}_{m_1,m_2} = iL\mathrm{e}^{\frac{\left(\lambda^p_{m_3}-\lambda^s_{m_1}-\lambda^i_{m_2}\right)z}{2}} \mathrm{sinc}\left(\frac{\left(\lambda^p_{m_3}-\lambda^s_{m_1}-\lambda^i_{m_2}\right)z}{2}\right) \times \sum_{n_3} U_3\left(n_3,m_3\right) U_1\left(n_3,m_1\right) U_2\left(n_3,m_2\right) E^s_{m_1} E^i_{m_2}. \quad \text{(2.23)}$$

Bibliography

[1] C. L. . Tang, *Handbook of Optics: Devices, Measurements, and Properties (part 5)* (McGraw-Hill Professional, Volume II, 2nd Edition, 1994). 4

[2] R. W. Boyd, *Nonlinear Optics*, 3rd ed. (Academic Press, San Diego, 2008). 4, 6, 52, 63, 64, 66

[3] W. P. Grice and I. A. Walmsley, "Spectral information and distinguishability in type-II down-conversion with a broadband pump," Phys. Rev. A **56**, 1627- 1634 (1997). 5

[4] M. Halder, A. Beveratos, N. Gisin, V. Scarani, C. Simon, and H. Zbinden, "Entangling independent photons by time measurement," Nature Physics **3**, 692 - 695 (2007). 5

[5] W. P. Schleich, *Quantum Optics in Phase Space* (WILEY-VCH Verlag Berlin, 2001). 6, 9

[6] M. O. Scully and M. S. Zubairy, *Quantum Optics* (Cambridg University Press, 1997).

[7] L. Mandel and E. Wolf, *Optical Coherence and Quantum Optics* (Cambridge University Press, New York, 1995). 9, 15, 17, 74, 76

[8] S. Braunstein and A. Pati, eds., *Quantum Information with Continuous Variables* (Kluwer Academic Publisher, 2003). 6

[9] C. K. Hong, Z. Y. Ou, and L. Mandel, "Measurement of subpicosecond time intervals between two photons by interference," Phys. Rev. Lett. **59**, 2044-2046 (1987). 6, 75

[10] D. Bouwmeester, J. Pan, K. Mattle, M. Eible, H. Weinfurter, and A. Zeilinger, "Experimental quantum teleportation," Nature, London **390**, 575-579 (1997). 6, 15

[11] K. Mattle, H.Weinfurter, P. Kwiat, and A. Zeilinger, "Dense Coding in Experimental Quantum Communication," Phys. Rev. Lett. **76**, 4656 (1996).

[12] C. Bennett, G. Brassard, C. Crepeau, R. Jozsa, A. Peres, and W. Wootters, "Teleporting an unknown quantum state via dual classical and Einstein-Podolsky-Rosen channels," Phys. Rev. Lett. **70**, 1895 (1993).

[13] D. Boschi, S. Branca, F. De Martini, L. Hardy, and S. Popescu, "Experimental realization of teleporting an unknown pure quantum state via dual classical and Einstein-Podolsky-Rosen channels," Phys. Rev. Lett. **80**, 1121-1125 (1998). 15

[14] S. Braunstein and H. Kimble, "Teleportation of Continuous Quantum Variables," Phys. Rev. Lett. **80**, 869 (1998).

[15] T. C. Ralph and P. K. Lam, "Teleportation with Bright Squeezed Light," Phys. Rev. Lett. **81**, 5668 (1998).

[16] D. Gottesman and J. Preskill, "Secure quantum key distribution using squeezed states," Phys. Rev. A **63**, 022309 (2001).

[17] N. Cerf, M. Levy, and G. V. Assche, "Quantum distribution of Gaussian keys using squeezed states," Phys. Rev. A **63**, 052311 (2001).

[18] T. Ralph, "Security of continuous-variable quantum cryptography," Phys. Rev. A **62**, 062306 (2000).

[19] F. Grosshans, V. Gilles, J. Wenger, R. Brouri, N. Cerf, and P. Grangier, "Quantum key distribution using gaussian-modulated coherent states," Nature **421**, 238-241 (2003).

[20] A. U'Ren, K. Banaszek, and I. Walmsley, "Photon engineering for quantum information processing," Quant. Inf. and Comp **3**, 480-502 (2003). 6, 8, 47

[21] P. Kwiat, K. Mattle, H. Weinfurter, A. Zeilinger, A. Sergienko, and Y. Shih, "New High-Intensity Source of Polarization-Entangled Photon Pairs," Phys. Rev. Lett. **75**, 4337-4341 (1995). 6

[22] Y. R. Shen, "Surface properties probed by second-harmonic and sum-frequency generation," Nature **337**, 519 - 525 (1989). 6

[23] Z. Kuprionis, V. Kod, G. Niaura, and A. Malinauskas, "Application of infrared-visible sum-frequency generation spectroscopy for studies of surfaces of conjugated polymers." Technical Digest. Summaries of Papers Presented at the Conference on Lasers & Electro-Optics. Postconference Technical Digest (IEEE CLEO) **01CH37170**, 162-162 (2001). 6

[24] J. Shah, "Ultrafast luminescence spectroscopy using sum frequency generation," Quant. Electr., IEEE **24**, 276 - 288 (1988). 6

[25] D. Logan, M. Giguere, A. Villeneuve, and A. S. Helmy, "Widely tunable mid-infrared generation via frequency conversion in semiconductor waveguides," Opt. Lett. **38(21)**, 4457-4460 (2013). 7

[26] K. Fradkin-Kashi, A. Arie, P. Urenski, and G. Rosenman, "Mid-infrared differencefrequency generation in periodically poled KTiOAsO4 and application to gas sensing," Opt. Lett. **25**, 743-745 (2000). 7

[27] S. Both, P. Cancio, G. Giusfredi, D. Mazzotti, and P. D. Natale, "Difference-frequency generation as a precise tool for high-resolution spectroscopy," Proceedings of SPIE **5137**, 339- 346 (2003). 7

[28] M. A. Belkin, F. Capasso, A. Belyanin, D. L. Sivco, A. Y. Cho, D. C. Oakley, C. J. Vineis, and G. W. Turner, "Terahertz quantum-cascade-laser source based on intracavity difference-frequency generation," Nat. Phot. **1**, 288 - 292 (2007). 7

[29] K. Asatani, "Lightwave subscriber toward broadband ISDN," J. Lightwave Technol. **7**, 1705-1747 (1989). 7

[30] M. Kawachi, "Silica waveguides on silicon and their application to integrated-optical components," Opt. and quant. Electron. **22**, 391-416 (1990).

[31] D. B. Keck, A. J. Morrow, D. A. Nolan, and D. A. Thompson, "Passive components in the subscriber loop," J. Lightwave Technol. **7**, 1623-163 (1989). 7

[32] H. Jin, F. M. Liu, P. Xu, J. L. Xia, M. L. Zhong, Y. Yuan, J. W. Zhou, Y. X. Gong, W. Wang, and S. N. Zhu, "On-Chip Generation and Manipulation of Entangled Photons Based on Reconfigurable Lithium-Niobate Waveguide Circuits," Phys. Rev. Lett. **113**, 103601 (2014). 8, 47

[33] J. C. F. Matthews, A. Politi, A. Stefanov, and J. L. O'Brien, "Manipulation of multiphoton entanglement in waveguide quantum circuits," Nature Photon. **3**, 346-350 (2009). 8, 11, 47

[34] T. Meany, M. Gräfe, R. Heilmann, A. Prez-Leija, S. Gross, M. J. Steel, M. J. Withford, and A. Szameit, "Laser written circuits for quantum photonics," Laser Photon. Rev. **9**, 363-384 (2015). 8, 39, 40

[35] A. Politi, M. J. Cryan, J. G. Rarity, S. Y. Yu, and J. L. O'Brien, "Silica-on-silicon waveguide quantum circuits," Science **320**, 646-649 (2008). 8

[36] B. J. Metcalf, J. B. Spring, P. C. Humphreys, N. Thomas-Peter, M. Barbieri, W. S. Kolthammer, X. M. Jin, N. K. Langford, D. Kundys, J. C. Gates, B. J. Smith, P. G. R. Smith, and I. A. Walmsley, "Quantum teleportation on a photonic chip," Nature Photonics **8**, 770-774 (2014). 47

[37] M. Grafe, R. Heilmann, A. Perez-Leija, R. Keil, F. Dreisow, M. Heinrich, H. Moya-Cessa, S. Nolte, D. N. Christodoulides, and A. Szameit, "On-chip generation of high-order single-photon W-states," Nature Photonics **8**, 791-795 (2014). 47

[38] F. Najafi, J. Mower, N. C. Harris, F. Bellei, A. Dane, C. Lee, X. L. Hu, P. Kharel, F. Marsili, S. Assefa, K. K. Berggren, and D. Englund, "On-chip detection of non-classical light by scalable integration of single-photon detectors," Nat. Commun. **6**, 5873-5878 (2015).

[39] A. Crespi, R. Ramponi, R. Osellame, L. Sansoni, I. Bongioanni, F. Sciarrino, G. Vallone, and P. Mataloni, "Integrated photonic quantum gates for polarization qubits," Nat. Commun. **2**, 566-6 (2011). 8

[40] S. Longhi, "Optical Bloch Oscillations and Zener Tunneling with Nonclassical Light," Phys. Rev. Lett. **101**, 193902-4 (2008). 8, 85

[41] A. Rai, G. S. Agarwal, and J. H. H. Perk, "Transport and quantum walk of nonclassical light in coupled waveguides," Phys. Rev. A **78**, 042304-5 (2008). 8

[42] M. J. Collins, C. Xiong, I. H. Rey, T. D. Vo, J. He, S. Shahnia, C. Reardon, T. F. Krauss, M. J. Steel, A. S. Clark, and B. J. Eggleton, "Integrated spatial multiplexing of heralded single-photon sources," Nat. Commun. **4**, 2582-7 (2013). 8

[43] J. W. Silverstone, D. Bonneau, K. Ohira, N. Suzuki, H. Yoshida, N. Iizuka, M. Ezaki, C. M. Natarajan, M. G. Tanner, R. H. Hadfield, V. Zwiller, G. D. Marshall, J. G. Rarity, J. L. O'Brien, and M. G. Thompson, "On-chip quantum interference between silicon photon-pair sources," Nature Photonics **8**, 104-108 (2014).

[44] N. C. Harris, D. Grassani, A. Simbula, M. Pant, M. Galli, T. Baehr-Jones, M. Hochberg, D. Englund, D. Bajoni, and C. Galland, "Integrated Source of Spectrally Filtered Correlated Photons for Large-Scale Quantum Photonic Systems," Phys. Rev. X **4**, 041047-10 (2014). 8

[45] Q. Zhang, X. P. Xie, H. Takesue, S. W. Nam, C. Langrock, M. M. Fejer, and Y. Yamamoto, "Correlated photon-pair generation in reverse-proton-

exchange PPLN waveguides with integrated mode demultiplexer at 10 GHz clock," Opt. Express **15**, 10288-10293 (2007). 8, 15, 47

[46] X. Q. Yu, P. Xu, Z. D. Xie, J. F. Wang, H. Y. Leng, J. S. Zhao, S. N. Zhu, and N. B. Ming, "Transforming Spatial Entanglement Using a Domain-Engineering Technique," Phys. Rev. Lett. **101**, 233601-4 (2008).

[47] S. Krapick, H. Herrmann, V. Quiring, B. Brecht, H. Suche, and C. Silberhorn, "An efficient integrated two-color source for heralded single photons," New J. Phys. **15**, 033010-19 (2013). 73

[48] A. S. Solntsev, F. Setzpfandt, A. S. Clark, C. W. Wu, M. J. Collins, C. Xiong, A. Schreiber, F. Katzschmann, F. Eilenberger, R. Schiek, W. Sohler, A. Mitchell, C. Silberhorn, B. J. Eggleton, T. Pertsch, A. A. Sukhorukov, D. N. Neshev, and Y. S. Kivshar, "Generation of Nonclassical Biphoton States through Cascaded Quantum Walks on a Nonlinear Chip," Phys. Rev. X **4**, 031007-13 (2014). 47, 64, 65, 85

[49] H. Jin, F. M. Liu, P. Xu, J. L. Xia, M. L. Zhong, Y. Yuan, J. W. Zhou, Y. X. Gong, W. Wang, and S. N. Zhu, "On-Chip Generation and Manipulation of Entangled Photons Based on Reconfigurable Lithium-Niobate Waveguide Circuits," Phys. Rev. Lett. **113**, 103601-5 (2014). 8, 11

[50] Y. Bromberg, Y. Lahini, R. Morandotti, and Y. Silberberg, "Quantum and Classical Correlations inWaveguide Lattices," Phys. Rev. Lett. **102**, 253904 (2009). 8, 85

[51] A. Peruzzo, M. Lobino, J. C. F. Matthews, N. Matsuda, A. Politi, K. Poulios, X. Q. Zhou, Y. Lahini, N. Ismail, K. Worhoff, Y. Bromberg, Y. Silberberg, M. G. Thompson, and J. L. O'Brien, "Quantum Walks of Correlated Photons," Science **329**, 1500-1503 (2010). 8, 15, 28, 29, 85

[52] M. A. Broome, A. Fedrizzi, S. Rahimi-Keshari, J. Dove, S. Aaronson, T. C. Ralph, and A. G. White, "Photonic Boson Sampling in a Tunable Circuit," Science **339**, 794-798 (2013). 8, 15

[53] J. B. Spring, B. J. Metcalf, P. C. Humphreys, W. S. Kolthammer, X. M. Jin, M. Barbieri, A. Datta, N. Thomas-Peter, N. K. Langford, D. Kundys, J. C. Gates, B. J. Smith, P. G. R. Smith, and I. A. Walmsley, "Boson Sampling on a Photonic Chip," Science **339**, 798-801 (2013).

[54] M. Tillmann, B. Dakic, R. Heilmann, S. Nolte, A. Szameit, and P. Walther, "Experimental boson sampling," Nature Photonics **7**, 540-544 (2013).

[55] A. Crespi, R. Osellame, R. Ramponi, D. J. Brod, E. F. Galvao, N. Spagnolo, C. Vitelli, E. Maiorino, P. Mataloni, and F. Sciarrino, "Integrated multimode interferometers with arbitrary designs for photonic boson sampling," Nature Photonics **7**, 545-549 (2013). 8, 15

[56] A. S. Solntsev, A. A. Sukhorukov, D. N. Neshev, and Y. S. Kivshar, "Spontaneous Parametric Down-Conversion and Quantum Walks in Arrays of Quadratic Nonlinear Waveguides," Phys. Rev. Lett. **108**, 023601-5 (2012). 8, 15, 24, 28, 29, 73, 78, 80

[57] A. S. Solntsev, A. A. Sukhorukov, D. N. Neshev, and Y. S. Kivshar, "Photon-pair generation in arrays of cubic nonlinear waveguides," Opt. Express **20**, 27441-27446 (2012). 73

[58] M. Gräfe, A. S. Solntsev, R. Keil, A. A. Sukhorukov, M. Heinrich, A. Tunnermann, S. Nolte, A. Szameit, and Y. S. Kivshar, "Biphoton generation in quadratic waveguide arrays: A classical optical simulation," Sci. Rep. **2**, 562-5 (2012). 12, 26, 35, 36, 47, 85

[59] R. Kruse, F. Katzschmann, A. Christ, A. Schreiber, S. Wilhelm, K. Laiho, A. Gabris, C. S. Hamilton, I. Jex, and C. Silberhorn, "Spatio-spectral characteristics of parametric down-conversion in waveguide arrays," New J. Phys. **15**, 083046-24 (2013). 8, 15, 24, 28, 85

[60] R. W. Heeres, L. P. Kouwenhoven, and V. Zwiller, "Quantum interference in plasmonic circuits," Nat. Nanotechnol. **8**, 719-722 (2013). 8, 11

[61] J. S. Fakonas, H. Lee, Y. A. Kelaita, and H. A. Atwater, "Two-plasmon quantum interference," Nature Photonics **8**, 317-320 (2014). 8, 11

[62] C. M. Caves and D. D. Crouch, "Quantum wide-band traveling-wave analysis of a degenerate parametric-amplifier," J. Opt. Soc. Am. B **4**, 1535-1545 (1987). 8, 16, 17, 18, 48, 74

[63] D. Klyshko, *Photons and Nonlinear Optics* (Gordon and Breach, 1988). 15, 18, 21, 22, 42

[64] S. P. Kulik, G. A. Maslennikov, S. P. Merkulova, A. N. Penin, L. K. Radchenko, and V. N. Krasheninnikov, "Two-photon interference in the presence of absorption," JETP **98**, 31-38 (2004). 16, 20, 48

[65] D. A. Antonosyan, A. S. Solntsev, and A. A. Sukhorukov, "Effect of loss on photon-pair generation in nonlinear waveguide arrays," Phys. Rev. A **90**, 043845-10 (2014). 42, 48

[66] L. G. Helt, M. J. Steel, and J. E. Sipe, "Spontaneous parametric downconversion in waveguides: what's loss got to do with it?" New J. Phys. **17**, 013055-17 (2015). 8

[67] V. Scarani, H. Bechmann-Pasquinucci, N. J. Cerf, M. Duek, N. Ltkenhaus, and M. Peev, "The security of practical quantum key distribution," Rev. Mod. Phys. **81**, 1301-1350 (2009). 9

[68] R. Dong, M. Lassen, J. Heersink, C. Marquardt, R. Filip, G. Leuchs, and U. Andersen, "Experimental entanglement distillation of mesoscopic quantum states," Nat. Phys. **4**, 919-923 (2008). 9

[69] M. Mičuda, I. Straka, M. Mikovä, M. Duek, N. J. Cerf, J. Fiuräsek, and M. Ježek, "Noiseless Loss Suppression in Quantum Optical Communication," Phys. Rev. Lett. **109**, 180503 (2012). 9

[70] C. Kittel, *Introduction to Solid State Physics* (Wiley, NewYork, 2005). 9

[71] R. D. Astumian and P. Hänggi, "Brownian motions," Physics Today **55**, 33-39 (2002).

[72] P. Reimann, "Brownian Motors: Noisy Transport far from Equilibrium," Phys. Rep. **57**, 361-365 (2002). 9

[73] B. E. A. Saleh and M. C. Teich, *Fundamentals of Photonics* (Wiley, New York, 1991). 9

[74] R. Philip, M. Anija, C. Yelleswarapu, and D. Rao, "Passive all-optical diode using asymmetric nonlinear absorption," Appl. Phys. Lett. **91**, 141118 (2007). 9

[75] K. Gallo, G. Assanto, K. R. Parameswaran, and M. M. Fejer, "All-optical diode in a periodically-poled Lithium Niobate waveguide," Appl. Phys. Lett. **79**, 314316 (2001). 9

[76] M. Scalora, J. Dowling, C. Bowden, and M. Bloemer, "The photonic band edge optical diode," J. Appl. Phys **76**, 2023-2026 (1994). 9

[77] N. Moiseyev, ed., *Non-Hermitian Quantum Mechanics* (Cambridge University Press, UK, 2011). 9, 10

[78] C. M. Bender and S. Böttcher, "Real spectra in non-Hermitian Hamiltonians having PT symmetry." Phys. Rev. Lett. **80**, 5243-5246 (1998). 9

[79] N. Bender, S. Factor, J. D. Bodyfelt, H. Ramezani, D. N. Christodoulides, F. M. Ellis, and T. Kottos, "Observation of Asymmetric Transport in Structures with Active Nonlinearities," Phys. Rev. Lett. **110**, 234101-5 (2013). 9, 71

[80] R. El Ganainy, K. G. Makris, D. N. Christodoulides, and Z. H. Musslimani, "Theory of coupled optical PT-symmetric structures," Opt. Lett. **32**, 2632 - 2634 (2007). 9, 10, 48

[81] A. Guo, G. J. Salamo, D. Duchesne, R. Morandotti, M. Volatier-Ravat, V. Aimez, G. A. Siviloglou, and D. N. Christodoulides, "Observation of PT-Symmetry Breaking in Complex Optical Potentials," Phys. Rev. Lett. **103**, 093902-4 (2009). 10, 11, 48, 63, 65, 66, 68

[82] C. E. Ruter, K. G. Makris, R. El Ganainy, D. N. Christodoulides, M. Segev, and D. Kip, "Observation of parity-time symmetry in optics," Nature Physics **6**, 192-195 (2010). 9, 10, 11, 65, 66, 68

[83] A. Ruschhaupt, F. Delgado, and J. Muga, "Physical realization of-symmetric potential scattering in a planar slab waveguide," Journal of Physics A **38**, L171 - L176 (2005). 9

[84] K. G. Makris, R. El-Ganainy, D. N. Christodoulides, and Z. H. Musslimani, "Beam Dynamics in PT Symmetric Optical Lattices," Phys. Rev. Lett. **100**, 103904 (2008). 48

[85] Z. H. Musslimani, K. G. Makris, R. El-Ganainy, and D. N. Christodoulides, "Optical solitons in PT periodic potentials," Phys. Rev. Lett. **100**, 030402 (2008). 9, 48

[86] A. Ruschhaupt, F. Delgado, and J. G. Muga, "Physical realization of PT-symmetric potential scattering in a planar slab waveguide," J. Phys. A **38**, L171-L176 (2005). 10

[87] L. Feng, Z. J. Wong, R. M. Ma, Y. Wang, and X. Zhang, "Single-mode laser by parity-time symmetry breaking," Science **346**, 972-975 (2014). 10, 67, 71

[88] H. Hodaei, M. A. Miri, M. Heinrich, D. N. Christodoulides, and M. Khajavikhan, "Parity-time-symmetric microring lasers," Science **346**, 975-978 (2014). 10, 67, 71

[89] H. Ramezani, T. Kottos, R. El-Ganainy, and D. N. Christodoulides, "Unidirectional nonlinear PT -symmetric optical structures," Phys. Rev. A **82**, 043803 (2010). 10, 48

[90] S. V. Suchkov, A. A. Sukhorukov, J. Huang, S. V. Dmitriev, C. Lee, and Y. S. Kivshar, "Nonlinear switching and solitons in PT-symmetric photonic systems," Laser Phot. Rev. **10**, 177-213 (2016). 11, 48

[91] S. Longhi, "Quantum simulation of decoherence in optical waveguide lattices," Opt. Lett. **38**, 4884-4887 (2013). 12, 35, 36, 45

[92] B. H. Liu, L. Li, Y. F. Huang, C. F. Li, G. C. Guo, E. M. Laine, H. P. Breuer, and J. Piilo, "Experimental control of the transition from Markovian to non-Markovian dynamics of open quantum systems," Nat. Phys. **7**, 931-934 (2011). 12

[93] H. P. Breuer and F. Petruccione, *The Theory of Open Quantum Systems* (Oxford University Press, Oxford, 2002).

[94] H. Lee, Y. C. Cheng, and G. R. Fleming, "Coherence dynamics in photosynthesis: Protein protection of excitonic coherence," Science **316**, 14621465 (2007). 12

[95] M. M. e. a. Wolf, "Assessing non-Markovian quantum dynamics." Phys. Rev. Lett. **101**, 150402 (2008). 12

[96] H. P. Breuer, E. M. Laine, and J. Piilo, "Measure for the degree of non-Markovian behavior of quantum processes in open systems." Phys. Rev. Lett. **103**, 210401 (2009). 12

[97] S. Longhi, "Quantum-optical analogies using photonic structures," Laser Photon. Rev. **3**, 243-261 (2009). 12, 35, 47

[98] M. Liscidini and J. E. Sipe, "Stimulated Emission Tomography," Phys. Rev. Lett. **111**, 193602-5 (2013). 12, 35, 47

[99] L. G. Helt and M. J. Steel, "Effect of scattering loss on connections between classical and quantum processes in second-order nonlinear waveguides," Opt. Lett. **40**, 1460-1463 (2015). 12, 35, 47, 48

[100] D. Bouwmeester, A. K. Ekert, and A. Zeilinger, eds., *The physics of quantum information: quantum cryptography, quantum teleportation, quantum computation* (Springer, New York, 2000). 15

[101] Y. Shih, *An Introduction to Quantum Optics: Photon and Biphoton Physics* (Taylor & Francis, New York, 2011). 15

[102] S. E. Harris, M. K. Oshman, and R. L. Byer, "Observation of tunable optical parametric fluorescence," Phys. Rev. Lett. **18**, 732 (1967). 15

[103] J. W. Pan, D. Bouwmeester, H. Weinfurter, and A. Zeilinger, "Experimental entanglement swapping: Entangling photons that never interacted," Phys. Rev. Lett. **80**, 3891-3894 (1998). 15

[104] A. Furusawa, J. L. Sorensen, S. L. Braunstein, C. A. Fuchs, H. J. Kimble, and E. S. Polzik, "Unconditional quantum teleportation," Science **282**, 706-709 (1998). 15

[105] A. K. Ekert, J. G. Rarity, P. R. Tapster, and G. M. Palma, "Practical quantum cryptography based on 2-photon interferometry," Phys. Rev. Lett. **69**, 1293-1295 (1992). 15

[106] M. Giustina, A. Mech, S. Ramelow, B. Wittmann, J. Kofler, J. Beyer, A. Lita, B. Calkins, T. Gerrits, S. Nam, R. Ursin, and A. Zeilinger, "Bell violation using entangled photons without the fair-sampling assumption," Nature **497**, 227-230 (2013). 15

[107] R. Fickler, M. Krenn, R. Lapkiewicz, S. Ramelow, and A. Zeilinger, "Real-Time Imaging of Quantum Entanglement," Sci. Rep. **3**, 1914-5 (2013). 15

[108] S. Tanzilli, H. De Riedmatten, W. Tittel, H. Zbinden, P. Baldi, M. De Micheli, D. B. Ostrowsky, and N. Gisin, "Highly efficient photon-pair source using periodically poled lithium niobate waveguide," Electron. Lett. **37**, 26-28 (2001). 15

[109] K. Banaszek, A. B. U'Ren, and I. A. Walmsley, "Generation of correlated photons in controlled spatial modes by downconversion in nonlinear waveguides," Opt. Lett. **26**, 1367-1369 (2001). 15, 47

[110] Q. Zhang, H. Takesue, C. Langrock, X. P. Xie, M. M. Fejer, and Y. Yamamoto, "Hong-Ou-Mandel Dip Using Degenerate Photon Pairs from a Single Periodically Poled Lithium Niobate Waveguide with Integrated Mode Demultiplexer," Jpn. J. Appl. Phys. **49**, 064401-4 (2010).

[111] A. Eckstein and C. Silberhorn, "Broadband frequency mode entanglement in waveguided parametric downconversion," Opt. Lett. **33**, 1825-1827 (2008).

[112] M. F. Saleh, G. Di Giuseppe, B. E. A. Saleh, and M. C. Teich, "Photonic Circuits for Generating Modal, Spectral, and Polarization Entanglement," IEEE Photonics J. **2**, 736-752 (2010). 15, 47

[113] A. B. U'Ren, K. Banaszek, and I. A. Walmsley, "Photon engineering for quantum information processing," Quantum Inform. Comput. **3**, 480-502 (2003). 15

[114] R. Loudon, *The Quantum Theory of Light*, 3rd ed. (Oxford University Press, New York, 2000). 16, 17, 18, 87

[115] S. Lloyd, "Universal quantum simulators," Science **273**, 1073-1078 (1996). 17

[116] S. Prasad, M. O. Scully, and W. Martienssen, "A quantum description of the beam splitter," Opt. Commun. **62**, 139-145 (1987). 18

[117] M. S. Tame, C. Lee, J. Lee, D. Ballester, M. Paternostro, A. V. Zayats, and M. S. Kim, "Single-Photon Excitation of Surface Plasmon Polaritons," Phys. Rev. Lett. **101**, 190504-4 (2008). 18

[118] X. Y. Zou, L. J. Wang, and L. Mandel, "Induced coherence and indistinguishability in optical interference," Phys. Rev. Lett. **67**, 318-321 (1991). 20

[119] G. B. Lemos, V. Borish, G. D. Cole, S. Ramelow, R. Lapkiewicz, and A. Zeilinger, "Quantum imaging with undetected photons," Nature **512**, 409 - 412 (2014). 22

[120] D. Kalashnikov, A. V. Paterova, S. P. Kulik, and L. A. Krivitsky, "Infrared spectroscopy with visible light," Nature Photonics **10**, 98 - 101 (2015). 22

[121] A. Ekert and P. L. Knight, "Entangled quantum-systems and the schmidt decomposition," Am. J. Phys. **63**, 415-423 (1995). 29

[122] H. Huang and J. H. Eberly, "Correlations and one-quantum pulse shapes in photon pair generation," J. Mod. Opt. **40**, 915-930 (1993). 29

[123] A. B. U'Ren, C. Silberhorn, K. Banaszek, I. A. Walmsley, R. Erdmann, W. P. Grice, and M. G. Raymer, "Generation of pure-state single-photon wavepackets by conditional preparation based on spontaneous parametiric downconversion," Laser Phys. **15**, 146-161 (2005). 29

[124] P. Ginzburg and A. V. Zayats, "Non-exponential decay of dark localized surface plasmons," Opt. Express **20**, 6720-6727 (2012). 35

[125] F. Lederer, G. I. Stegeman, D. N. Christodoulides, G. Assanto, M. Segev, and Y. Silberberg, "Discrete solitons in optics," Phys. Rep. **463**, 1-126 (2008). 37

[126] K. M. Davis, K. Miura, N. Sugimoto, and K. Hirao, "Writing waveguides in glass with a femtosecond laser," Opt. Lett. **21**, 1729-1731 (1996). 39

[127] S. Nolte, M. Will, J. Burghoff, and A. Tuennermann, "Femtosecond waveguide writing: a new avenue to three-dimensional integrated optics," Appl. Phys. A **77**, 109111 (2003). 39

[128] D. Blömer, A. Szameit, F. Dreisow, T. Schreiber, S. Nolte, and A. Tünnermann, "Nonlinear refractive index of fs-laser-written waveguides in fused silica," Opt. Express **14**, 2151-2157 (2006). 39, 40

[129] K. Miura, J. Qiu, H. Inouye, T. Mitsuyu, and K. Hirao, "Photowritten waveguides in various glasses with ultrashort pulse laser," Appl. Phys. Lett. **71**, 33293331 (1997). 39

[130] W. Watanabe, T. Asano, K. Yamada, K. Itoh, and J. Nishii, "Wavelength division with three-dimensional couplers fabricated by filamentation of femtosecond laser pulses," Opt. Lett. **28**, 24912493 (2003). 39

[131] T. Pertsch, U. Peschel, F. Lederer, J. Burghoff, M. Will, S. Nolte, and A. Tünnermann, "Discrete diffraction in two-dimensional arrays of coupled waveguides in silica," Opt. Lett. **29**, 468470 (2004). 39, 52

[132] A. Szameit, D. Blömer, J. Burghoff, T. Pertsch, S. Nolte, and A. Tünnermann, "Hexagonal waveguide arrays written with fs-laser pulses," Appl. Phys. B **82**, 507-512 (2006). 39, 40

[133] Z. Yang, M. Liscidini, and J. E. Sipe, "Spontaneous parametric down-conversion in waveguides: A backward Heisenberg picture approach," Phys. Rev. A **77**, 033808 (2008). 47

[134] M. A. Foster, A. C. Turner, R. Salem, M. Lipson, and A. L. Gaeta, Opt. Express **15**, 12949 (2007).

[135] C. Monat, A. Clark, C. Xiong, C. Grillet, G. Marshall, M. J. Steel, J. A. Dionne, L. OFaolain, T. F. Krauss, and B. J. Eggleton, "Correlated photon-pair generation in an ultra-compact silicon photonic crystal waveguide," CLEO:2011, Baltimore p. PDPC4 (2011). 47

[136] M. Fiorentino, S. M. Spillane, R. G. Beausoleil, T. D. Roberts, P. Battle, and M. W. Munro, "Spontaneous parametric down-conversion in periodically poled KTP waveguides and bulk crystals," Opt. Express **15**, 7479-7488 (2007). 47

[137] G. Harder, V. Ansari, B. Brecht, T. D. C. Marquardt, and C. Silberhorn, "An optimized photon pair source for quantum circuits," Opt. Express **21**, 13975-13985 (2013). 47

[138] A. A. Sukhorukov, Z. Y. Xu, and Y. S. Kivshar, Phys. Rev. A **82**, 043818 (2010). 48

[139] B. A. Malomed, G. D. Peng, , and P. L. Chu, "Nonlinearoptical amplifier based on a dual-core fiber," Opt. Lett. **21**, 330-332 (1996). 48

[140] I. V. Barashenkov, S. V. Suchkov, A. A. Sukhorukov, S. V. Dmitriev, and Y. S. Kivshar, Phys. Rev. A **86**, 053809 (2012). 48

[141] L. A. Rozema, C. Wang, D. H. Mahler, A. Hayat, A. M. Steinberg, . E. Sipe, and M. Liscidini, "Characterizing an entangled-photon source with classical detectors and measurements," Opt. Lett. **2**, 430-433 (2015). 48

[142] J. Wilkinson, *The Algebraic Eigenvalue Problem* (Oxford, Clarendon Press, 1988). 50

[143] D. A. Antonosyan, A. S. Solntsev, and A. A. Sukhorukov, "Parity-time anti-symmetric parametric amplifier," Opt. Lett. **40**, 4575-4578 (2015). 52

[144] A. Guo, G. Salamo, D. Duchesne, R. Morandotti, M. Volatier-Ravat, V. Aimez, G. Siviloglou, and D. Christodoulides, Phys. Rev. Lett. **103** (2009). 55

[145] C. M. Bender, D. Brody, and H. F. Jones, Am. J. Phys. **71**, 1095-1102 (2003). 55

[146] B. Bagchi and C. Quesne, Phys. Lett. A **273**, 285292 (2000). 55

[147] H. Alaeian and J. A. Dionne, Phys. Rev. A (in press). 60, 61

[148] A. Lupu, H. Benisty, and A. Degiron, Optics Express **21**, 21651-21668 (2013). 60

[149] E. Verhagen, R. de Waele, L. Kuipers, and A. Polman, "Three-Dimensional Negative Index of Refraction at Optical Frequencies by Coupling Plasmonic Waveguides," Phys. Rev. Lett. **105**, 223901 (2010). 60

[150] T. Xu, A. Agrawal, M. Abashin, K. J. Chau, and H. J.Lezec, Nature **497**, 470474 (2013). 60

[151] J. Valentine, S. Zhang, T. Zentgraf, E. U. Avila, D. A. Genov, G. Bartal, and X. Zhang, Nature **455**, 376-379 (2008). 60

[152] J. Yao, Z. Liu, , Y. Liu, Y.Wang, C. Sun, G. Bartal, A. M. Stacy, and X. Zhang, Science **321**, 930 (2008). 60

[153] K. Li, D. A. Zezyulin, P. G. Kevrekidis, V. V. Konotop, and F. K. Abdullaev, "PT-symmetric coupler with $\chi^{(2)}$ nonlinearity," Phys. Rev. A **88**, 053820-11 (2013). 63

[154] F. C. Moreira, F. K. Abdullaev, V. V. Konotop, and A. V. Yulin, "Localized modes in $\chi^{(2)}$ media with PT-symmetric localized potential," Phys. Rev. A **86**, 053815-7 (2012). 63

[155] F. C. Moreira, V. V. Konotop, and B. A. Malomed, "Solitons in PT-symmetric periodic systems with the quadratic nonlinearity," Phys. Rev. A **87**, 013832-11 (2013). 63

[156] L. Ge and H. E. Tureci, "Antisymmetric PT-photonic structures with balanced positive- and negative-index materials," Phys. Rev. A **88**, 053810-5 (2013). 66

[157] B. Peng, S. K. Ozdemir, F. C. Lei, F. Monifi, M. Gianfreda, G. L. Long, S. H. Fan, F. Nori, C. M. Bender, and L. Yang, "Parity-time-symmetric whispering-gallery microcavities," Nature Physics **10**, 394-398 (2014). 71

[158] A. Rai and D. G. Angelakis, "Dynamics of nonclassical light in integrated nonlinear waveguide arrays and generation of robust continuous-variable entanglement," Phys. Rev. A **85**, 052330-5 (2012). 73

[159] S. Sensarn, G. Y. Yin, and S. E. Harris, "Generation and Compression of Chirped Biphotons," Phys. Rev. Lett. **104**, 253602-4 (2010). 73

[160] T. Guerreiro, E. Pomarico, B. Sanguinetti, N. Sangouard, J. S. Pelc, C. Langrock, M. M. Fejer, H. Zbinden, R. T. Thew, and N. Gisin, "Interaction of independent single photons based on integrated nonlinear optics," Nat. Commun. **4**, 2324-5 (2013). 73

[161] H. Hubel, D. R. Hamel, A. Fedrizzi, S. Ramelow, K. J. Resch, and T. Jennewein, "Direct generation of photon triplets using cascaded photon-pair sources," Nature **466**, 601-603 (2010). 73

[162] N. K. Langford, S. Ramelow, R. Prevedel, W. J. Munro, G. J. Milburn, and A. Zeilinger, "Efficient quantum computing using coherent photon conversion," Nature **478**, 360-363 (2011). 73, 75

[163] D. Markis, K.G.and Christodoulides, O. Peleg, M. Segev, and D. Kip, "Optical transitions and Rabi oscillations in waveguide arrays," Opt. Express **16**, 10309-10314 (2008). 74

[164] Y. Kartashov, V. Vysloukh, and L. Torner, "Resonant Mode Oscillations in Modulated Waveguiding Structures," Phys. Rev. Lett. **99**, 233903 (2007). 74

[165] I. Bayala, P. Panchadhyayeeb, and P. K. Mahapatrac, "Optical analogue of Rabi oscillations in optical waveguides via structured continuum," J. of Modern Opt. **62**, 1412 -1418 (20015). 74

[166] S. A. Podoshvedov, J. Noh, and K. Kim, "A full quantum theory of parametric down conversion and its application to coincidence measurements," J. Korean Phys. Soc. **47**, 213-222 (2005). 75

[167] M. I. Kolobov, "The spatial behavior of nonclassical light," Rev. Mod. Phys. **71**, 1539 -1589 (1999). 85

[168] A. Christ, K. Laiho, A. Eckstein, T. Lauckner, P. J. Mosley, and C. Silberhorn, "Spatial modes in waveguided parametric down-conversion." Phys. Rev. A **80**, 033829 (2009). 85